NMR analyses on recognition of the mitochondrial targeting signal by Tim50

(Tim50 によるミトコンドリア移行シグナル認識機構の NMR 解析)

2014, PhD Thesis

Md. Bytul Mokaddesur RAHMAN

Department of Chemistry
Graduate School of Science
Nagoya University

Acknowledgements

Foremost I would like to express my cordial gratitude to Professor Toshiya Endo for the excellent scientific forms in his laboratory, for his permanent enthusiasm to discuss scientific matters, his openness towards all kinds of scientific directions, his constant support and his kind encouragements throughout the present study.

I am truly grateful to Dr. Shin Kawano for his continuous guidance and kind cooperation which enabling me to finish my PhD thesis at Nagoya University.

I want to express my sincere thanks to Professor Tohru Yoshihisa, Hyogo University, Japan. He greatly helped me to develop my ideas with basic methodology at an early stage of this research. I like to thank Dr. Yohei Miyanoiri and Dr. Masatsune Kainosho for NMR measurements.

Furthermore, I am very thankful for the great help I received from Takahiro Anzai. Life in the lab and outside of the lab would not be smooth without his support. I am grateful to Dr. Kaori Esaki for her supports and valuable suggestions. I would like to thank all other former and present members of the “Prof. Endo lab” for helpful discussion, for giving me the nice and friendly working atmosphere and their parts in the lab life.

I am deeply grateful for the support and the friendship that I received from my colleagues from the University of Rajshahi, Bangladesh.

And finally, I wish to express my deepest gratitude to all of my beloved family members for their understanding and encouragement.

Md. Bytul Mokaddesur RAHMAN

Contents

List of abbreviations

ATP	adenosine 5’ triphosphate
CBB	coomassie brilliant blue
CD	circular dichroism
Cyt. c	cytochrome *c*
EDTA	di-sodium dihydrogen ethylenediamine tetra-acetic acid dehydrate
GST	glutathione S-transferase
Hsp60	heat shock protein 60
HSQC	heteronuclear single quantum coherence spectroscopy
IMM	inner mitochondrial membrane
IMS	Intermembrane space
IPTG	isopropyl β-D-1-thiogalactopyranoside
III	the respiratory chain complex III
IV	the respiratory chain complex IV
kDa	kilodalton
MIA	mitochondrial intermembrane space import and assembly
mtHsp70	mitochondrial heat shock protein 70
Ni-NTA	nickel-nitrilotriacetic acid-agarose
NMR	nuclear magnetic resonance
N-terminal	amino-terminal
OD	optic density
OMM	outer mitochondrial membrane
PAM	precursor-associated motor
PBD	presequence binding domain
sPBD	shorter variant of presequence binding domain
PBS	phosphate buffered saline
PCR	polymerase chain reaction

SAM	sorting and assembly machinery
SDS-PAGE	sodium dodecyl sulfate-polyacrylamide gel electrophoresis
TCA	trichloric acid
TFA	trifluoroacetic acid
TEMED	*N*,*N*,*N´*,*N´*-Tetramethylethan-1,2-diamin
TIM	translocase of the inner mitochondrial membrane
TMS	transmembrane segment
TOB	topogenesis of mitochondrial outer membrane β-barrel proteins
TOM	translocase of the outer mitochondrial membrane
Tris	tris(hydroxymethyl)aminomethane
Ura	uracil
U	unit
WT	wild type
v/v	volume per volume
w/v	weight per volume
Δψ	mitochondrial inner membrane potential

Chapter 1

General Introduction

1.1. Mitochondria and mitochondrial proteins

Mitochondria are ubiquitous organelles consisting of two highly specialized membrane systems, the OM (Outer Membrane) and IM (Inner Membrane), and two aqueous compartments, the matrix and the IMS (Intermembrane Space). In addition to their fundamental role in ATP synthesis, mitochondria hold central metabolic pathways, like the Krebs cycle and the β-oxidation of fatty acids. Based on proteomic analyses, it is estimated that mitochondria contain ~1500 different proteins in mammals and ~1000 different proteins in yeast [1–3]. Because of their endosymbiotic origin, mitochondria still contain their own small genome encoding a limited number of proteins, which are mostly subunits of respiratory chain complexes and F_1F_o-ATP synthase. Thus, nearly all mitochondrial proteins are encoded by nuclear genes, synthesized as precursor forms on cytosolic ribosomes and subsequently transported into mitochondria. Transport of proteins from their site of synthesis to the final destination within mitochondria is a complicated task and requires the help of distinct import machineries, which have been identified and extensively characterized over the last few decades [4–14].

1.2. Targeting and sorting signals of mitochondrial proteins

Targeting of newly synthesized mitochondrial precursor proteins to mitochondria and their sorting to distinct mitochondrial sub-compartments require the presence of specific import signals within the transported polypeptides (Figure 1.2.1). The most typical mitochondrial import signal is contained in an N-terminal extension termed a presequence. Presequences can form amphipathic α-helical segments with a net positive charge and show a prevalent length distribution of 15 to 55 amino acids [15]. The helix therefore shows two

faces, one hydrophobic and the other hydrophilic, and possesses a net positive charge(s). These properties of the mitochondrial presequences are important in view of the specific interaction with the receptors on the outer mitochondrial membrane. In general, N-terminal presequences are proteolytically removed after import into the matrix by matrix processing peptidase and other proteases [16,17]. A second group of precursor proteins lacks a cleavable amino-terminal extension but contains often less well defined internal targeting signals. These internal targeting signals are used by β-barrel proteins of the outer membrane, soluble IMS proteins and polytopic inner membrane proteins. Most precursor proteins, with or without presequence, can be imported into mitochondria post-translationally, although a co-translational mechanism can also occur [18].

1.3. An overview of mitochondrial protein translocases

Most mitochondrial proteins enter mitochondria by crossing the outer membrane, and then the protein-sorting pathway branches out elaborately for different sub-mitochondrial compartments with the aid of distinct sorting-specific import machineries (Figure 1.3.1). The protein import machineries of mitochondria include four main translocators, named the TOM40, TOB/SAM, TIM23 and TIM22 complexes. The outer mitochondrial membrane contains the TOM40 translocation complex, whereas the other two are present in the inner membrane. Virtually all mitochondrial proteins utilize the TOM40 complex as the main entry point for the transport across the outer mitochondrial membrane. The outer mitochondrial membrane additionally contains the SAM (sorting and assembly machinery) complex, also termed the TOB complex, which is required for the assembly of β-barrel proteins into the outer membrane [19]. However, these β-barrel proteins are first imported through the TOM40 complex prior to relocation to the SAM/TOB

complex.

The TIM23 and TIM22 complexes represent two distinct inner membrane translocases. The TIM23 complex is responsible for the import of presequence-containing preproteins, while TIM22 complex facilitates the assembly of precursor proteins bearing internal targeting signals into the inner membrane. A further pathway involving Mia40/Tim40 (mitochondrial intermembrane space assembly machinery) and Erv1 directs small soluble proteins to the intermembrane space of mitochondria, and links their sorting to their oxidative folding by a disulfide relay mechanism [20].

1.3.1. Protein translocation across the outer membrane: the TOM40 complex

The TOM40 complex is a particularly fascinating protein translocase, as it mediates the transport of various types of precursors with diverse import signals across the outer membrane and then selectively distributes them to multiple downstream protein sorting machineries. Tom40, the central subunit of the TOM40 complex, is integrated into the outer membrane in a β-barrel conformation and forms an aqueous pore, through which mitochondrial precursor proteins cross the outer membrane [21–23]. To function as receptors, the cytosolic domains of three primary receptor subunits Tom20, Tom22 and Tom70 recognize and bind specific signals of mitochondrial precursor proteins. Tom20 mainly recognizes N-terminal presequences by binding the hydrophobic face of their amphipathic α-helical structure [24,25]. Precursor proteins with hydrophobic internal targeting signals are preferentially bound by Tom70 with the assistance of Hsp90 and Hsp60, which deliver precursor proteins to the TOM40 complex [26-28]. The receptor Tom22 is critical for the integrity of the TOM40 complex and exposes presequence binding domains to both the cytosol and the IMS [29–32]. Tom22 is thought to bind to the hydrophilic face of the amphipathic α-helical structure of presequences. The TOM40 core complex also

contains three small proteins Tom5, Tom6 and Tom7, which also play a role in stabilization and organization of the TOM40 complex [33–35], but Tom5 was also reported to have a more direct role in protein translocation [35]. After passage through the TOM40 complex, the precursor proteins are further sorted to their respective mitochondrial sub-compartments.

The pathway of precursor passage through the TOM40 complex is best understood for presequence-containing proteins [36,37]. The increasing affinity for the presequence from the cis binding site to the trans binding site is considered to drive the inward-directed movement of the presequence. For presequence-containing proteins, the transport across the outer membrane is tightly coupled to the translocation across or into the inner membrane via the TIM23 machinery through a direct hand-over of substrates as soon as they emerge from the TOM40 complex [38,39].

1.3.2. The SAM/TOB complex

β-barrel proteins are a unique species of evolutionarily conserved membrane proteins that are exclusively found in the outer membranes of mitochondria and chloroplasts and of gram-negative bacteria. All β-barrel proteins in mitochondria are encoded by the nuclear genome and are transported through the outer membrane by the TOM40 complex [40].

After passage through the TOM40 complex, the soluble small Tim chaperone complexes in the IMS guide the β-barrel proteins to the SAM/TOB complex in the outer membrane [41,42]. The central essential subunit of the SAM/TOB complex is Sam50 (Tob55, Omp85), which is a β-barrel protein itself and is related to BamA of the bacterial β-barrel assembly machinery [43-45]. In the SAM/TOB complex, Sam50 acts together with

another essential subunit Sam35 (Tob38, Tom38) and two other subunits Sam37 (Mas37, Tom37) and Mdm10. The two peripheral subunits Sam35 and Sam37 and the polypeptide transport associated domain (POTRA) of Sam50 help to recognize incoming precursors and to release folded β-barrel proteins into the lipid phase [40,46-50]. Mdm10 is specifically required for the assembly of Tom40, where Mdm10 in the presence of Tom7 contributes to a role in discharge of Tom40 from the SAM/TOB complex [51]. In addition to its localization at the SAM/TOB complex, Mdm10 also forms a complex with Tom7 and is also a crucial subunit of the ER (endoplasmic reticulum)-mitochondria encounter structure (ERMES), which tethers the membrane of the ER to the outer mitochondrial membrane [52-54]. In the ERMES complex, the mitochondrial outer membrane proteins Mdm10 and Gem1 are connected with the help of Mdm12 and Mdm34 to the integral ER membrane protein Mmm1 [55-57]. In addition, the ERMES complex was proposed to facilitate ER-mitochondria lipid transport, which is crucial for mitochondrial biogenesis as well [55,58-59].

The SAM/TOB complex also physically interacts with the mitochondrial inner membrane organization system (MINOS, MICOS, MitOS), which is required for the maintenance of the mitochondrial cristae architecture [60-63]. In order to build cristae junctions, the inner boundary membrane must be connected to the outer membrane. This connection is mediated by the inner membrane protein Fcj1 (mitofilin), which facilitates the formation of cristae junctions [64, 65].

1.3.3. The MIA pathway

Numerous proteins in the IMS with masses smaller than 20 kDa carry characteristic conserved cysteine motifs that are required for binding to cofactors, for example metal ions. These proteins are equipped with internal mitochondrial targeting information and go

through the TOM40 complex into the IMS with the help of the Tim40/Mia40 (mitochondrial intermembrane space import and assembly) [66,67] and its mode of action differs significantly from the typical import pathways into mitochondria. Perhaps the most exclusive feature of this pathway compared with other mitochondrial import pathways and also other cellular translocation systems is the use of cysteine chemistry to stabilize translocation intermediates and mature folded proteins *via* disulfide bonds. Disulfide bond formation by Tim40/Mia40 leads to trapping of proteins in the IMS of mitochondria. Tim40/Mia40 contains six conserved cysteine residues and mediates oxidative folding of substrate proteins by forming a mixed-disulfide [68-70]. Like Tim40/Mia40, a sulfhydryl oxidase Erv1 (essential for respiration and viability 1) is an essential IMS protein for yeast cell viability and is involved in mitochondrial disulfide bond formation with Tim40/Mia40 [68,71]. Tim40/Mia40 is reoxidized by Erv1, which passes the electrons over cytochrome *c* to the respiratory chain [68,71]. In addition to Tim40/Mia40 and Erv1, another IMS protein known as Hot13, with similarity to zinc-finger proteins, was suggested to play a role in the biogenesis of IMS proteins. The precise function of this protein in the biogenesis of IMS proteins is not clear yet. However, it is plausible at this point that further regulatory proteins can also be involved in the MIA pathway.

1.3.4. The TIM22 complex

Carrier proteins with internal targeting information are guided to the TIM22 translocase by the small Tim complexes, i.e. soluble, hexameric chaperone complexes Tim9-Tim10 and/or Tim8-Tim13 [72-74]. The translocase TIM22 complex consists of the integral membrane proteins Tim22, Tim54, and Tim18, and docking of small Tim complexes to the TIM22 complex mediated by Tim12 passes the carrier substrate to the TIM22

complex [75-77]. Tim22 is a channel-forming protein with sequence homologies to Tim23 and Tim17 [78]. It forms a twin pore, whose gating is dependent on $\Delta\psi$ (the membrane potential across the inner membrane) and on the binding of the precursor substrate [79-81]. Tim54 could exert a similar function as Tim50 in regulating the Tim23 pore, whereas Tim18 acts in the TIM22 complex assembly [76, 82].

1.3.5. The TIM23 complex

The majority of mitochondrial precursor proteins in yeast carry N-terminal, cleavable presequences that govern targeting and sorting of these proteins to the mitochondrial inner membrane or matrix [83]. After translocation through the TOM40 complex, the incoming precursors with N-terminal targeting sequences are handed over to the presequence translocase of the inner membrane (the TIM23 complex). The TIM23 complex consists of three essential membrane-integrated core components Tim23, Tim17 and Tim50, and multiple peripheral subunits. Tim23 consists of four transmembrane helices and an N-terminal domain in the IMS and partly in the outer membrane and is thought to be the channel forming component of the TIM23 complex [84]. Furthermore, the N-terminal IMS domain of Tim23 associates with the IMS domain of Tim50 through coiled-coil interactions [85,86], and this association is essential for guiding the precursors protein through the Tim23 channel [85]. Tim17, a homolog of Tim23, was demonstrated to play a multi-functional role in the TIM23 complex. It is crucial for stabilization of the translocase complex and was suggested to act as a voltage sensor of the TIM23 complex [87]. Tim17 functions in lateral sorting into the inner membrane as well as in import of preproteins into the matrix [88].

Tim50 is a single membrane spanning protein and exposes a large C-terminal domain into the IMS. Crosslinking studies indicate that Tim50IMS is located in close

proximity to the Tom22 subunit of the TOM40 complex [32]. This spatial arrangement allows Tim50IMS to interact with precursor proteins at an early stage of import, when the bulk of the precursor protein in still inside the TOM40 complex [89-91]. Tim50IMS domain is involved in closing the Tim23 channel to preserve $\Delta\psi$ [92]. The crystal structure of the conserved core domain of Tim50IMS (residue 176-361) forms a monomer and consists of five α-helices and nine β- strands [93]. The crystal structure also shows the presence of an extended groove on the surface with negatively charged amino acid residues at the bottom that could accommodate an amphipathic α-helical peptide [93]. Adjacent to this groove, a β-hairpin that is crucial for the binding of Tim50IMS to Tim23IMS protrudes from the surface of the molecule [93]. Recently, two distinct presequence binding sites within yeast Tim50IMS have been proposed: one in the conserved core domain and the other in the C-terminal region [93,94]. Furthermore the IMS domain of Tim23 is responsible for binding and handover of incoming precursors from Tim50IMS [86,95-97]. The fourth subunit, Tim21 may possess a unique regulatory role in promoting a transient coupling of the TIM23 complex with the respiratory chain complexes III and IV [98-100]. Altogether, the Tim23/Tim50 receptor module is engaged in multiple interactions with an incoming precursor protein, which cooperatively functions to mediate efficient transfer of the precursor protein from the outer mitochondrial membrane to the protein-conducting channel of the inner membrane.

From the energetic perspective, complete transfer of precursor proteins from the TOM40 complex to the TIM23 complex and the initiation of preprotein translocation across the inner membrane are driven by $\Delta\psi$, which also triggers opening of the TIM23 protein-conducting channel and exerts an electrophoretic force on the positively charged presequence [101,102]. For the complete translocation of preproteins into the matrix,

mtHsp70 and the energy derived from ATP hydrolysis in the mitochondrial matrix is required.

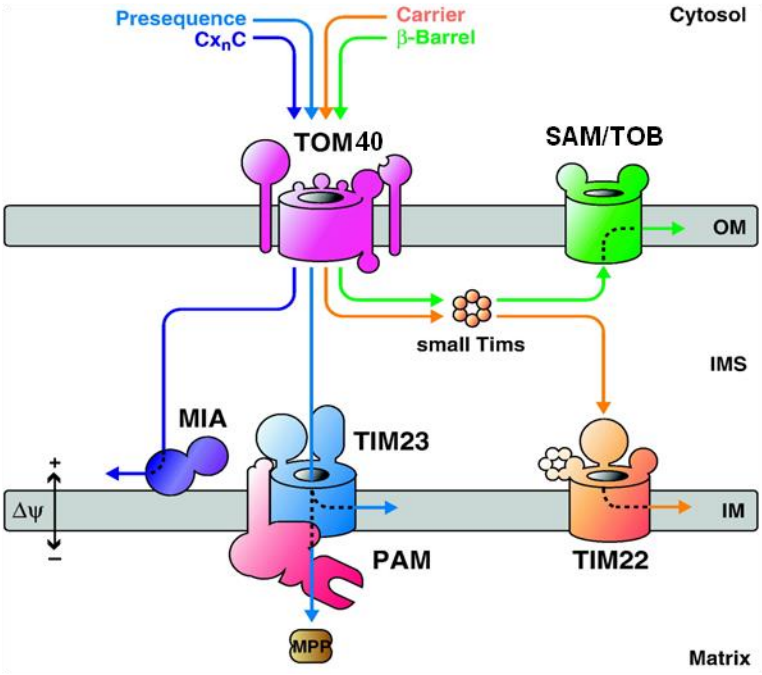

Figure 1.2.1. Mitochondrial translocation map for different targeting signals [103]
Various mitochondrial targeting signals target proteins for mitochondrial import. Biogenesis of β-barrel proteins of the outer membrane (OM) requires the small Tim chaperones of the IMS and the sorting and assembly machinery (SAM). Proteins of the IMS that contain cysteine-rich signals (CxnC) are imported via the mitochondrial intermembrane space import and assembly (MIA) pathway. Carrier proteins of the inner membrane (IM) are transported with the help of the small Tims and the translocase of the inner membrane 22 (the TIM22 complex). Presequence containing proteins are inserted into the inner membrane or imported into the matrix by the translocase of the inner membrane 23 (the TIM23 complex; presequence translocase). Matrix translocation requires the activity of the presequence translocase-associated import motor (PAM). Presequences are proteolytically removed by the matrix processing peptidase (MPP) upon import. Δψ, membrane potential across the inner mitochondrial membrane.

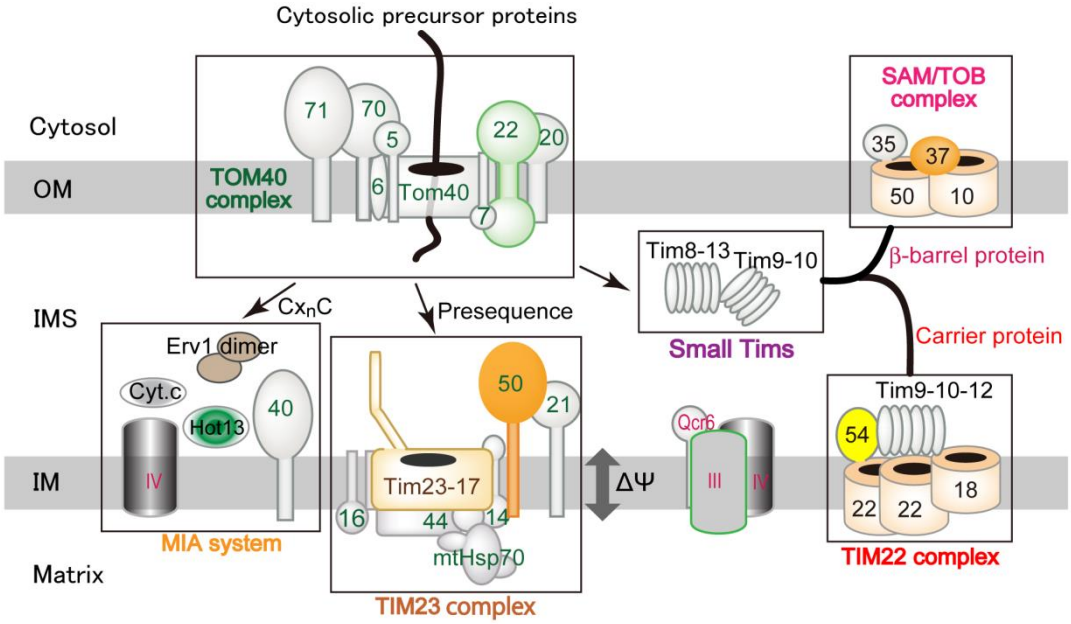

Figure 1.3.1. Mitochondrial protein import pathways and translocators.

Cytosolic precursor proteins are transported via specialized import machineries into mitochondria. The translocase of the outer membrane 40 (TOM40) facilitates transport across the outer membrane. Subsequently the translocases of the inner membrane (TIM23, TIM22), the sorting and assembly machinery (SAM) or the mitochondrial inter membrane space assembly machinery (MIA) are required for transport to the respective submitochondrial destination and maturation of the protein. TOM40 complex (20, Tom20; 22, Tom22; 7, Tom7; 71, Tom71; 70, Tom70; 6, Tom6; 5, Tom5); TOB/SAM complex (50, Sam50/Tob55; 35, Sam35/Tob38; 37, Sam37/Mas37/Tom37); MIA system (Cyt. c, cytochrome c; IV, the respiratory chain complex IV); TIM23 complex (50, Tim50; 23, Tim23; 17, Tim17; 21, Tim21; 14, Tim14; 44, Tim44; 16, Tim16;); TIM22 complex (54, Tim54; 22, Tim22; 18, Tim18); III, the respiratory chain complex III.

1.4. General objective

The majority of mitochondrial precursor proteins in yeast carry N-terminal, cleavable presequences that govern targeting and sorting of these proteins to the mitochondrial matrix or inner membrane using the TOM40-TIM23 pathway (Figure1.4.1). The presequence-containing precursor proteins pass through the import channel of Tom40 to reach the presequence binding site on the IMS side of the TOM40 complex and are subsequently handed over from the TOM40 complex to the TIM23 complex; presequences are then received by Tim50 of the TIM23 complex and transferred to the import channel of Tim23. Tim50 was found to have two presequence binding sites, one in the C-terminal PBD (presequence binding domain) and the second in the conserved core domain. However, how Tim50 recognizes the presequence and how it regulates the protein transport process are not clear at the moment.

PBD, which is conserved only among fungal Tim50, is in a close proximity to another presequence receptor Tim50IMS-core, which may reflect a mechanism that cooperatively directs the mitochondrial presequence for translocation. So I decided to probe how the presequence is recognized by PBD, and how PBD and Tim50core functions cooperatively to mediate efficient transfer of the presequence to the Tim23 channel.

Two experimental methods, NMR and X-ray crystallography, can provide an insight into the comprehensive understanding of the presequence-receptor interactions as well as their dynamics at a molecular level. In particular, NMR has evolved as a powerful tool in identification of presequence-receptor binding and offers some key advantages over other techniques. Although NMR can never compete with X-ray crystallography in the pace of structure determination, NMR can provide insights into the dynamics of the molecules, their folding/unfolding as well as the effects of interactions with binding partners including competitive binding on these processes. Besides, NMR studied in solution gives the

opportunity to vary a wide range of conditions that are closer to the physiological ones (like pH, temperature and different solvents etc). Furthermore, NMR can detect weak protein-protein or protein-nucleic acid or protein-peptide interactions, which are more difficult to analyze through crystallization followed by X-ray analyses, and enables the determination of binding constants. In addition to gaining information on whether a receptor protein is interacting with the presequence peptide or not, mechanistic insights of their binding and structural information can be obtained by NMR for both the receptor protein and the presequence peptide. The above quotation refers to this fact and highlights the distinctive position of NMR analyses on understanding of the mitochondrial presequence-receptor interaction mechanisms, of which I have tried to show in this thesis.

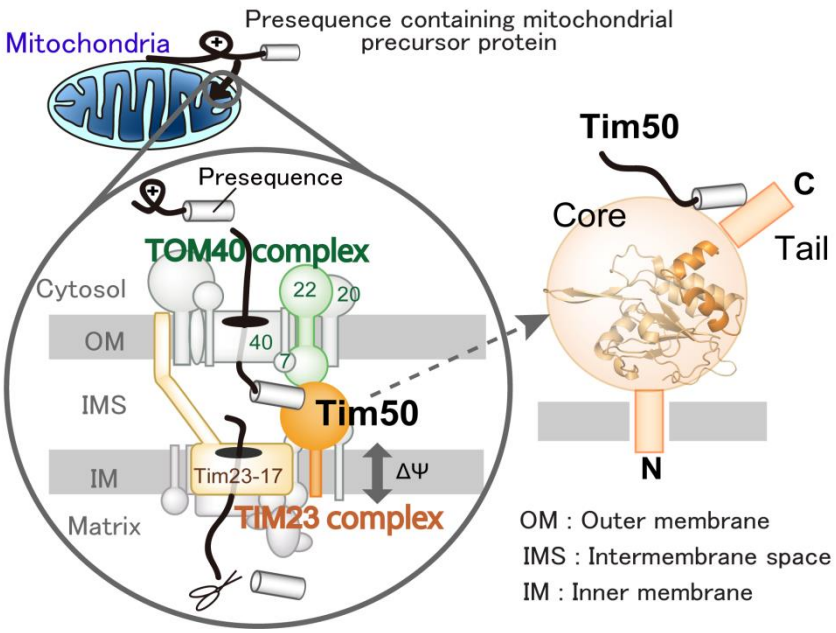

Figure 1.4.1. Presequence containing mitochondrial precursor protein pathway to matrix through TOM40-TIM23 complexes

1.5. References

1. Sickmann, A., Reinders, J., Wagner, Y., Joppich, C., Zahedi, R., Meyer, H. E., Schönfisch, B., Perschil, I., Chacinska, A., Guiard, B., Rehling, P., Pfanner, N. and Meisinger, C. (2003) The proteome of Saccharomyces cerevisiae mitochondria. Proc. Natl. Acad. Sci. USA 100, 13207–13212.
2. Reinders, J., Zahedi, R., Pfanner, N., Meisinger, C. and Sickmann, A. (2006) Toward the complete yeast mitochondrial proteome: multidimensional separation techniques for mitochondrial proteomics. J. Proteome Res. 5, 1543–1554.
3. Pagliarini, D.J., et al. (2008) A mitochondrial protein compendium elucidates complex I disease biology. Cell 134, 112–123.
4. Neupert, W. (1997) Protein import into mitochondria. Annu. Rev. Biochem. 66, 863–917.
5. Paschen, S.A. and Neupert, W. (2001) Protein import into mitochondria. IUBMB Life 52, 101–112.
6. Pfanner, N. and Wiedemann, N. (2002) Mitochondrial protein import: two membranes, three translocases. Curr. Opin. Cell Biol. 14, 400–411.
7. Truscott, K.N., Brandner, K. and Pfanner N. (2003) Mechanisms of protein import into mitochondria. Curr. Biol. 13, R326–R337.
8. Wiedemann, N., Frazier, A.E. and Pfanner, N. (2004) The protein import machinery of mitochondria. J. Biol. Chem. 279, 14473–14476.
9. Baker, M.J., Frazier, A.E., Gulbis, J.M. and Ryan, M.T. (2007) Mitochondrial protein-import machinery: correlating structure with function. Trends Cell Biol. 17, 456–464.
10. Neupert, W. and Herrmann, J.M. (2007) Translocation of proteins into mitochondria. Annu. Rev. Biochem. 76, 723–749.
11. Bolender, N., Sickmann, A., Wagner, R., Meisinger, C. and Pfanner, N. (2008) Multiple pathways for sorting mitochondrial precursor proteins. EMBO Rep. 9, 42–49.
12. Chacinska, A., Koehler, C.M., Milenkovic, D., Lithgow, T. and Pfanner, N. (2009) Importing mitochondrial proteins: machineries and mechanisms, Cell 138, 628–644.
13. Schmidt, O., Pfanner, N. and Meisinger C. (2010) Mitochondrial protein import: from proteomics to functional mechanisms. Nat. Rev. Mol. Cell Biol. 11, 655–667.
14. Becker, T., Böttinger, L. and Pfanner N. (2012) Mitochondrial protein import: from transport pathways to an integrated network. Trends Biochem. Sci. 37, 85–91.

15. Vögtle, F.-N., Wortelkamp, S., Zahedi, R.P., Becker, D., Leidhold, C., Gevaert, K., Kellermann, J., Voos, W., Sickmann, A., Pfanner, N. and Meisinger, C. (2009) Global analysis of the mitochondrial N-proteome identifies a processing peptidase critical for protein stability. Cell 139, 428–439.
16. Taylor, A., Smith, B., Kitada, S., Kojima, K., Miyaura, H., Otwinowski, Z., Ito, A. and J. Deisenhofer, J. (2001) Crystal structures of mitochondrial processing peptidase reveal the mode for specific cleavage of import signal sequences. Structure 9, 615–625.
17. Mossmann, D., Meisinger, C. and Vögtle, F.-N. (2012) Processing of mitochondrial presequences. Biochim. Biophys. Acta. 1819, 1098-106.
18. Beddoe, T. and Lithgow T. (2002) Delivery of nascent polypeptides to the mitochondrial surface. Biochim. Biophys. Acta 1592, 35–39.
19. Wiedemann, N., Kozjak, V., Chacinska, A., Schönfisch, B., Rospert, S., Ryan, M.T., Pfanner, N. and Meisinger, C. (2003) Machinery for protein sorting and assembly in the mitochondrial outer membrane. Nature 424, 565–571.
20. Mesecke, N., Terziyska, N., Kozany, C., Baumann, F., Neupert, W., Hell, K. and Herrmann, J.M. (2005) A disulfide relay system in the intermembrane space of mitochondria that mediates protein import. Cell 121, 1059–1069.
21. Hill, K., Model, K., Ryan, M.T., Dietmeier, K., Martin, F., Wagner, R. and Pfanner, N. (1998) Tom40 forms the hydrophilic channel of the mitochondrial import pore for preproteins. Nature 395, 516–521.
22. Künkele, K.P., Heins, S., Dembowski, M., Nargang, F.E., Benz, R., Thieffry, M., Walz, J., Lill, R., Nussberger, S. and Neupert W. (1998) The preprotein translocation channel of the outer membrane of mitochondria. Cell 93, 1009–1019.
23. Model, K., Meisinger, C. and Kühlbrandt, W. (2008) Cryo-electron microscopy structure of a yeast mitochondrial preprotein translocase. J. Mol. Biol. 383, 1049–1057.
24. Abe, Y., Shodai, T., Muto, T., Mihara, K., Torii, H., Nishikawa, S., Endo, T. and Kohda, D. (2000) Structural basis of presequence recognition by the mitochondrial protein import receptor Tom20. Cell 100, 551–560.
25. Saitoh, T., Igura, M., Obita, T., Ose, T., Kojima, R., Maenaka, K., Endo, T. and Kohda, D. (2007) Tom20 recognizes mitochondrial presequences through dynamic equilibrium among multiple boand states. EMBO J. 26 , 4777–4787.
26. Young, J.C., Hoogenraad, N.J. and Hartl, F.U. (2003) Molecular chaperones Hsp90 and

Hsp70 deliver preproteins to the mitochondrial import receptor Tom70. Cell 112, 41–50.

27. Wu, Y. and Sha B. (2006) Crystal structure of yeast mitochondrial outer membrane translocon member Tom70p. Nat. Struct. Mol. Biol. 13, 589–593.
28. Chan, N.C., Likić, V.A., Waller, R.F., Mulhern, T.D. and Lithgow T. (2006) The C-terminal TPR domain of Tom70 defines a family of mitochondrial protein import. J. Mol. Bio. 358. 1010-1022.
29. Moczko, M., Bömer, U., Kübrich, M., Zufall, N., Hönlinger, A. and Pfanner, N. (1997) The intermembrane space domain of mitochondrial Tom22 functions as a trans binding site for preproteins with N-terminal targeting sequences. Mol. Cell. Biol. 17, 6574–6584.
30. Komiya, T., Rospert, S., Koehler, C., Looser, R., Schatz, G. and Mihara, K. (1998) Interaction of mitochondrial targeting signals with acidic receptor domains along the protein import pathway: evidence for the 'acid chain' hypothesis. EMBO J. 17, 3886–3898.
31. van Wilpe, S., Ryan, M.T., Hill, K., Maarse, A.C., Meisinger, C., Brix, J., Dekker, P.J., Moczko, M., Wagner, R., Meijer, M., Guiard, B., Hönlinger, A. and Pfanner N. (1999) Tom22 is a multifunctional organizer of the mitochondrial preprotein translocase. Nature 401, 485–489.
32. Shiota, T., Mabuchi, H., Tanaka-Yamano, S., Yamano, K. and Endo, T. (2011) In vivo protein-interaction mapping of a mitochondrial translocator protein Tom22 at work. Proc. Natl. Acad. Sci. USA. 108, 15179–15183.
33. Kassenbrock, C.K., Cao, W. and Douglas, M.G. (1993) Genetic and biochemical characterization of ISP6, a small mitochondrial outer membrane protein associated with the protein translocation complex. EMBO J. 12, 3023–3034.
34. Hönlinger, A., Bömer, U., Alconada, A., Eckerskorn, C., Lottspeich, F., Dietmeier, K. and Pfanner, N. (1996) Tom7 modulates the dynamics of the mitochondrial outer membrane translocase and plays a pathway-related role in protein import. EMBO J. 15, 2125–2137.
35. Dietmeier, K., Hönlinger, A., Bömer, U., Dekker, P.J., Eckerskorn, C., Lottspeich, F., Kübrich, M. and Pfanner, N. (1997) Tom5 functionally links mitochondrial preprotein receptors to the general import pore. Nature 388, 195–200.
36. Kanamori, T., Nishikawa, S., Nakai, M., Shin, I., Schultz, P.G. and Endo, T. (1997) Uncoupling of transfer of the presequence and unfolding of the mature domain in precursor translocation across the mitochondrial outer membrane. Proc. Natl. Acad. Sci. USA 96, 634–3639.

37. Esaki, M., Shimizu, H., Ono, T., Yamamoto, H., Kanamori, T., Nishikawa, S.-I. and Endo, T. (2004) Mitochondrial protein import. Requirement of presequence elements and tom components for precursor binding to the TOM complex. J. Biol. Chem. 279, 45701–45707.
38. Dekker, P.J., Martin, F., Maarse, A.C., Bömer, U., Müller, H., Guiard, B., Meijer, M., Rassow, J. and Pfanner, N. (1997) The Tim core complex defines the number of mitochondrial translocation contact sites and can hold arrested preproteins in the absence of matrix Hsp70-Tim44. EMBO J. 16, 5408–5419.
39. Chacinska, A., Rehling, P., Guiard, B., Frazier, A.E., Schulze-Specking, A., Pfanner, N., Voos, W. and Meisinger, C. (2003) Mitochondrial translocation contact sites: separation of dynamic and stabilizing elements in formation of a TOM–TIM–preprotein supercomplex. EMBO J. 22, 5370–5381.
40. Wiedemann, N., Kozjak, V., Chacinska, A., Schönfisch, B., Rospert, S., Ryan, M.T., Pfanner, N. and Meisinger, C. (2003) Machinery for protein sorting and assembly in the mitochondrial outer membrane. Nature 424, 565–571.
41. Hoppins, S.C. and Nargang, F.E. (2004) The Tim8–Tim13 complex of Neurospora crassa functions in the assembly of proteins into both mitochondrial membranes. J. Biol. Chem. 279, 12396–12405.
42. Wiedemann, N., Truscott, K.N., Pfannschmidt, S., Guiard, B., Meisinger, C. and Pfanner, N. (2004) Biogenesis of the protein import channel Tom40 of the mitochondrial outer membrane: intermembrane space components are involved in an early stage of the assembly pathway. J. Biol. Chem. 279, 18188–18194.
43. Kozjak, V., Wiedemann, N., Milenkovic, D., Lohaus, C., Meyer, H.E., Guiard, B., Meisinger, C. and Pfanner, N. (2003) An essential role of Sam50 in the protein sorting and assembly machinery of the mitochondrial outer membrane. J. Biol. Chem. 278, 48520–48523.
44. Paschen, S.A., Waizenegger, T., Stan, T., Preuss, M., Cyrklaff, M., Hell, K., Rapaport, D. and Neupert, W. (2003) Evolutionary conservation of biogenesis of beta-barrel membrane proteins. Nature 426, 862–866.
45. Gentle, I., Gabriel, K., Beech, P., Waller, R. and Lithgow, T. (2004) The Omp85 family of proteins is essential for outer membrane biogenesis in mitochondria and bacteria. J. Cell Biol. 164, 19–24.
46. Milenkovic, D., Kozjak, V., Wiedemann, N., Lohaus, C., Meyer, H.E., Guiard, B., Pfanner, N. and Meisinger, C. (2004) Sam35 of the mitochondrial protein sorting and assembly

machinery is a peripheral outer membrane protein essential for cell viability. J. Biol. Chem. 279, 22781–22785.

47. Ishikawa, D., Yamamoto, H., Tamura, Y. Moritoh, K. and Endo, T. (2004) Two novel proteins in the mitochondrial outer membrane mediate beta-barrel protein assembly. J. Cell Biol. 166, 621–627.
48. Waizenegger, T., Habib, S.J., Lech, M., Mokranjac, D., Paschen, S.A., Hell, K., Neupert, W. and Rapaport, D. (2004) Tob38, a novel essential component in the biogenesis of β-barrel proteins of mitochondria. EMBO Rep. 5, 704–709.
49. Chan, N.C. and Lithgow, T. (2008) The peripheral membrane subunits of the SAM complex function codependently in mitochondrial outer membrane biogenesis. Mol. Biol. Cell 19, 126–136.
50. Stroud, D.A., Becker, T., Qiu, J., Stojanovski, D., Pfannschmidt, S., Wirth, C., Hunte, C., Guiard, B., Meisinger, C., Pfanner, N. and Wiedemann, N. (2011) Biogenesis of mitochondrial β-barrel proteins: the POTRA domain is involved in precursor release from the SAM complex. Mol. Biol. Cell 22, 2823–2833.
51. Yamano, K., Tanaka-Yamano, S. and Endo, T. (2010) Mdm10 as a dynamic constituent of the TOB/SAM complex directs coordinated assembly of Tom40. EMBO Rep. 11, 187–193.
52. Meisinger, C., Wiedemann, N., Rissler, M., Strub, A., Milenkovic, D., Schönfisch, B., Müller, H., Kozjak, V. and Pfanner, N. (2006) Mitochondrial protein sorting: differentiation of beta-barrel assembly by Tom7-mediated segregation of Mdm10. J. Biol. Chem. 281, 22819–22826.
53. Yamano, K., Tanaka-Yamano, S. and Endo, T. (2010) Tom7 regulates Mdm10-mediated assembly of the mitochondrial import channel protein Tom40. J. Biol. Chem. 285, 41222–41231.
54. Becker, T., Wenz, L.S., Thornton, N., Stroud, D., Meisinger, C., Wiedemann, N. and Pfanner, N. (2011) Biogenesis of mitochondria: dual role of Tom7 in modulating assembly of the preprotein translocase of the outermembrane. J. Mol. Biol. 405, 113–124.
55. Kornmann, B., Currie, E., Collins, S.R., Schuldiner, M., Nunnari, J., Weissman, J.S. and Walter, P. (2009) An ER–mitochondria tethering complex revealed by a synthetic biology screen. Science 325, 477–481.
56. Kornmann, B. and Walter, P. (2010) ERMES-mediated ER–mitochondria contacts: molecular hubs for the regulation of mitochondrial biology. J. Cell Sci. 123, 1389–1393.

57. Stroud, D.A., Oeljeklaus, S., Wiese, S., Bohnert, M., Lewandrowski, U., Sickmann, A., Guiard, B., van der Laan, M., Warscheid, B. and Wiedemann, N. (2011) Composition and topology of the endoplasmic reticulum–mitochondria encounter structure. J. Mol. Biol. 413, 743–750.
58. Nguyen, T.T., Lewandowska, A., Choi, J.-Y., Markgraf, D.F., Junker, M., Bilgin, M., Ejsing, C.S., Voelker, D.R., Rapoport, T.A. and Shaw, J.M. (2012) Gem1 and ERMES do not directly affect phosphatidylserine transport from ER to mitochondria or mitochondrial inheritance. Traffic 13, 880–890.
59. Voss, C., Lahiri, S., Young, B.P., Loewen, C.J. and Prinz, W.A. (2012) ER-shaping proteins facilitate lipid exchange between the ER and mitochondria in *S. cerevisiae*. J. Cell Sci. 125, 4791–4799.
60. von der Malsburg, K. et al. (2011) Dual role of mitofilin in mitochondrial membrane organization and protein biogenesis. Dev. Cell 21, 694–707.
61. Hoppins, S., Collins, S.R., Cassidy-Stone, A., Hummel, E., Devay, R.M., Lackner, L.L., Westermann, B., Schuldiner, M., Weissman, J.S. and Nunnari, J. (2011) A mitochondrial-focused genetic interaction map reveals a scaffold-like complex required for inner membrane organization in mitochondria. J. Cell Biol. 195, 323–340.
62. Harner, M., Körner, C., Walther, D., Mokranjac, D., Kaesmacher, J., Welsch, U., Griffith, J., Mann, M., Reggiori, F. and Neupert, W. (2011) Themitochondrial contact site complex, a determinant of mitochondrial architecture. EMBO J. 30, 4356–4370.
63. Alkhaja, A.K., Jans, D.C., Nikolov, M., Vukotic, M., Lytovchenko, O., Ludewig, F., Schliebs, W., Riedel, D., Urlaub, H., Jakobs, S. and Deckers, M. (2012) MINOS1 is a conserved component of mitofilin complexes and required for mitochondrial function and cristae organization. Mol. Biol. Cell 23, 247–257.
64. John, G.B., Shang, Y., Li, L., Renken, C., Mannella, C.A., Selker, J.M.L., Rangell, L., Bennett, M.J. and Zha, J. (2005) The mitochondrial inner membrane protein mitofilin controls cristae morphology. Mol. Biol. Cell 16, 1543–1554.
65. Rabl, R., Soubannier, V., Scholz, R., Vogel, F., Mendl, N., Vasiljev-Neumeyer, A., Körner, C., Jagasia, R., Keil, T., Baumeister, W., Cyrklaff, M., Neupert, W. and Reichert, A.S. (2009) Formation of cristae and crista junctions in mitochondria depends on antagonism between Fcj1 and Su e/g. J. Cell Biol. 185, 1047–1063.
66. Chacinska, A. et el. (2004) Essential role of Mia40 in import and assembly of mito-chondrial

intermembrane space proteins. EMBO J. 23 [19], 3735-3746.

67. Naoe, M.; Ohwa, Y.; Ishikawa, D.; Ohshima, C.; Nishikawa, S.; Yamamoto, H. and Endo, T. (2004) Identification of Tim40 that mediates protein sorting to the mitochondrial intermembrane space. J. Biol. Chem. 279 [46], 47815-47821.
68. Mesecke, N.; Terziyska, N.; Kozany, C.; Baumann, F.; Neupert, W.; Hell, K. and Herrmann, J. M. (2005) A disulfide relay system in the intermembrane space of mitochondria that mediates protein import. Cell 121 [7], 1059-1069.
69. Milenkovic, D.; Gabriel, K.; Guiard, B.; Schulze-Specking, A.; Pfanner, N. and Chacinska, A. (2007) Biogenesis of the essential Tim9-Tim10 chaperone complex of mitochondria: site-specific recognition of cysteine residues by the intermembrane space receptor Mia40. J. Biol. Chem. 282 [31], 22472-22480.
70. Sideris, D. P. and Tokatlidis, K. (2007) Oxidative folding of small Tims is mediated by site-specific docking onto Mia40 in the mitochondrial intermembrane space. Mol. Microbiol. 65 [5], 1360-1373.
71. Allen, S.; Balabanidou, V.; Sideris, D. P.; Lisowsky, T. and Tokatlidis, K. (2005) Erv1 mediates the Mia40-dependent protein import pathway and provides a functional link to the respiratory chain by shuttling electrons to cytochrome c. J. Mol. Biol. 353 [5], 937-944.
72. Davis, A. J.; Alder, N. N.; Jensen, R. E. and Johnson, A. E. (2007) The Tim9p/10p and Tim8p/13p complexes bind to specific sites on Tim23p during mitochondrial protein import. Mol. Biol. Cell 18 [2], 475-486.
73. Vial, S.; Lu, H.; Allen, S.; Savory, P.; Thornton, D.; Sheehan, J. and Tokatlidis, K. (2002) Assembly of Tim9 and Tim10 into a functional chaperone. J. Biol. Chem. 277 [39], 36100-36108.
74. Webb, C. T.; Gorman, M. A.; Lazarou, M.; Ryan, M. T. and Gulbis, J. M. (2006) Crystal structure of the mitochon-drial chaperone TIM9.10 reveals a six-bladed alpha-propeller. Mol. Cell 21 [1], 123-133.
75. Gebert, N.; Chacinska, A.; Wagner, K.; Guiard, B.; Koehler, C. M.; Rehling, P.; Pfanner, N. and Wiedemann, N. (2008) Assembly of the three small Tim proteins precedes docking to the mitochondrial carrier translocase. EMBO Rep. 9 [6], 548-554.
76. Kerscher, O.; Holder, J.; Srinivasan, M.; Leung, R. S. and Jensen, R. E. (1997) The Tim54p-Tim22p complex medi-ates insertion of proteins into the mitochondrial inner membrane. J. Cell Biol. 139 [7], 1663-1675

77. Koehler, C. M.; Murphy, M. P.; Bally, N. A.; Leuenberger, D.; Oppliger, W.; Dolfini, L.; Junne, T.; Schatz, G. and Or, E. (2000) Tim18p, a new subunit of the TIM22 complex that mediates insertion of imported proteins into the yeast mitochondrial inner membrane. Mol. Cell Biol. 20 [4], 1187-1193.
78. Sirrenberg, C.; Bauer, M. F.; Guiard, B.; Neupert, W. and Brunner, M. (1996) Import of carrier proteins into the mitochondrial inner membrane mediated by Tim22. Nature 384 [6609], 582-585.
79. Kovermann, P.; Truscott, K. N.; Guiard, B.; Rehling, P.; Sepuri, N. B.; Muller, H.; Jensen, R. E.; Wagner, R. and Pfanner, N. (2002) Tim22, the essential core of the mitochondrial protein insertion complex, forms a voltage-activated and signal-gated channel. Mol. Cell 9 [2], 363-373.
80. Peixoto, P. M.; Grana, F.; Roy, T. J.; Dunn, C. D.; Flores, M.; Jensen, R. E. and Campo, M. L. (2007) Awaking TIM22, a dynamic ligand-gated channel for protein insertion in the mitochondrial inner membrane. J. Biol. Chem. 282 [26], 18694-18701.
81. Rehling, P.; Model, K.; Brandner, K.; Kovermann, P.; Sickmann, A.; Meyer, H. E.; Kuhlbrandt, W.; Wagner, R.; Trus-cott, K. N. and Pfanner, N. (2003) Protein insertion into the mitochondrial inner membrane by a twin-pore translocase. Science 299 [5613], 1747-1751.
82. Wagner, K.; Gebert, N.; Guiard, B.; Brandner, K.; Truscott, K. N.; Wiedemann, N.; Pfanner, N. and Rehling, P. (2008) The assembly pathway of the mitochondrial carrier translocase involves four preprotein translocases. Mol. Cell Biol. 28 [13], 4251-4260.
83. F.-N. Vögtle, S. Wortelkamp, R.P. Zahedi, D. Becker, C. Leidhold, K. Gevaert, J. Kellermann, W. Voos, A. Sickmann, N. Pfanner, C. Meisinger, Global analysis of the mitochondrial N-proteome identifies a processing peptidase critical for protein stability, Cell 139 (2009) 428–439.
84. Truscott, K.N., Kovermann, P., Geissler, A., Merlin, A., Meijer, M., Driessen, A.J., Rassow, J., Pfanner, N. and Wagner, R. (2001) A presequence- and voltage-sensitive channel of the mitochondrial preprotein translocase formed by Tim23. Nat. Struct. Biol. 8, 1074–1082.
85. Tamura, Y., Harada, Y., Shiota, T., Yamano, K., Watanabe, K., Yokota, M., Yamamoto, H., Sesaki, H. and Endo, T. (2009) Tim23–Tim50 pair coordinates functions of translocators and motor proteins in mitochondrial protein import. J. Cell Biol. 184, 129–141.
86. Mokranjac, D., Sichting, M., Popov-Čeleketić, D., Mapa, K., Gevorkyan-Airapetov, L., Zohary, K., Hell, K., Azem, A. and Neupert, W. (2009) Role of Tim50 in the transfer of precursor

proteins from the outer to the inner membrane in mitochondria. Mol. Biol. Cell 20, 1400–1407.

87. Martinez-Caballero, S., Grigoriev, S.M., Herrmann, J.M., Campo, M.L. and Kinnally, K.W. (2007) Tim17p regulates the twin pore structure and voltage gating of the mitochondrial protein import complex TIM23. J. Biol. Chem. 282, 3584–3593.
88. Chacinska, A., Lind, M., Frazier, A.E., Dudek, J., Meisinger, C., Geissler, A., Sickmann, A., Meyer, H.E., Truscott, K.N., Guiard, B., Pfanner, N. and Rehling, P. (2005) Mitochondrial presequence translocase: switching between TOM tethering and motor recruitment involves Tim21 and Tim17. Cell 120, 817–829.
89. Geissler, A., Chacinska, A., Truscott, K.N., Wiedemann, N., Brandner, K., Sickmann, A., Meyer, H.E., Meisinger, C., Pfanner, N. and Rehling, P. (2002) The mitochondrial presequence translocase: an essential role of Tim50 in directing preproteins to the import channel. Cell 111, 507–518.
90. Yamamoto, H., Esaki, M., Kanamori, T., Tamura, Y., Nishikawa, S. and Endo, T. (2002) Tim50 is a subunit of the TIM23 complex that links protein translocation across the outer and inner mitochondrial membranes. Cell 111, 519–528.
91. Mokranjac, D., Paschen, S.A., Kozany, C., Prokisch, H., Hoppins, S.C., Nargang, F.E., Neupert, W. and Hell, K. (2003) Tim50, a novel component of the TIM23 preprotein translocase of mitochondria. EMBO J. 22, 816-825.
92. Meinecke, M., Wagner, R., Kovermann, P., Guiard, B., Mick, D.U., Hutu, D.P., Voos, W., Truscott, K.N., Chacinska, A., Pfanner, N. and Rehling, P. (2006) Tim50 maintains the permeability barrier of the mitochondrial inner membrane. Science 312, 1523–1526.
93. Qian, X., Gebert, M., Höpker, J., Yan, M., Li, J., Wiedemann, N., van der Laan, M., Pfanner, N. and Sha, B. (2011) Structural basis for the function of Tim50 in the mitochondrial presequence translocase. J. Mol. Biol. 411, 513–519.
94. Schulz, C., Lytovchenko, O., Melin, J., Chacinska, A., Guiard, B., Neumann, P., Ficner, R., Jahn, O., Schmidt, B. and Rehling, P. (2011) Tim50's presequence receptor domain is essential for signal driven transport across the TIM23 complex. J. Cell Biol. 195, 643–656.
95. Bauer, M.F., Sirrenberg, C., Neupert, W. and Brunner, M. (1996) Role of Tim23 as voltage sensor and presequence receptor in protein import into mitochondria. Cell 87, 33–41.
96. de la Cruz, L., Bajaj, R., Becker, S. and Zweckstetter, M. (2010) The intermembrane space

domain of Tim23 is intrinsically disordered with a distinct binding region for presequences. Protein Sci. 19, 2045–2054.

97. Marom, M., Dayan, D., Demishtein-Zohary, K., Mokranjac, D., Neupert, W. and Azem A. (2011) Direct interaction of mitochondrial targeting presequences with purified components of the TIM23 complex. J. Biol. Chem. 286, 43809–43815.
98. van der Laan, M. Wiedemann, N., Mick, D.U., Guiard, B., Rehling, P. amd Pfanner, N. (2006) A role for Tim21 in membrane-potential-dependent preprotein sorting in mitochondria. Curr. Biol. 16, 2271–2276.
99. Wiedemann, N., van der Laan, M., Hutu, D.P., Rehling, P. and Pfanner, N. (2007) Sorting switch of mitochondrial presequence translocase involves coupling of motor module to respiratory chain. J. Cell Biol. 179, 1115–1122.
100. Dienhart, M.K. and Stuart, R.A. (2008) The yeast Aac2 protein exists in physical association with the cytochrome bc1-COX supercomplex and the TIM23 machinery. Mol. Biol. Cell 19, 3934–3943.
101. Truscott, K.N., Kovermann, P., Geissler, A., Merlin, A., Meijer, M., Driessen, A.J, Rassow, J., Pfanner, N. and Wagner, R. (2001) A presequence- and voltage-sensitive channel of the mitochondrial preprotein translocase formed by Tim23. Nat. Struct. Biol. 8, 1074–1082.
102. Martin, J., Mahlke, K. and Pfanner, N. (1991) Role of an energized inner membrane in mitochondrial protein import: Δψ drives the movement of presequences. J. Biol. Chem. 266, 18051–18057.
103. Dudek, J. *et al*. (2013) Mitochondrial protein import: Common principles and physiological networks. Biochimica et Biophysica Acta. 1833, 274–285.

Chapter 2

Mechanistic insights of the sPBD for presequence and Tim50core binding

2.1. Introduction

Mitochondria are essential organelles in eukaryotic cells and consist of two membranes, the outer and the inner membrane, and two aqueous compartments, the matrix and the intermembrane space (IMS). Mitochondria contain about 1000–1500 different proteins, most of which are encoded by nuclear genes and are consequently synthesized on cytosolic ribosome as precursor proteins and imported into mitochondria for their functioning. Precursor proteins need the presence of specific targeting signals for targeting to mitochondria through specific transport pathways and sorting to their final destination within different mitochondrial sub-compartments [1-5]. Most extensively studied mitochondrial targeting signals are the ones-encoded in N-terminal presequences and are characterized as an ability to form amphipathic α-helical segments that are rich in net positive charges [6]. Generally, N-terminal presequences are cleaved off after import into the matrix by processing peptidase, resulting in formation of the mature protein [7-9]. Import and subsequent intra-mitochondrial sorting of mitochondrial proteins are mediated by membrane-protein complexes called translocators in the outer (the TOM40 complex and TOB/SAM complex) and inner membranes (the TIM23 complex and TIM22 complex) and soluble factors in the cytosol, IMS, and matrix [1,2,10-13]. After translocation of precursors through the general entry gate formed by the TOM40 complex, several distinct downstream intra-mitochondrial sorting pathways can operate with the aid of other specific translocators. The targeting signal in a presequence is recognized by Tom20 and Tom22, receptor subunits of the outer membrane translocator TOM40 complex [9]. The presequence then pass through the import channel of Tom40 to reach the presequence binding site on the IMS side of the TOM40 complex and is subsequently handed over from the TOM40 complex to the TIM23 complex (Figure 2.1.1). Accumulated evidence suggests

that the presequence is received by Tim50 of the TIM23 complex and is transferred to the import channel of Tim23 in a manner dependent on the membrane potential (ΔΨ) across the inner membrane [1,2,9].

Tim50 plays a key role in the link of the translocation across the outer and inner membranes. Yeast Tim50 contains a N-terminal cleavable presequence (residues 1-43), a small matrix domain (residues 44-112), a transmembrane segment (residues 113-132) for anchoring to the inner membrane, and a large C-terminal domain exposed to the IMS (Tim50IMS: residues 133-476) [5-7, 14-16] (Figure 2.1.2). Tim50IMS contains a well-conserved domain (residues 159-362) followed by the C-terminal tail that is conserved only among fungal species (residues 363-476). Tim50IMS is located in close proximity to the Tom22 subunit of the TOM40 complex [17], which permits Tim50IMS to interact with precursors at an early stage of protein import [14-16]. A trypsin resistant core domain (IMS-core: residues 164-361) in the conserved IMS domain was subjected to crystallization, and its X-ray structure was reported [18]. The determined X-ray structure of residues 176-361 consists of 5 α-helices and 9 β-strands, and a negatively charged groove near the protruding β-hairpin was proposed to bind to a positively charged presequence [18]. Interestingly it was reported that not only the crystallized conserved core domain but also the C-terminal region, which is conserved among fungal species, can interact with presequences [19, 20]. Tim50 receptor is thus linked in multiple interactions with an incoming precursor, thereby mediating the transfer of the precursor proteins from the outer mitochondrial membrane to the protein-conducting channel of the inner membrane.

It is currently not clear how presequence peptides are recognized by Tim50 during protein import. Furthermore, little is known about the role of C-terminal region of Tim50 in the protein transport process. To gain a clear understanding of protein-peptide

interactions and their dynamics in the inner mitochondrial membrane at a molecular level, I analyzed here the minimal variant of presequence binding domain (PBD) of yeast Tim50 (400-450, sPBD) by NMR. The analyses show that sPBD is folded and recognizes the same sequence elements of a model presequence peptide, pSu9N (the N-terminal half of presequence of the precursor to subunit 9 of *Neurospora crassa* F_o-ATPase) [21] as that for binding to dTom20, the cytosolic receptor domain (residues 51-145) [12] of yeast Tom20. Two functionally distinct presequence-binding sites at N- and C-terminal parts of sPBD were mapped out and the interactions were found to be partly hydrophobic. Mutational analyses revealed that the N-terminal binding site of sPBD is more important for recognition of presequences. sPBD can also bind to the core domain of Tim50 (171-362, Tim50core) through the presequence binding region, which could promote transfer of the presequence from sPBD to the core domain in Tim50; binding of Tim50core to sPBD was found to result in partial formation of ternary complex in the presence of presequence. A possible scenario of presequence recognition by Tim50 in protein import will be discussed.

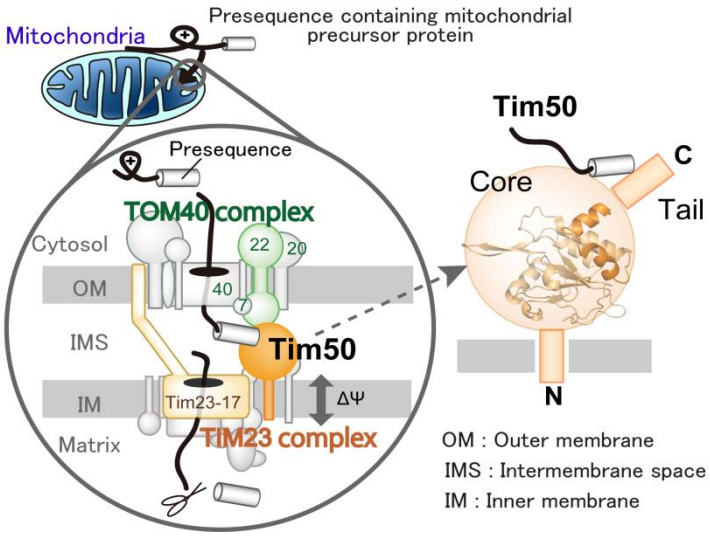

Figure 2.1.1. Presequence pathway to matrix through TOM40-TIM23 complexes

A

```
MLSILRNSVR LNSRALRVVP SAANTLTSVQ ASRRLLTSYS SFLQKETKDD   50
KPKSILTDDM LFKAGVDVDE KGQGKNEETS GEGGEDKNEP SSKSEKSRRK  100
RQTSTDIKRE KYANWFYIFS LSALTGTAIY MARDWEPQES EELKKDIDNG  150
YTLSLMYKRF KARFNSMFTY FQEPPFPDLL PPPPPPPYQR PLTLVITLED  200
FLVHSEWSQK HGWRTAKRPG ADYFLGYLSQ YYEIVLFSSN YMMYSDKIAE  250
KLDPIHAFVS YNLFKEHCVY KDGVHIKDLS KLNRDLSKVI IIDTDPNSYK  300
LQPENAIPME PWNGEADDKL VRLIPFLEYL ATQQTKDVRP ILNSFEDKKN  350
LAEEFDHRVK KLKDKFYGDH KSGGNWAMTA LGLGNSLGGS TKFPLDLIHE  400
EGQKNYLMFM KMIEEEKEKI RIQQEQMGGQ TFTLKDYVEG NLPSPEEQMK  450
IQLEKQKEVD ALFEEEKKKK KIAESK  476
```

B

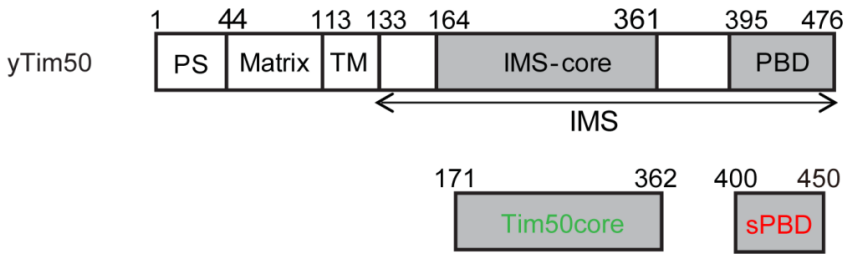

Figure 2.1.2. Yeast Tim50 (yTim50) and its segments

(A) Amino acid sequence of yeast Tim50

(B) Schematic representations of yeast Tim50 and its segments used in this study. PS, presequence; IM, inner membrane; IMS, intermembrane space; PBD, presequence binding domain; sPBD, shorter variant of presequence binding domain.

2.2. Materials and Methods

2.2.1. Amplification of DNA fragments by polymerase chain reaction (PCR)

PCR enables rapid and specific amplification of DNA fragments. A typical 25 µl reaction mix contained 2.5 µl supplied 10x PCR buffer, 2.5 µl dNTPs mix (each 10 mM), 1 µl each primer (10 µM), 0.5 µl of *Taq* polymerase and 1 µl of the genomic DNA library (W3031A).

A typical program for PCR cycler is given below:

PCR cycler			
1	94°C, 5 min		Inactivation of nucleases and denaturation of DNA template
2	30 cycles	94°C, 30 s	Denaturation
		50°C, 30 s	Primer annealing
		72°C, 2 min	Primer extension
3	72°C, 7 min		Final extension step
4	Cooling to 4°C		

The PCR product was analyzed by agarose gel electrophoresis to confirm that the target DNA fragments have been amplified successfully.

2.2.2. Gel-electrophoresis of DNA

Horizontal agarose gel electrophoresis was used for separation of DNA fragments according to their sizes. Agarose was prepared in TAE buffer (TRIS/EDTA/Glacial acetic acid), mixed with biothium and, while still hot, poured into precasted molds where it can

solidify. DNA-containing solution was mixed with 10x loading dye (50% (v/v) glycerol, 0.21% (w/v) bromphenol-blue, 0.21% (w/v) xylene Cyanol, 0.2 M EDTA, pH8.0) and loaded on an 1-1.5% (w/v) agarose gel, depending on the size of DNA fragments to be separated. Gels were run in TAE buffer at 100 V depending on the size. Separated DNA fragments were visualized under UV light.

2.2.3. Purification of PCR DNA product by GFX kit

For isolation and concentration of DNA fragments from PCR mixtures, the GFX kit (Healthcare) was used.

2.2.4. Cloning of DNA fragments into the vector by In-Fusion cloning kit

In-Fusion HD Cloning Kits were used for fast, directional cloning of one or more fragments of DNA into any vector. After purification by GFX kit, 1 µl of the DNA fragment was put into a 5 µl reaction mixture that contained 1 µl of vector solution, and 1 µl of In-Fusion HD enzyme premix. The reaction mixture was incubated for 15 min at 50°C, then placed on ice.

2.2.5. Transformation of *E. coli* with plasmid DNA

The prepared plasmids were introduced into competent *E. coli* cells. The strain used was XL2 Blue. Then the cells were placed and spreaded on LBAmp plates (LB with 2% (w/v) agar supplemented with 50 µg/ml ampicillin). Plates were incubated overnight at 37°C. The plasmid DNA was purified from overnight cultures using the Wizard plus SV Minipreps purification system (Promega).

2.2.6. Plasmids

pET15b(+)-PBD, a plasmid for expression of the C-terminal region of Tim50 (residues 395-476 with a N-terminal hexahistidine-tag) in *E. coli* cells, was amplified by PCR, with a *Saccharomyces cerevisiae* genomic DNA as a template using the primers listed in Table 2.2.1. The amplified DNA fragment was digested with *Nde*I and *Bam*HI. By using In-Fusion HD Cloning Kit (Clontech), the PCR product was cloned into *Nde*I/*Bam*HI-digested pET15b(+) (Novagen) vector containing hexahistidine-tag and a thrombin site for its cleavage.

pET15b(+)-PBD(395-460), a plasmid for expression of the C-terminal region of Tim50 (residues 395-460 with a N-terminal hexahistidine-tag) in *E. coli* cells, was amplified by PCR, with a *S. cerevisiae* genomic DNA as a template using the primers listed in Table 2.2.1. The amplified DNA fragment was digested with *Nde*I and *Bam*HI. By using In-Fusion HD Cloning Kit (Clontech), the PCR product was cloned into *Nde*I/*Bam*HI-digested pET15b(+) (Novagen) vector containing hexahistidine-tag and a thrombin site for its cleavage.

pET15b(+)-PBD(395-450), a plasmid for expression of the C-terminal region of Tim50 (residues 395-450 with a N-terminal hexahistidine-tag) in *E. coli* cells, was amplified by PCR, with a *S. cerevisiae* genomic DNA as a template using the primers listed in Table 2.2.1. The amplified DNA fragment was digested with *Nde*I and *Bam*HI. By using In-Fusion HD Cloning Kit (Clontech), the PCR product was cloned into *Nde*I/*Bam*HI-digested pET15b(+) (Novagen) vector containing hexahistidine-tag and a thrombin site for its cleavage.

pET15b(+)-PBD(390-450), a plasmid for expression of the C-terminal region of Tim50 (residues 390-450 with a N-terminal hexahistidine-tag) in *E. coli* cells, was amplified by PCR, with a *S. cerevisiae* genomic DNA as a template using the primers listed in Table 2.2.1. The amplified DNA fragment was digested with *Nde*I and *Bam*HI. By using In-Fusion HD Cloning Kit (Clontech), the PCR product was cloned into *Nde*I/*Bam*HI-digested pET15b(+)

(Novagen) vector containing hexahistidine-tag and a thrombin site for its cleavage.

pET15b(+)-PBD(400-450), a plasmid for expression of the C-terminal region of Tim50 (residues 400-450 with a N-terminal hexahistidine-tag) in *E. coli* cells, was amplified by PCR, with a *S. cerevisiae* genomic DNA as a template using the primers listed in Table 2.2.1. The amplified DNA fragment was digested with *Nde*I and *Bam*HI. By using In-Fusion HD Cloning Kit (Clontech), the PCR product was cloned into *Nde*I/*Bam*HI-digested pET15b(+) (Novagen) vector containing hexahistidine-tag and a thrombin site for its cleavage.

pET15b(+)-PBD(405-450), a plasmid for expression of the C-terminal region of Tim50 (residues 405-450 with a N-terminal hexahistidine-tag) in *E. coli* cells, was amplified by PCR, with a *S. cerevisiae* genomic DNA as a template using the primers listed in Table 2.2.1. The amplified DNA fragment was digested with *Nde*I and *Bam*HI. By using In-Fusion HD Cloning Kit (Clontech), the PCR product was cloned into *Nde*I/*Bam*HI-digested pET15b(+) (Novagen) vector containing hexahistidine-tag and a thrombin site for its cleavage.

I413A, E414A, E415A, L434Q, K435A, and D436A point mutations, and I413A/D436A double mutations were introduced into the sPBD gene by PCR using pET-15b(+)-sPBD as template, and primers sets listed in Table 2.2.1. The resulting plasmids were named as pET-15b(+)-sPBD(I413A), pET15b(+)-sPBD(E414A), pET15b(+)-sPBD(E415A), pET15b(+)-sPBD(L434Q), pET15b(+)-sPBD(K435A), pET15b(+)-sPBD(D436A) and pET15b(+)-sPBD(I413A/D436A), respectively .

pColdGST-Tim50core, a plasmid for expression of the conserved core domain of Tim50 (residues 171-362) in *E. coli* cells, was amplified by PCR, with a *S. cerevisiae* genomic DNA as a template using the primers listed in Table 2.2.1. The amplified DNA fragment was digested with *Nde*I and *Eco*RI, and was cloned into pColdGST vector that was digested with same set of of restriction enzymes.

The DNA fragment containing the promoter, the ORF and the terminator of the TIM50 gene was amplified by PCR from a *S. cerevisiae* genomic DNA. The amplified DNA fragment was ligated into the *Xho*I and *Bam*HI sites of pRS314 vector [22]. ACCTAC sequence corresponding to residues Thr169-Tyr170 was replaced by *Nde*I restriction site, resulting in T169H/Y170M mutations, and TTTT sequence just after the TAA terminal codon was replaced by *Eco*RI restriction site, using the Quik-Change mutagenesis protocol (Agilent, La Jolla, CA) to produce pRS314-Tim50^{WT}. The genes for the truncated Tim50 segments (residues 1-366 or 450) of Tim50 were amplified by PCR from pRS314-Tim50^{WT}. The amplified DNA fragments were ligated into the *Nde*I and *Eco*RI sites of pRS314-Tim50^{WT} to produce pRS314-Tim50$^{1-366}$ and Tim50$^{1-450}$.

pET21a-dTom20, a plasmid for expression of the cytosolic receptor domain of yeast Tom20 (residues 51-145) and pET17xb-pSu9N, a plasmid for expression of the N-terminal half of presequence pSu9N (residues 1-34) in *E. coli* cells, were kind gifts of Dr. Shin Kawano of Professor Endo's lab of Biochemistry.

2.2.7. Site-directed mutagenesis of plasmids

The QuikChange Site-Directed Mutagenesis Kit (Agilent) was used to introduce point mutations in the previously cloned gene for sPBD. Mutagenesis was performed according to the manufacturer's instructions and was verified by sequencing.

2.2.8. Sequencing of DNA

Sequencing of DNA was performed by the Sanger method using the BigDye Terminator v1.1 Cycle Sequencing Kit: the sequencing reaction was performed in 5 µl scale containing 1 µl plasmid, 1 µl primer (1.6 µM), 1 µl BigDye sequencing-mix and 1 µl sequencing-buffer. After the sequencing reaction (25 cycles: 96°C, 10 sec; 50°C, 5 sec;

60°C, 4 min), DNA was precipitated by adding 12.5 µl 100% ethanol that contained 0.5 µl of 3 M sodium acetate. Subsequently the DNA was pelleted (10,000 × g, 10 min), washed with 70% ethanol and dried (vacuum concentrator). After being resuspended in 15 µl Hi-Diformamide, the DNA was analyzed using the Genetic Analyzer 3130 (Applied Biosystems).

2.2.9. Yeast Strains and growth conditions

The strain Tim50-316 (tim50Δ, MATa ade2 his3 ura3 leu2 trp1 can1 tim50Δ::CgHIS3 [pRS316-Tim50^{WT}]) was described previously [15, 23]. Tim50-316 was transformed with pRS314, pRS314-Tim50^{WT}, Tim50$^{1-366}$ or Tim50$^{1-450}$. Cells were grown on SCD (-Trp, -Ura) (0.67% yeast nitrogen base without amino acids, 0.5% casamino acid, and 2% glucose, 20 mg/L Adenine sulfate, 30 mg/L L-Leucine, 20 mg/L L-Histidine-HCl, 30 mg/L L-Lysine-HCl). For plasmid shuffling experiment, cells were grown on SCD -Trp (SCD -Trp -Ura, +20 mg/L Uracil, +1 mg/ml 5'-fluoroorotic acid) at 30°C for 2 days to eliminate the URA3-containing plasmid.

2.2.10. The medium for *E. coli*

For preparation of non-labeled protein from *E. coli*, cells were grown in the LB medium (1% tryptophan, 0.5% yeast extract and 0.5% NaCl) containing 50 µg/ml ampicillin. For preparation of uniformly ^{15}N-labeled or ^{15}N/^{13}C-labeled protein, *E. coli* cells were grown in M9 minimal medium (42 mM Na_2HPO_4, 22 mM KH_2HPO_4, 0.1% NaCl, 1 mM $MgSO_4$, 0.1 mM $CaCl_2$, 3.3 µM $FeCl_3$, 30 µM thiamine-HCl) supplemented with $^{15}NH_4Cl$ (1.0 g/L) and/or [U-^{13}C]-glucose (2.0 g/l), respectively.

2.2.11. Protein and peptide preparation from *E. coli* cells

2.2.11.1. sPBD

The *E. coli* strain Rosetta (DE3) was used as a host for the expression of pET15b -sPBD fusion proteins to express the protein as a soluble form at a high level. Briefly, bacterial cells were grown for ~ 3 h at 37°C in 1 L of LB medium containing 50 µg/ml ampicillin. Upon reaching an OD_{600} of 0.5, temperature was lowered to 16°C, and protein expression was induced with 0.5 mM IPTG (isopropyl β-D-1-thiogalactopyranoside) for overnight. Cells were harvested by centrifugation at 4,400 × g for 10 min and pelleted cells were disrupted by sonication using 20 mM Tris-HCl (pH 7.4) containing 300 mM NaCl. After disrupting the cell by using a microfluidizer, insoluble material was removed by centrifugation at 14,000 × g for 40 min at 4°C. The supernatant was loaded onto a Ni-NTA (nickel-nitrilotriacetic acid-agarose, Qiagen) column (20 ml), which was pre-equilibrated with buffer A (20 mM Tris-HCl, pH 7.4, 300 mM NaCl). The column was washed with three volumes of buffer B (20 mM Tris-HCl, pH 7.4, 300 mM NaCl, 20 mM imidazole) until a stable baseline was obtained. The fusion protein was eluted with buffer C (buffer A containing 0.5 M imidazole) and was further purified by gel-filtration chromatography using a superdex-75 10/300 GL (GE Healthcare) column (pre-equilibrated with 20 mM Tris-HCl, pH 7.4, 50 mM NaCl). The eluted fusion protein was treated with thrombin (2.5 unit/mg fusion protein) at 23°C for 16 hours. The digested protein was concentrated and loaded further into a Superdex-75 10/300 GL column (GE Healthcare) to separate target protein from the cleaved His-tag and SDS-PAGE electrophoresis was performed to assess protein purity. Fractions with the desired protein were concentrated using Amicon ultra 3K device (molecular weight cut-off of 3,000). Protein concentration

was determined by absorbance at λ=280 nm with a molar extinction coefficient (ε) of 2,980 $(M\ cm)^{-1}$. All the purification procedures were carried out at 4°C.

2.2.11.2. Truncated PBD

Purification of the non-labeled truncated PBD proteins was performed essentially by the same procedure for sPBD.

2.2.11.3. Mutant sPBD

Purification of the non-labeled or uniformly labeled mutants sPBD proteins was performed essentially by the same procedure for sPBD.

2.2.11.4. Preparation of dTom20

The *E. coli* strain Rosetta (DE3) was used as a host for expression of pET21a-dTom20 fusion proteins as a soluble form at a high level. Briefly, cells were grown at 37°C to OD_{600} ~0.5, and protein expression was induced by addition of 0.5 mM IPTG (isopropyl-β-D-1-thiogalactopyranoside) for overnight at 16°C. Cells were harvested by centrifugation at 4400 × g for 10 minutes. The harvested cells were disrupted by sonication in 20 mM Tris-HCl (pH 7.4) containing 300 mM NaCl. The fusion protein was purified from cell lysates by using a Ni-NTA (nickel-nitrilotriacetic acid-agarose, Qiagen) column followed by SDS-PAGE electrophoresis to assess protein purity. The purified proteins were concentrated by using Amicon ultra 3K device (molecular weight cut-off of 3,000) and concentration was determined by absorbance at λ=280 nm with a molar extinction coefficient (ε) of 1,490 $(M\ cm)^{-1}$.

2.2.11.5. Preparation of Tim50core

The gene for Tim50core (residues 171-362) was inserted into the pCold-GST vector using the NdeI and EcoRI sites and was over expressed as a soluble form at a high level in *E. coli* cells. Briefly, cells were grown at 37°C to OD_{600} ~0.5, and expression was induced by addition of 0.5 mM IPTG (isopropyl-β-D-1-thiogalactopyranoside) for overnight at 16°C. The harvested cells were disrupted by sonication in 20 mM Tris-HCl (pH 7.4) containing 50 mM NaCl. Tim50core was purified from cell lysates by glutathione sepharose column chromatography. The GST-tag of Tim50core (171-362) was cleaved off with HRV3C protease at 25°C for overnight, and Tim50core was further purified by gel filtration chromatography using a Superdex-200 10/300 GL column. Protein concentration was determined by absorbance at λ=280 nm with a molar extinction coefficient (ε) of 32,890 $(M\ cm)^{-1}$.

2.2.11.6. Preparation of presequence peptide pSu9N

To prepare a non-labeled or uniformly labeled pSu9N peptide, pET-17xb (Novagen) a fusion protein consisting of the gene10 protein plus one glutamate followed by the presequence was expressed in *E. coli* cells in LB medium or M9-minimal medium containing $^{15}NH_4Cl$ (1.0 g⁄L). Briefly, cells were cultivated to an absorbance of 0.5 at 600 nm (A600) in the presence of 50 μg/ml ampicillin in LB medium or M9-minimal medium at 37°C, and induced with 0.5 mM IPTG (isopropyl-β-D-thiogalactopyranoside) at 16°C for 16 h. Cells were harvested by centrifugation at 4400 × g for 10 min. , and the harvested cell pellets were resuspended in 20 mM Tris-HCl (pH 7.4) containing 50 mM NaCl and 1% Triton-X, and disrupted by sonication. The supernatant was discarded after centrifugation at 8,000 × g for 10 minutes, and the pellet was then resuspended in 20 mM Tris-HCl (pH 7.4) containing

50 mM NaCl and 0.1% Triton-X. The supernatant was discarded after centrifugation at 14,000 × g for 10 minutes, and the pellet was resuspended and washed with water until it became a white-creamy color. The fusion proteins were found as inclusion bodies, which were solubilized using 4 M urea, and subjected to V8 protease treatment (1⁄50 wt⁄wt) at 30°C for overnight to yield the presequence peptide. The presequence peptide was finally purified satisfactorily by reversed phase HPLC as follows. The digested protein solution was loaded onto a Develosil column (Nomura) pre-equilibrated with 80% of buffer A (0.1% TFA in water) and 20% of buffer B (0.1% TFA in acetonitrile). The target peptide was eluted with a linear gradient of acetonitrile (20–35%). The fractions containing the target peptide were collected by monitoring the absorbance at 214 nm and checked by mass spectrometry analyses. The solvent of the purified peptide fraction was evaporated completely using a vacuum centrifugal rotor machine and the peptide was stored at -30°C. The concentration of the peptide was determined by absorbance at λ=280 nm with a molar extinction coefficient (ε) of 1,490 $(M\ cm)^{-1}$. Chemically synthesized pHsp60 and pSu9NQ were purchased from CS Bio (Shanghai) Ltd.

2.2.12. Analytical protein methods

2.2.12.1. SDS-polyacrylamide gel electrophoresis (SDS-PAGE)

Proteins were separated according to their sizes on a vertical, discontinuous SDS-PAGE system. A large gel was used and acrylamide concentration in the running gel (running gel: 14 x 6 x 0.1cm) was chosen according to the sizes of proteins to be separated.

Protein samples were dissolved in 2 x SDS buffer (0.25 M TRIS/HCl, pH 6.8, 2% (w/v) SDS, 4 mM EDTA, 20% (w/v) sucrose, 0.05% (w/v), 0.05% (w/v) bromphenol-blue) and

heated for 2 min at 95°C before loading on the gel. Gels were run at 46 mA until the blue front reached bottom of the gel (ca. 70 min). Separated proteins were stained with CBB.

Compositions of buffers	
Running gel	16% (w/v) acrylamide, 0.42% (w/v) bis-acrylamide, 375 mM Tris-HCl (pH 8.8), 2 mM EDTA, 0.1% (w/v) SDS, 0.06% (w/v) APS, 0.08% (v/v) TEMED
Stacking gel	4.5% (w/v) acrylamide, 0.2% (w/v) bis-acrylamide, 125 mM Tris-HCl (pH 6.8), 2 mM EDTA, 0.1% (w/v) SDS, 0.06% (w/v) APS, 0.08% (v/v) TEMED
Electrophoresis buffer	24.7 mM Tris, 189 mM glycine, 0.1% (w/v) SDS, 0.9 mM EDTA

2.2.12.2. Staining SDS-PAGE with Coomassie Brilliant Blue (CBB)

SDS-PAGE was briefly washed with water and then immersed into the CBB staining solution (2.5% CBB or R-250, 45% (v/v) methanol, 10% (v/v) acetic acid). Staining can be speeded up by heating the solution for 5 min in the microwave. Background staining was removed by repeated washes in 30% (v/v) methanol, 10% (v/v) acetic acid.

2.2.13. Circular dichroism

The CD measurement was carried out with a JASCO CD spectrometer model J720 over the range of 200-240 nm at a scan rate of 100 nm/min, using a cell with a path length of 0.2 cm. Each spectrum is an average of four scans. The raw data were collected by subtracting the contribution of the buffer to the CD signal. The data were smoothed and converted to molar ellipticity units. The measurements were taken at a constant

temperature of 25°C in buffer containing 20 mM KPi, pH 6.7, 50 mM KCl, with a protein concentration of 10 µM.

2.2.14. NMR resonance assignments

NMR spectra of 0.1 mM uniformly [^{15}N, ^{13}C]-labeled sPBD in 20 mM KPi, pH 6.7, 50 mM KCl, D_2O/ H_2O (7/93) were recorded on a Bruker AVANCE 600 MHz spectrometer equipped with a TCI cryogenic probe at a sample temperature of 25°C by triple resonance experiments including HNCANNH measurements for sequential backbone resonance assignments. All spectra were processed with TopSpin 1.3 (Bruker BioSpin) and analyzed with Sparky 3.114 (http://www.cgl.ucsf.edu/home/sparky/).

2.2.14.1. Sample preparation

sPBD protein for an NMR study were conventionally prepared by recombinant expression, typically in bacterium *E. coli*. The recombinant expression procedure provides typically easier production in sufficient quantity, and allows isotopic labeling of proteins. The ^{13}C enriched glucose and ^{15}N enriched ammonium chloride are used most frequently as a source of carbon ^{13}C and nitrogen ^{15}N, respectively. The typical volume of the purified protein sample is 300–500 µl with the protein in the concentration range 2–3 mM dissolved in 20 mM KPi, pH 6.7, 50 mM KCl solution. Ideally behaving protein should be well soluble, stable for several weeks.

2.2.14.2. Resonance assignment of backbone atoms

The NMR structure determination procedure is based mainly on the inter-proton distances, thus the first step is the assignment of proteins resonances for the target protein.

However, it is also important to assign ^{13}C and ^{15}N resonances as well. The reason is as follows. First, these nuclei also carry useful structural information, and second, correlation of protons with ^{13}C and ^{15}N can allows one to distinguish protons of identical frequencies and to establish covalent bond connectivity in the molecule.

For assignment of chemical shifts from backbone atoms (H, N, C^{α}, C^{β} and C') to specific amino-acid residues, I performed the following NMR experiments.

• [^{1}H, ^{15}N]-HSQC - a double resonance experiment correlating H–N from amide groups

• HNCACB - a triple resonance experiment correlating atoms Hi–Ni with atoms C^{α}_{i} and C^{β}_{i}

• CBCA(CO)NH - a triple resonance experiment correlating amide atoms Hi–Ni with atoms C^{α}_{i-1} and C^{β}_{i-1} from the preceding residue

• HNCO - a triple resonance experiment correlating atoms Hi–Ni with atoms C'_{i-1} from the preceding residue

• HN(CA)NNH experiment – a triple-resonance experiment specifically designed to provide information on sequential assignment between the amide NH proton of one residue and the amide nitrogen of the preceding and the following residues via the intervening ^{13}CA spin by means of the $^{1}J(NH)$ and $^{1,2}J(N,CA)$ coupling constants.

2.2.15. NMR titration experiments

Titrations of ^{15}N uniformly labeled sPBD and presequence peptides or ^{15}N uniformly labeled presequence peptide and sPBD or ^{15}N uniformly labeled sPBD and Tim50core were performed on Bruker AVANCE 600 MHz spectrometer equipped with a room temperature TXI probe at a sample temperature of 26°C in 20 mM KPi, pH 6.7, 50 mM KCl, D_2O/ H_2O (7/93). Assignments of [^{1}H, ^{15}N] amide resonances of ^{15}N-labeled pSu9N were described previously [21]. For estimation of dissociation constants in pSu9N binding to sPBD,

titration curves were analyzed with a program xcrvfit v5.0.3 (http://www.bionmr.ualberta.ca/bds/software/xcrvfit/), developed by Drs. R. Boyko and B. Sykes (University of Alberta, Canada), with a fitting function, “chemical shift XY1”.

For each cross-peak, the weighted chemical shift difference $\Delta\delta$ was calculated as $[(\Delta\delta\ (^{1}H))^{2} + (\Delta\delta\ (^{15}N)/15)^{2}]^{1/2}$. For the analysis of intensity changes, each cross-peak was normalized by the intensity of the C-terminal residue as an internal reference.

2.3. Results

2.3.1. A segment of suitability of C-terminal PBD (residue 400-450, sPBD) for NMR analyses

Tim50 acts as a central presequence receptor of the TIM23 complex and interacts with Tim23 in order to promote efficient precursor translocation across the inner membrane [14,15,18,19,24]. The C-terminal PBD (presequence binding domain) of Tim50 (residues 395-476), which is conserved among fungal species, was found to bind to presequences [19]. To characterize presequence binding of the C-terminal PBD of yeast Tim50 by NMR, I first tried to purify $PBD^{395-476}$ from *E. coli* cells. $PBD^{395-476}$ was well expressed in *E. coli* cells and purified to homogeneity successfully (Figure 2.3.1). The CD spectrum suggested that the recombinant $PBD^{395-476}$ protein is folded (Figure 2.3.2), although it tended to form aggregates at 25°C (not shown). A two-dimensional [^{1}H, ^{15}N]-heteronuclear single-quantum coherence spectrum (HSQC) of $PBD^{395-476}$ (Figure 2.3.3) at 20 mM KPi, pH 6.7, containing 50 mM KCl showed a large number of overlapped signals which indicates that PBD is not suitable for NMR analyses under these conditions. Then I made several recombinant constructs, $PBD^{395-460}$, $PBD^{395-450}$, $PBD^{400-450}$, and $PBD^{405-450}$ (Table 2.3.1) by truncating several residues from the N- and C-terminus of the previously suggested Tim50 PBD (residues 395-476) [19]. All of the truncated recombinant proteins were well expressed in *E. coli* cells and purified successfully (Figure 2.3.1, not shown all). The CD spectra indicate that the truncated PBD proteins have α-helix rich structures (Figure 2.3.2). Then, NMR spectra of the ^{15}N-labeled several truncated PBD proteins were recorded at 20 mM KPi, pH 6.7, containing 50 mM KCl at 26°C (Figure 2.3.3). However, HSQC signals of the truncated PBD were not well dispersed except for $PBD^{400-450}$, a segment corresponding to residues 400-450 of Tim50 (sPBD). Therefore, I concluded that sPBD is

the most suitable for further detailed NMR analyses.

2.3.2. C-terminal part of PBD in Tim50 is not essential for cell viability

I asked if two Tim50 C-terminal truncation mutants were able to complement the lethal growth phenotype of a strain lacking Tim50. A full-length $Tim50^{WT}$, $Tim50^{1–366}$ and $Tim50^{1–450}$ were expressed in yeast cells, in which a chromosomal deletion of TIM50 was complemented by a plasmid-encoded wild type Tim50 expressed from a URA3-containing plasmid. Cells that contain a plasmid are typically selected using nutritional markers. The *S. cerevisiae URA3* gene is a useful marker of plasmid selection analysis, which has both positive and negative selection properties. *S. cerevisiae ura3* mutants require the gene to grow in the absence of uracil, but when the gene is present, they become sensitive to the toxic uracil analogue produced from 5'-FOA (5'-fluoro-orotic acid) by the enzyme encoded by *URA3*. So, cells transformed with plasmids that contain the wild-type genes and a *ura* marker can be isolated by selecting for growth without uracil, and plasmid-free cells can be recovered by growth in 5'-FOA. This is the basis for plasmid shuffling that allows mutations of a gene on a second plasmid to be tested, even though they may be lethal. Here, expression of full-length Tim50 rescued the lethal growth phenotype of a strain lacking Tim50 upon 5'-FOA treatment. Another plasmid construct encoding $Tim50^{1–450}$, not $Tim50^{1–366}$, (PBD deletion mutant; Figure 2.3.4B) could rescue the lethal growth phenotype as well. This suggests that $Tim50^{1–450}$, not $Tim50^{1–366}$, is still functional as Tim50 because it was able to grow upon 5'-FOA treatment alike $Tim50^{WT}$. This is consistent with the results by Schulz C*. et al*. that PBD of Tim50 (residues 395-476) is essential for cell viability [19], but my result further indicates that the residues 451-476 in PBD is not essential for the function of Tim50.

2.3.3. Secondary structure prediction for sPBD

Circular dichroism (CD) is a spectroscopic technique commonly used to investigate secondary structures of proteins. Major secondary structure types, α-helices and β-strands, produce distinctive CD spectra. Thus, by comparing the CD spectrum of a protein of interest to a reference set consisting of CD spectra of proteins of known structure, predictive methods were proposed to estimate the secondary structure of the protein. In order to perform secondary structure analysis of PBD of yeast Tim50 (400-450, sPBD), sPBD was purified using Ni-NTA and gel-filtration chromatography (Figure 2.3.5A and B). To gain insight into the secondary structure content of sPBD, a CD spectrum was recorded at 10 μM protein concentration (Figure 2.3.6). The spectrum shows strong negative ellipticities at 206 and 222 nm, suggesting that sPBD in the native state predominantly contains α-helix rich regions. On the basis of the standard secondary structure prediction method (K2D3 method) [25], the overall secondary structural content was estimated to be 42% for α-helix and 5% for β-sheets.

2.3.4. Backbone signal assignments of the HSQC spectra of the sPBD

Then I performed NMR analyses of sPBD. The key point of NMR analyses is to assign NMR signals to specific positions/residues of target proteins. Therefore I started assignment of the backbone resonances of the sPBD. For this purpose uniformly [^{15}N, ^{13}C]-labeled sPBD was prepared from *E. coli* cells cultured in M9 medium. The spectra used for the resonance assignments are summarized in Table 2.3.2. To obtain the best NMR signal sensitivity and stability of the sample throughout the 3D NMR experiments, sample and measurement conditions were optimized. First, two-dimensional [^{1}H, ^{15}N]-heteronuclear single-quantum coherence spectra (HSQC) of different concentrations of

sPBD (0.1 mM, 0.2 mM, 0.3 mM) at 20 mM KPi, pH 6.7, containing 50 mM KCl were recorded at 30°C and 25°C. A [^{1}H, ^{15}N]-HSQC spectrum of 0.1 mM of ^{15}N-sPBD (Figure 2.3.7) at 20 mM KPi, pH 6.7, containing 50 mM KCl showed a sufficiently well dispersed spectrum with only a very limited number of overlapped signals. The spectra of sPBD were analyzed as strips of peaks, and strips from a pair of experiments has presented together side by side or as an overlay of two spectra. In HNCACB spectra, 4 peaks are usually present in each strip, i.e. the C_α and C_β of one residue as well as those of its preceding residue. The peaks from the preceding residue were identified from the CBCA(CO)NH, HNCO, and HNCANNH experiments. Each strip of peaks was therefore linked to the next strip of peaks from an adjoining residue, allowing the strips to be connected sequentially. The residue type was identified from the chemical shifts of the peaks, but some amino acids such as serine, glycine and alanine, can be easily identified. The resonances were then assigned to specific residues by comparing the sequence of a series of peaks with the amino acid sequence of sPBD. sPBD consists of 51 amino acids, and among them, two are proline residues and a large number of glutamic acid residues (about 20%) are present. A repeat of glutamic acid residues made the assignment little complicated but nevertheless, by using 3D data, [^{1}H, ^{15}N]-HSQC, HNCACB, CBCA(CO)NH, HNCO, and HNCANNH, 96% of the expected backbone (NH) signals of sPBD were successfully assigned to specific residues except for two proline residues, which lack backbone NHs.

2.3.5. Secondary structure propensity (SSP) of sPBD

The chemical shifts of ^{13}C signals of proteins and peptides, in particular of C_α and C_β atoms, can be used to characterize the secondary structure because of their sensitivity to

local magnetic environment. Thus I performed secondary structure propensity (SSP) analysis [26]. This method combines chemical shifts from different nuclei into a single score representing the expected fraction of α-helix or β-strand for each residue. The score is calculated relative to an average chemical shift of nuclei in known α-helix or β-strand structures, and ranges between 1 or −1 for the two types of secondary structure, respectively. Here, I used the chemical shifts obtained for the C_α and C_β nuclei in sPBD (Table 2.3.3) to calculate secondary structure propensities (Figure 2.3.8). Calculated secondary structure propensity (SSP) scores for individual residues show that α-helical structures reflected by positive SSP values prevail in sPBD, especially around residues 405-425, which is consistent with the CD spectrum with a negative band at around 222 nm (Figure 2.3.6).

2.3.6. pSu9N has common recognition elements for sPBD and dTom20 binding

Mitochondrial presequences have recognition elements for several presequence-binding receptor proteins for mitochondrial protein translocation. Potential recognition elements of precursor presequences for Tim50 have not been characterized yet. Principally it is stimulating to ask if a presequence contains a common sequence motif that is recognized by multiple mitochondrial protein receptors.

Mitochondrial targeting signals in N-terminal presequences are recognized by Tom20 and Tom22 in the TOM40 complex [12,17,27]. Presequence recognition by Tom20 was extensively studied by NMR and X-ray method. Tom20 is anchored in the mitochondrial outer membrane by an N-terminal hydrophobic transmembrane segment, and exposes a C-terminal receptor domain to the cytosol [2,28]. NMR and X-ray structures of the cytosolic receptor domain of rat Tom20 in a complex with a presequence peptide was

determined [12,13]. The determined NMR and X-ray structure of the cytosolic domain of Tom20 contains a hydrophobic groove that can interact with the hydrophobic residues of the presequence peptides in an amphiphilic helical structure [12,13]. The size of the hydrophobic groove of Tom20 suggests that sequences recognized by Tom20 are as short as 8 amino acid residues, whereas the lengths of presequences are often longer than 40 amino acid residues. The interactions between Tom20 and such a long presequence can direct the targeting signal recognition and subsequent tethering of the presequence to the TOM40 complex to increase import efficiency [21]. It was revealed that Tom20 recognizes a diverse consensus motif $\phi\chi\chi\phi\phi$ (where ϕ is a hydrophobic amino acid, and χ is any amino acid) in the N-terminal presequences [13].

Then, what is the Tim50 PBD binding element or motif in presequences? To answer this question, a ^{15}N-labeled model presequence peptide, pSu9N (the N-terminal half of the presequence of subunit 9 of F_o-ATPase) [21], was prepared, and the peptide was checked by mass spectrometry (Figure 2.3.9). I recorded its NMR spectra with and without Tim50 sPBD or dTom20, the cytosolic receptor domain (residues 51-145) [12] of yeast Tom20 (Figure 2.3.10A). By calculating the chemical shift perturbation, I could successfully identify the residues of pSu9N involved in sPBD and dTom20 binding. The presence of sPBD caused chemical shift perturbation of a subset of the backbone amides of pSu9N (Figure 2.3.10B), indicating that pSu9N has a specific binding segment for sPBD. However, I found that the residues of pSu9N, which interact with sPBD, are mostly hydrophobic in nature. On the other hand, a pronounced chemical shift perturbation of a subset of the backbone amides of pSu9N was observed upon addition of dTom20 (Figure 2.3.10B), indicating that pSu9N has a specific binding segment for dTom20. Interestingly, the patterns of chemical shift changes are very similar between Tim50 sPBD and dTom20,

although dTim20 at a lower concentration tends to cause larger shifts for the signals in pSu9N than Tim50 sPBD (Figure 2.3.10B). These results suggest that both Tim50 sPBD and dTom20 bind to the similar segment(s) of pSu9N in a similar manner.

In order to assess the quantitative data on the affinity of the interactions between sPBD and pSu9N, chemical shift changes of ^{15}N-labeled pSu9N residues induced by different concentrations of sPBD were monitored in [^{1}H, ^{15}N]-HSQC spectra at 26°C (Figure 2.3.11A). The titration curves for the signals of L11, A12, A16, and V21 were analyzed by a nonlinear iterative fitting by assuming 1:1 binding stoichiometry (Figure 2.3.11B). The dissociation constant K_d of the pSu9N-sPBD complex was thus estimated to be 0.1-0.3 mM (Table 2.3.4), which is one-order larger than that for Tom20 reported previously [9]. The residues with the highest chemical shift changes, L7 and A8, were not used for K_d value calculation because the chemical shift changes could not be fitted well to binding curves but showed a straight line. It is supposed that these two residues may take part in some non-specific interactions in such high-concentrated conditions.

2.3.7. Two distinct sites of sPBD recognize the presequences

Which residues of sPBD are responsible for presequence binding? Interactions of PBD with a presequence are essential for the Tim50 function [19] and the putative presequence-binding region in the crystallized core of yeast Tim50 may not be sufficient for the Tim50 function in mitochondrial translocation [20]. I thus tried to identify presequence binding elements in sPBD by using NMR. Figure 2.3.12A shows a superposition of a section of [^{1}H, ^{15}N]-HSQC spectra of ^{15}N-labeled sPBD (0.1 mM) in the absence and presence of non-labeled pSu9N (0.8 mM). Pronounced chemical shift changes upon addition of pSu9N were observed mainly in two distinct segments, residues

410-415 and 433-439 in sPBD (Figure 2.3.12B). These segments appear to represent two sites that take part in the interactions with the presequence pSu9N.

Then I tested another presequence peptide of mitochondrial pHsp60 (pHsp60). The [^{1}H, ^{15}N]-HSQC spectra of ^{15}N-labeld sPBD (0.1 mM) was recorded in the absence and presence of the presequene peptide of mitochondrial pHsp60 (pHsp60) (0.8 mM) (Figure 2.3.13A). Interestingly, a similar chemical shift perturbation profile was observed for the titration of sPBD to pHsp60, with changes within 410-415 and 433-439 regions (Figure 2.3.13B). Notably, these two regions corresponded well with the parts of the sequence seen before to have the α-helix rich structure, residues 405–425 and 431–440 (Figure 2.3.8). Thus, two distinct binding sites of sPBD for different presequences were mapped out, one in the N-terminal site (410-415) and the other in the C-terminal site (433-439) of sPBD. Since sPBD is a rather small folded domain, these two segments likely constitute a single presequence binding site in sPBD.

2.3.8. N-terminal binding site is more important for sPBD-presequence interactions

Next, I analyzed the individual roles of the two presequence binding segments in sPBD in presequence recognition by mutagenesis analyses. One or two mutation(s) were introduced into various positions in the two presequence binding segments in sPBD. Then mutant sPBDs were subjected to NMR titration experiments to demarcate the residues or regions of sPBD that are functionally more important for presequence binding. The CD analysis revealed that all these mutant sPBD proteins take similar folding to that of wild type sPBD (Figure 2.3.14). Therefore, those mutations did not affect secondary structures of sPBD. [^{1}H, ^{15}N]-HSQC spectra of 0.2 mM ^{15}N-labeled pSu9N were recorded in the absence and then presence of each of the mutants sPBD (0.4 mM). Figure 2.3.15A shows

the chemical shift perturbation of backbone amides in [^{1}H, ^{15}N]-HSQC spectra of 0.2 mM ^{15}N-labeled pSu9N in presence of 2-fold excess wild-type sPBD or indicated mutant sPBD. All the mutants except for K435A exhibit a reduced binding ability for pSu9N, suggesting their importance in the presequence binding. To make clear understanding, "the average chemical shift perturbations" of the indicated sPBD mutants from NMR analyses were calculated (Figure 2.3.15B). It is now clear that replacement of Ile413 and Glu414 or Glu415 with Ala (I413A, E414A, and E415A) in the N-terminal presequence binding site of sPBD significantly reduces their binding abilities to pSu9N. Similarly, three sPBD mutants with a mutation of L434Q, K435A or D436A in the C-terminal presequence binding site also exhibited reduced capability for pSu9N binding. However, the reduction of pSu9N binding ability was smaller for sPBD mutants with C-terminal mutations than the ones with N-terminal mutations (Figure 2.3.15B). Since, the mutants of the N-terminal binding part of sPBD show smaller binding ability to presequences than C-terminal part mutants, the N-terminal presequence binding site could be more important for presequence binding than the C-terminal binding site. Furthermore, sPBD with double mutations (I413A/D436A) showed more reduced binding ability for pSu9N than the ones with single mutations. Therefore residue I413 and D436 appear to synergetically contribute to the interactions with the presequence pSu9N.

I also tried to make more mutants in the N and C-terminal presequence binding sites of sPBD, yet they were not suitable for NMR analyses. For example, the mutant with Lys to Ala mutation at residue 411 tends to aggregate at concentration above 0.15 mM, which made NMR experiments unfeasible. Another mutant with Val to Gln mutation at residue 438 was not expressed in *E. coli* cells.

2.3.9. sPBD-presequence interaction is partly hydrophobic

Since interactions between Tom20 and presequences are mainly hydrophobic [12], it is of interest to test if the nature of the Tim50 PBD–presequence interactions is also hydrophobic. Thus, five hydrophobic residues, L7, A8, A12, A16, and A17 around the Tim50 binding element of pSu9N were replaced with hydrophilic Gln to make a mutant presequence peptide, pSu9N(Q) (Figure 2.3.16A). Then, [^{1}H, ^{15}N]-HSQC spectra of ^{15}N-labeled Tim50 sPBD were recorded in the absence and presence of pSu9N(Q) (Figure 2.3.16B) and the amounts of chemical shift changes of backbone amides of ^{15}N-labeled Tim50 sPBD were compared with those with pSu9N (Figure 2.3.16C). The presequence peptide pSu9N(Q) induced much smaller chemical shift changes of sPBD than pSu9N, suggesting that the binding of pSu9N(Q) to sPBD was significantly suppressed as compared with pSu9N. Therefore, hydrophobic residues in pSu9N are important for presequence binding to sPBD.

Next, effects of salt concentrations on the sPBD–presequence interactions were examined. Figure 2.3.17 shows the pSu9N induced chemical shift changes of backbone amides of ^{15}N-labeled sPBD in the presence of different concentrations of KCl. Chemical shift changes upon addition of pSu9N were enhanced at higher KCl concentrations for the C-terminal segment of sPBD while those for the N-terminal segment of sPBD were not affected or even suppressed at higher KCl concentrations (Figure 2.3.18). Therefore the C-terminal segment, but not the N-terminal part of sPBD, interacts with pSu9N through hydrophobic interactions, which is consistent with the recent suggestion that the interactions between Tim50 and presequences are mainly hydrophobic rather than hydrophilic [18,21,24].

2.3.10. sPBD binds to the Tim50core domain through the presequence binding site

Both Tim50core domain (residues 164–361) and PBD (residues 395–476) were found to bind to presequences [18-20]. Why does yeast Tim50 have two distinct presequence-binding regions in the core domain and PBD? Perhaps the presequence can be transferred from Tim50 PBD to the core domain. I thus asked if presequence binding to Tim50 sPBD is affected by the presence of the core domain of Tim50 (Tim50core, residues 171-362). Tim50core was expressed in *E. coli* cells and was purified successfully (Figure 2.3.19). To analyze the sPBD-Tim50core interactions, the [^{1}H, ^{15}N]-HSQC spectra of ^{15}N-labeled PBDs were recorded with and without Tim50core at 26°C (Figure 2.3.20A). When Tim50core was added to ^{15}N-labeled sPBD, several signals arising from the residues involved in presequence binding changed their chemical shifts, indicating that Tim50core can bind to the presequence binding site of sPBD (Figure 2.3.20B). Besides, Tim50core caused the intensity loss in addition to the chemical shift perturbations of backbone amides in [^{1}H, ^{15}N]-HSQC spectra of ^{15}N-labeled sPBD (Figure 2.3.20C), which was more prominent for the N-terminal residues than C-terminal residues. This suggests that the kinetics of Tim50core binding falls in the intermediate-exchange regime on the NMR time scale. The signal intensities of the N-terminal part of sPBD decrease to about half at a molar ratio of 2 : 1 [Tim50core : sPBD]. Conversely, other residues and notably the residues from the C-terminal part of sPBD encoding “C-terminal binding site for presequences” are still clearly observed upon addition of Tim50core. Comparison of the shift directions of each signal of sPBD upon addition of pSu9N (Figure 2.3.12A) and Tim50core (Figure 2.3.20A) reveals that the shift directions are similar for the signals in the N-terminal presequence binding site, but are different for those in the C-terminal binding site (Figure 2.3.21). These results collectively suggest that Tim50core and pSu9N may share a common binding site mainly

consisting of the N-terminal half of sPBD.

2.3.11. N-terminal part of sPBD is likely more involved in Tim50core-sPBD interactions

I next asked which part of sPBD, the N-terminal or C-terminal site, is more involved in Tim50core-sPBD interactions. To define the residues that are functionally more important for Tim50core interactions, the ^{15}N-labeled sPBD mutants (I413A, E414A, E415A, L434Q, K435A, and D436A) were prepared and subjected to the NMR titration experiments. Then, the intensity of backbone amides of ^{15}N-labeled sPBD mutants were monitored in the presence and absence of Tim50core (Figure 2.3.22, 23 and 24). The results show that the I413A mutation in the N-terminal presequence binding segment suppressed the Tim50core binding while the L434Q mutation in the C-terminal binding segment did not (Figure 2.3.22 and 23). Furthermore, mutations including E414A, E415A, K435A, and D436A did not or only partially suppressed the Tim50core binding (Figure 2.3.24). These data collectively suggest that residue I413 of N-terminal presequence binding site of sPBD plays an important role in Tim50core binding.

2.3.12. sPBD likely forms a partial ternary complex

Because Tim50core can bind to the presequence binding site of sPBD, I next asked if Tim50core could bind to sPBD in a competitive manner with a presequence peptide such as pSu9N. To answer this question, the NMR spectra of ^{15}N-labeled sPBD were recorded in the absence and presence of 8-fold molar excess pSu9N, and then with further addition of 2-fold molar excess Tim50core over sPBD (Figure 2.3.25A). Interestingly, the pattern of chemical shift changes upon Tim50core binding in the presence of pSu9N, especially around residues 417-421, is different from that in the absence of pSu9N (Figure 2.3.25B). This

suggests that binding of Tim50core to sPBD does not force the pre-bound pSu9N to leave from sPBD completely. Instead, sPBD may partially form a ternary complex consisting of Tim50core, sPBD and pSu9N, which likely associates with the change of the Tim50core binding to residues 417-421 instead of residues 409-415 on sPBD.

Next I asked if sPBD and presequences interact with each other in the presence of Tim50core. NMR spectra of ^{15}N-labeled sPBD were monitored in the absence and presence of 2-fold molar excess of Tim50core, and then with further addition of 8-fold molar excess pSu9N (Figure 2.3.26A). Expectedly, the pattern of chemical shift changes and intensity loss upon pSu9N binding in the presence of Tim50core are nearly the same as those upon Tim50core binding in the presence of pSu9N (Figure 2.3.26B). This result again indicates that binding of pSu9N to sPBD does not force the pre-bound Tim50core to leave from sPBD completely and that sPBD likely forms a ternary complex consisting of Tim50core, sPBD and pSu9N.

Although isolation of the transient ternary complex may be difficult, formation of the binary complex of sPBD and Tim50core may be detected by using a method other than NMR, e.g. gel-filtration chromatography. I thus carried out analytical gel-filtration analysis. Mixtures of sPBD and Tim50core at molar ratios of 5:1 were subjected to gel-filtration using a Superdex-75 5/150 GL column, and their elution profiles were compared with those of the individual proteins (Figure 2.3.27). The elution pattern of the mixture exhibited two peaks, the peak tops of which are close to the ones for individual proteins. Therefore, gel-filtration analyses failed to offer evidence for formation of the binary complex. This is probably because, in gel-filtration experiments, the concentrations of sPBD and Tim50core are too low to achieve sufficient complex formation.

2.4. Discussion

The vast majority of mitochondrial proteins are synthesized on the cytosolic ribosomes as precursor proteins, which have to be transported into mitochondria to reach their sites of function. The whole process of recognition, translocation, intra-mitochondrial sorting and assembly of precursor proteins is achieved by the concerted action of different mitochondrial translocases. All proteins destined for the mitochondrial matrix and some inner membrane proteins are imported first by the TOM40 complex of the outer membrane and subsequently by the TIM23 complex of the inner membrane in an energy-driven manner.

In order to fully understand the precise functional mechanism of the TIM23 complex at the molecular level, it is essential to obtain a comprehensive knowledge on the Tim50-presequence interactions. Tim50IMS was proposed to have two distinct binding sites for presequences [20], yet it is still not clear how targeting signals are recognized by these two binding sites. Here, I analyzed interactions of yeast Tim50 sPBD (residues 400-450) with presequence peptides by NMR. SSP score analyses showed that sPBD has a propensity for forming α-helical structure in the N-terminal part of the sequence, which is followed by a short region with weak helical structural propensities in the C-terminal part. Then NMR analyses allowed me to identify the element for sPBD binding in the presequence peptide pSu9N. Interestingly, the sPBD binding element is similar to the element for binding to dTom20, the cytosolic domain of the presequence receptor Tom20 in the TOM40 complex. Therefore presequence-containing proteins are subjected to similar targeting signal recognition at the outer membrane by Tom20 and at the inner membrane by Tim50 PBD. This likely increases the fidelity of targeting and sorting of presequence-containing mitochondrial precursor proteins.

Recently, it was suggested that the presequence-Tim50 interaction precedes the guidance of the precursor protein to the Tim23 channel in the inner membrane [19]. Previous NMR studies indicated that K_d for the presequence–dTom20 complex is approximately 0.36 mM [21] and that for the presequence–Tim23 complex is approximately 0.47 mM [29]. However, the present NMR titration analyses indicated that presequence peptides, pSu9N and pHsp60, bind to sPBD with K_d of 0.1-0.3 mM. This result suggests that the low affinity of the presequence–PBD interactions reflects a basic transient nature in which both the outer and inner membrane translocators function cooperatively to direct the precursor proteins for translocation, but do not drive precursor protein transfer unidirectionally. Rather, direction of the precursor protein transfer may be determined by the downstream process such as the membrane potential ($\Delta\Psi$) driven presequence translocation through the TIM23 channel.

Next I found that two distinct segments of sPBD take part in the interactions with presequences probably in a cooperative manner. Several previous studies suggested that interactions between the presequence and Tim50 are mainly hydrophobic in nature [18,21,24]. Other studies, which employ fluorescence quenching, suggested that interaction between human Tim50IMS and presequence peptide is mainly electrostatic [30]. Here, the mutational study and salt dependency assay suggest that pSu9N binds to Tim50 sPBD at a binding site consisting of the segments involving residues 434-439 through hydrophobic interactions and residues 410-415 through interactions other than hydrophobic ones.

In addition to PBD, Tim50 has another presequence binding site in the core domain. However, since only fungal species have the conserved PBD, the significance of the presence of two distinct presequence binding sites in yeast Tim50 is not clear.

Interestingly, I found that sPBD binds to Tim50core through the presequence binding region including residues 409-415 in the N-terminal half of sPBD. This means that N-terminal part of sPBD has a dual function, one is for presequence binding and the other is for Tim50core binding. This suggests that binding of sPBD to Tim50core promotes release of the pre-bound presequence from sPBD. Nevertheless in the presence of the excess presequence over sPBD and Tim50core, sPBD appears to partially associate with Tim50core and pSu9N simultaneously by switching the Tim50core binding site from residues 409-415 to residues 417-421. Therefore, these results can lead to the following scenario of presequence recognition by Tim50. PBD of Tim50 may first receive the presequence from the TOM40 complex (Figure 2.3.28). Then the core domain of Tim50 interacts with residues 417-421 of presequence-bound PBD to form a transient ternary complex. Shift of the core domain to the presequence binding domain (residues 409-415) on PBD will release the presequence from PBD for its transfer to the core domain following the affinity gradient [20]. Although presequence binding to PBD is conserved only among fungal Tim50, that to the core domain is conserved among Tim50 from yeast to human, suggesting the importance of the core domain for further transfer of the presequence to the Tim23 channel for translocation across the inner membrane. It is still open to future studies why only fungi including yeast require presequence binding by PBD in addition to that by the core domain of Tim50.

In summary, the presequence is recognized by PBD in a similar manner to Tom20. PBD can also bind to the core domain of Tim50 through the presequence binding site, which could promote transfer of the presequence from PBD to the core domain in Tim50. Furthermore, binding of Tim50core to PBD may partially lead to formation of a transient ternary complex in the presence of a presequence, which may facilitate efficient and direct

transfer of the presequence from PBD to the core domain. These findings by NMR may provide a basis for understanding of the still-elusive presequence recognition by the complicated protein receptor system in mitochondria for future studies.

Table 2.2.1.

Primers used in this study

PBD (395-476)	CCGCGCGGCAGCCATATGCTCGATTTGATTCATG
	TGTTAGCAGCCGGATCCTTATTTGGATTCAGCAATCTTC
PBD (395-460)	CCGCGCGGCAGCCATATGCTCGATTTGATTCATG
	TGTTAGCAGCCGGATCCTTAGTCTACCTCCTTCTGCTTCTCC
PBD (395-450)	CCGCGCGGCAGCCATATGCTCGATTTGATTCATG
	TGTTAGCAGCCGGATCCTTATTTCATTTGTTCTTCTGGCGAAGG
PBD (390-450)	CCGCGCGGCAGCCATATGAGCACCAAGTTCCCGCTCG
	TGTTAGCAGCCGGATCCTTATTTCATTTGTTCTTCTGGCGAAGG
PBD (400-450)(sPBD)	CCGCGCGGCAGCCATATGGAAGAAGGACAAAAGAAC
	TGTTAGCAGCCGGATCCTTATTTCATTTGTTCTTCTGGCGAAGG
PBD (405-450)	CCGCGCGGCAGCCATATGAACTATTTAATGTTCATGAAG
	TGTTAGCAGCCGGATCCTTATTTCATTTGTTCTTCTGGCGAAGG
sPBD_I413A	TTCATGAAGATGGCAGAGGAAGAAAAG
	CTTTTCTTCCTCTGCCATCTTCATGAA
sPBD_E414A	ATGAAGATGATTGCAGAAGAAAAGGAA
	TTCCTTTTCTTCTGCAATCATCTTCAT
sPBD_E415A	AAGATGATTGAGGCAGAAAAGGAAAAA
	TTTTTCCTTTTCTGCCTCAATCATCTT
sPBD_L434Q	CAAACATTTACGCAGAAAGACTATGTTG
	CAACATAGTCTTTCTGCGTAAATGTTTG
sPBD_K435A	ACATTTACGCTGGCAGACTATGTTGAAG
	CTTCAACATAGTCTGCCAGCGTAAATGT
sPBD_D436A	TTTACGCTGAAAGCATATGTTGAAGG
	CCTTCAACATATGCTTTCAGCGTAAA
Tim50core	CAACTCAATGTTCCATATGTTCCAAGAGCCACC
	AAAGAATTCTTACAATTTTTTCACACGATGATC

Table. 2.3.1. Different constructs of peptide binding domain (PBD) of yeast Tim50

Region	Properties				
	N–terminal tag	Expression & purification	Propensity	Stability at 37 °C for 1 hr	NMR signal quality
PBD (395-476)	His-Tag	O	α- helix	△	×
PBD (395-460)	His-Tag	O	α- helix	△	×
PBD (395-450)	His-Tag	O	α- helix	△	×
PBD (400-450)	His-Tag	O	α- helix	O	O
PBD (405-450)	His-Tag	O	α- helix	O	Not checked

Table 2.3.2. NMR pulse programs used in the backbone assignments of sPBD

Pulse program	Solvent	Labeling	Number of scan	Time domain
[^{1}H, ^{15}N]-HSQC	93%H_2O/7%D_2O	^{15}N	16	^{1}H: 2048, ^{15}N: 256
HNCACB,	93%H_2O/7%D_2O	^{15}N, ^{13}C	16	^{1}H: 2048, ^{15}N: 28 , 13C: 128
CBCA(CO)NH	93%H_2O/7%D_2O	^{15}N, ^{13}C	16	^{1}H: 2048, ^{15}N: 40 , 13C: 128
HNCO	93%H_2O/7%D_2O	^{15}N, ^{13}C	4	^{1}H: 2048, ^{15}N: 40 , 13C: 128
HNCANNH	93%H_2O/7%D_2O	^{15}N, ^{13}C	16	^{1}H: 2048, ^{15}N: 40 , 13C: 128

Table 2.3.3.

Chemical shift index for sPBD based on 3D NMR experiments

Number	Amino	CA	CB	N	NH	CO
400	E	54.2	27.43	122	8.369	174.3
401	E	55.11	27.27	121.9	8.427	174.9
402	G	43.23	-	108.8	8.362	172.3
403	Q	54.16	26.25	120.1	8.003	174.1
404	K	55.38	29.83	121.2	8.183	174.7
405	N	51.83	35.72	118.3	8.292	173.5
406	Y	57.73	35.78	121.8	8.084	175.5
407	L	54.55	39.02	119.9	8.028	176.7
408	M	54.91	29.38	118.6	7.877	175.1
409	F	57.28	36.27	120.9	7.979	174.2
410	M	54.34	29.39	118.1	8.067	175.4
411	K	55.53	29.61	120.6	7.851	173.1
412	M	55.19	29.86	119.7	7.866	175.5
413	I	60.7	34.95	120.3	7.848	175.4
414	E	56.04	26.78	121.4	8.027	176.1
415	E	56.13	27	120.3	8.285	176.1
416	E	55.93	26.27	120.7	8.09	174.2
417	K	56.57	29.7	119.3	8.049	176.3
418	E	55.42	26.75	120.2	7.954	174.8
419	K	56.44	29.64	119.7	7.775	176.2
420	I	60.8	35.33	119.5	7.769	174.6
421	R	56.07	29.62	122.7	7.916	175.9
422	I	60.95	35.51	119.5	8.121	175.2
423	Q	55.35	26.07	120.9	7.945	175.1
424	Q	55.18	26.16	119.1	8.257	175.1
425	E	55.26	27.2	120.4	8.204	175.1
426	Q	53.98	26.36	118.7	8.073	174
427	M	53.42	29.91	119.4	8.043	174.4
428	G	42.91	-	109	8.161	172.1
429	G	42.66	-	108.4	8.184	172.7
430	Q	53.31	26.8	119.6	8.165	173.3
431	T	59.27	67.1	115.1	8.093	171.4
432	F	55.1	37.15	122.5	8.179	172.8

Number	Amino	CA	CB	N	NH	CO
433	T	58.86	67.58	116.3	8.124	171.4
434	L	52.94	39.68	124.6	8.182	174.6
435	K	53.99	30.23	121.6	8.142	173.5
436	D	52	38.31	120.2	8.075	173.1
437	Y	55.5	36.22	120.1	7.875	172.8
438	V	59.52	30.29	122.8	7.905	173.1
439	E	54.31	27.31	124.1	8.314	174.2
440	G	42.55	-	109.7	8.225	171.1
441	N	50.21	36.4	118.4	8.171	172
442	L	50.33	39.02	123.4	8.105	-
443	P	59.71	31.85	-	-	173.4
444	S	53.81	60.69	117.9	8.414	-
445	P	61.17	29.22	-	-	174.7
446	E	54.56	27.22	119.7	8.405	174.3
447	E	54.03	27.62	121.3	8.166	173.8
448	Q	53.28	26.77	120.6	8.158	173.2
449	M	53.06	30.16	122	8.234	172.5
450	K	55.12	31.02	127.9	7.823	-

Table 2.3.4

K_d values for sPBD binding elements in pSu9N

Residue	Sum of square of error (SSE)	Parameters	
		Shift (ppm)	K_d (mM)
L11	0.0008613	0.042	0.304
A12	0.001515	0.035	0.123
A16	0.0008404	0.031	0.286
V21	0.0005303	0.026	0.084

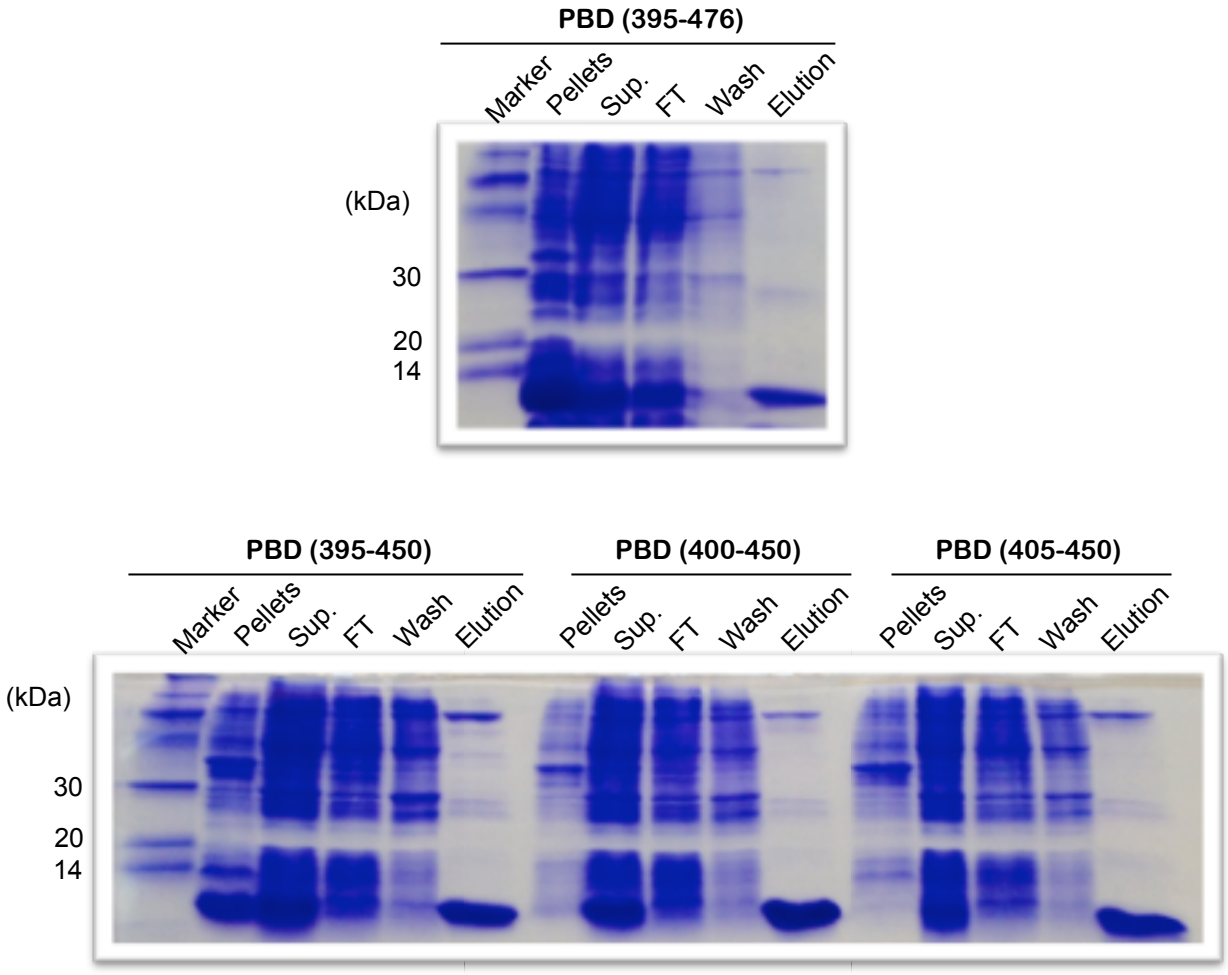

Figure 2.3.1. Expression and solubility level of PBD and its segments, and Ni-NTA column chromatography purification.

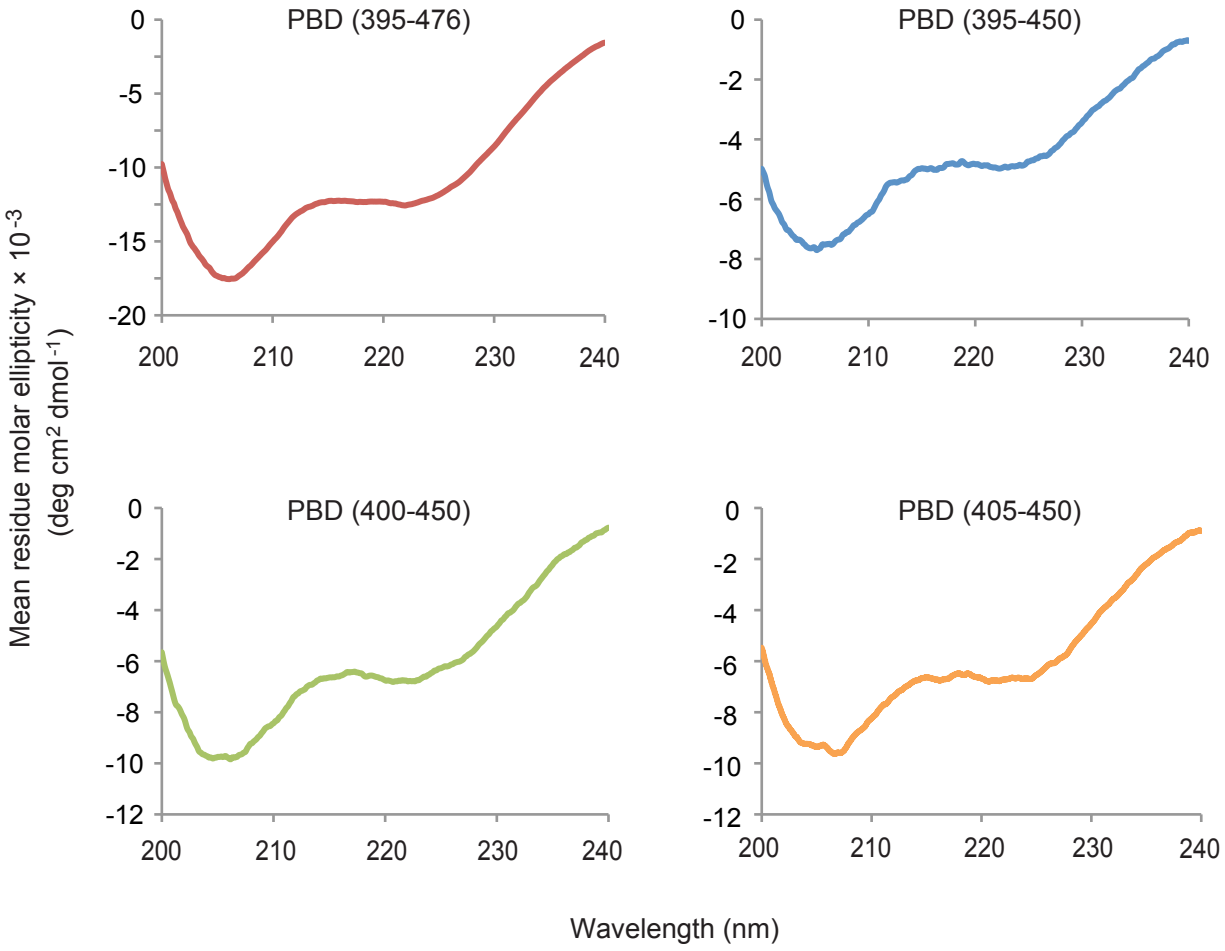

Figure 2.3.2. CD spectrum of indicated PBD constructs

A circular dichroism (CD) spectrum was recorded in 20 mM KPi (pH 6.7) containing 50 mM KCl at 25°C.

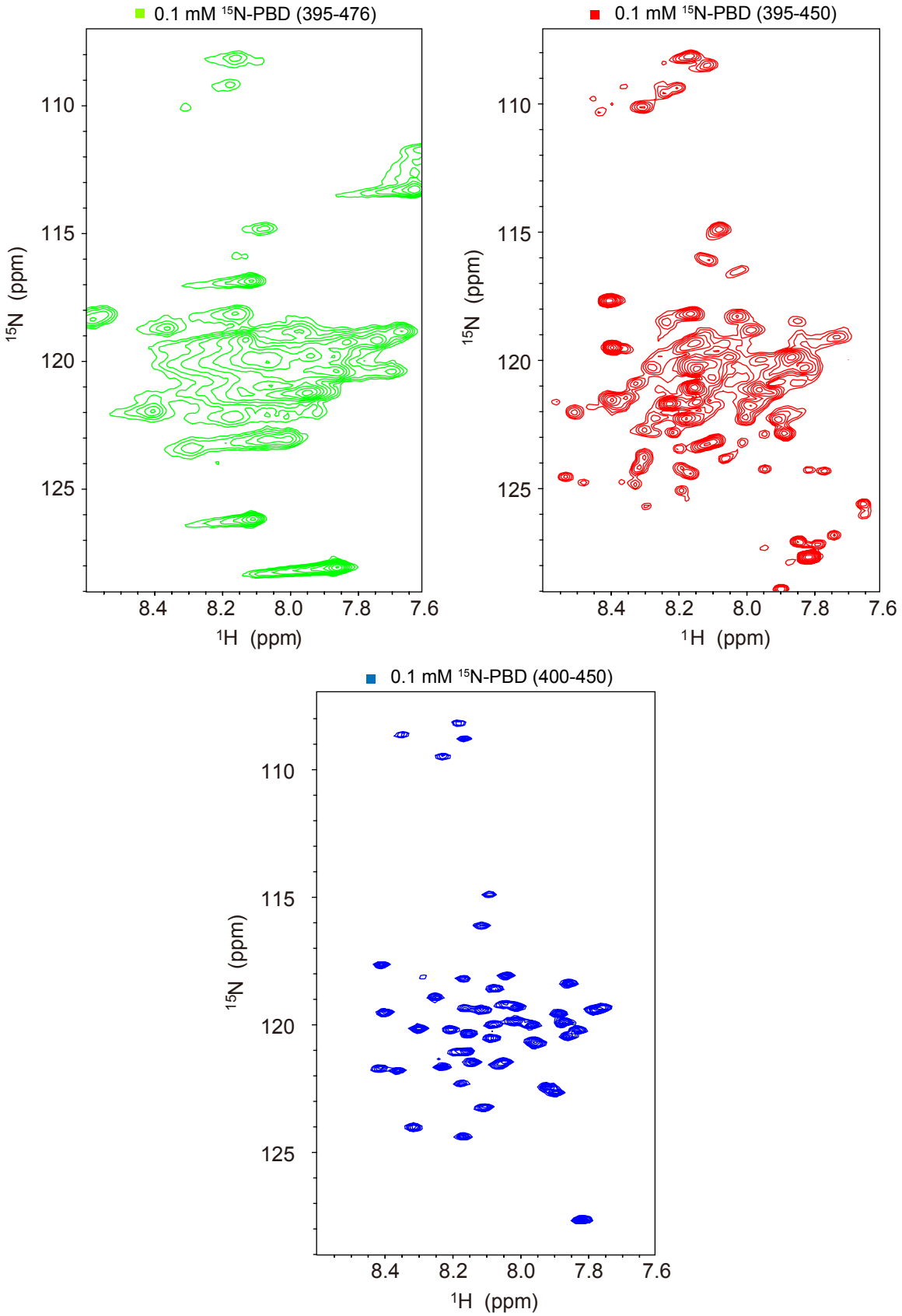

Figure 2.3.3. NMR spectra of PBD and its truncated segments

A two-dimensional [^{1}H, ^{15}N]-HSQC spectrum of PBD$^{395\text{-}476}$, PBD$^{395\text{-}450}$, and PBD$^{400\text{-}450}$ was recorded in the presence of 20 mM KPi, pH 6.7, 50 mM KCl, D_2O/H_2O (7/93) at 26°C.

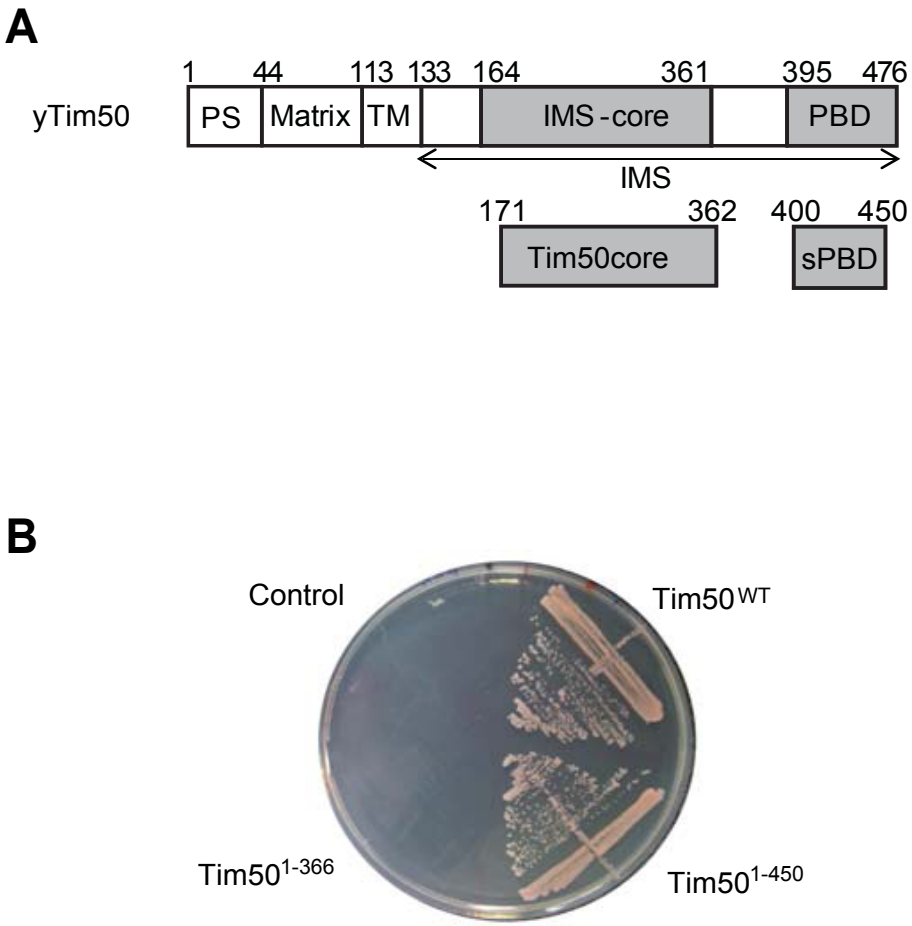

Figure 2.3.4. Tim50$^{1-450}$ can replace full-length Tim50 in yeast cells (Dr. Kaori Esaki of Professor Endo`s laboratory contributed to this result)

(A) Domain arrangement of yeast Tim50 (yTim50) and its segments used in this study

(B) Wild type Tim50 (WT) and Tim50 truncation mutants containing the first 366 or 450 amino acids (Tim50$^{1-366}$, Tim50$^{1-450}$) in pRS314 were used to replace the wild-type protein-encoding plasmid carrying URA3 in the gene deletion strain grown on 5-fluoroorotic acid-containing plates at 30°C. The empty pRS314 was used for negative control (control).

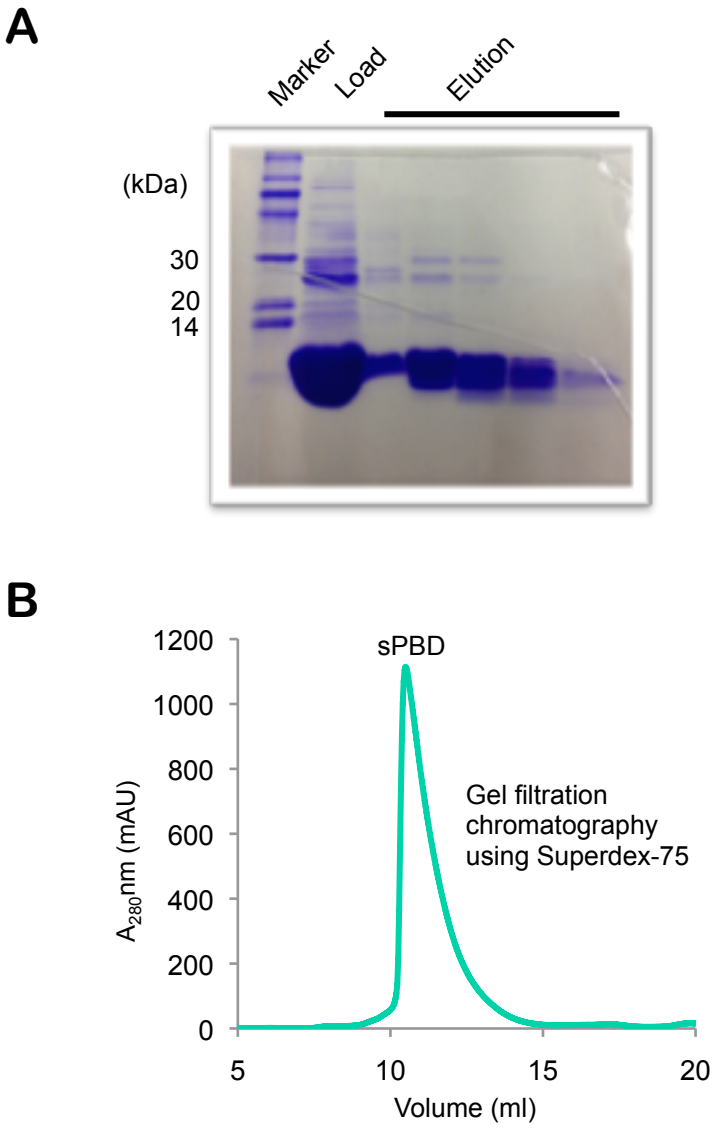

Figure 2.3.5. Purification of sPBD

(A) Purified sPBD protein was analysed by SDS-PAGE and CBB staining

(B) Elution pattern of sPBD was captured by gel-filtraion chromatography

.

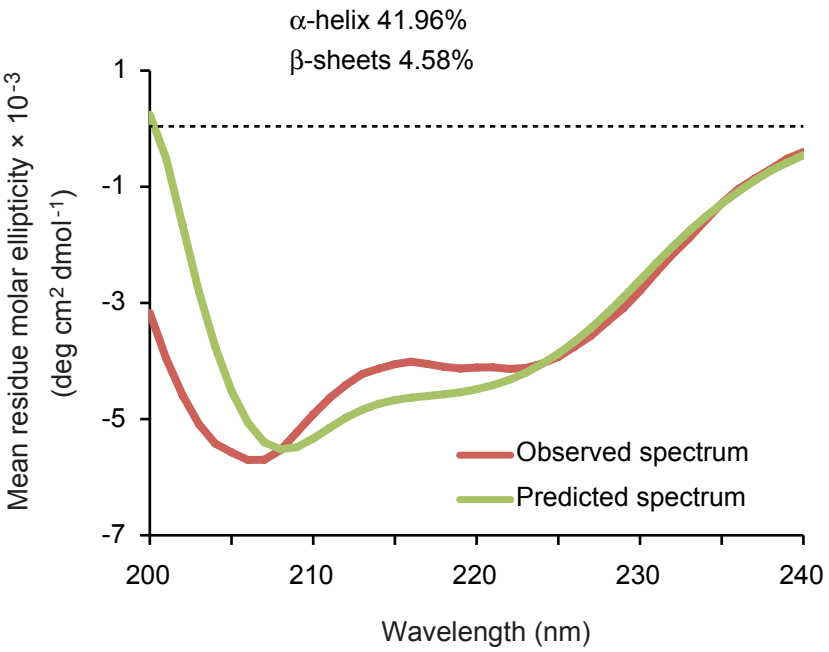

Figure 2.3.6. sPBD is an α-helix rich protein

A circular dichroism (CD) spectrum was recorded at 10 μM protein concentration in 20 mM KPi (pH 6.7) containing 50 mM KCl at 25°C. The overall secondary structural content was calculated using K2D3 method.

.

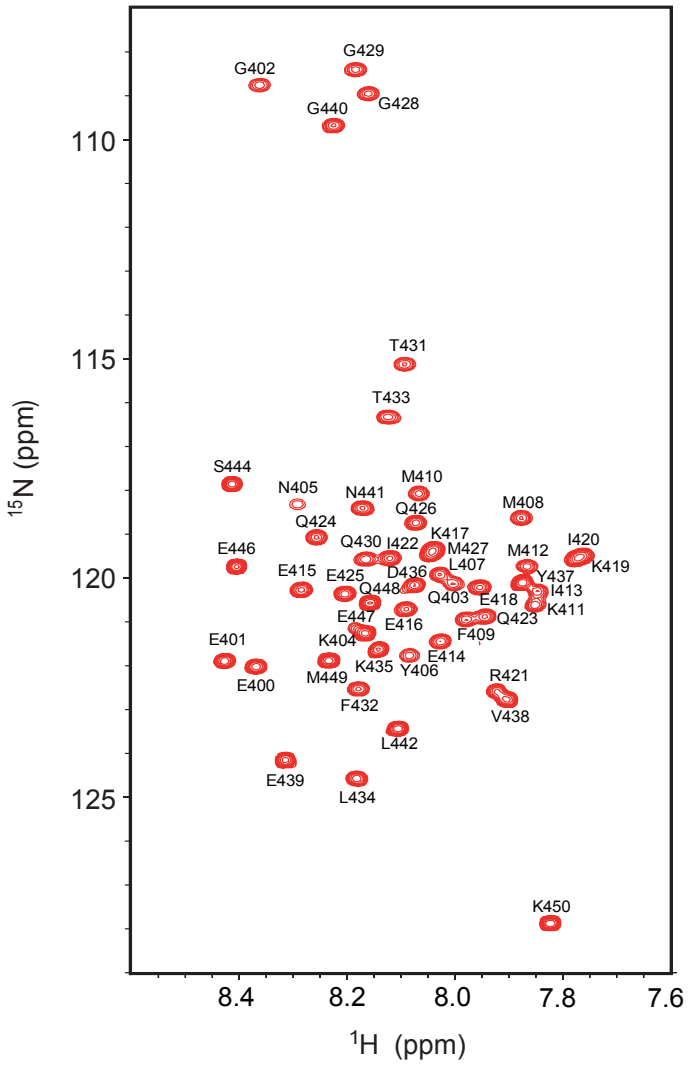

Figure 2.3.7. Backbone signal assignments of sPBD

Two-dimensional [^{1}H, ^{15}N]-HSQC spectrum of sPBD was recorded in the presence of 20 mM KPi, pH 6.7, 50 mM KCl, D_2O/H_2O (7/93) at 25°C.

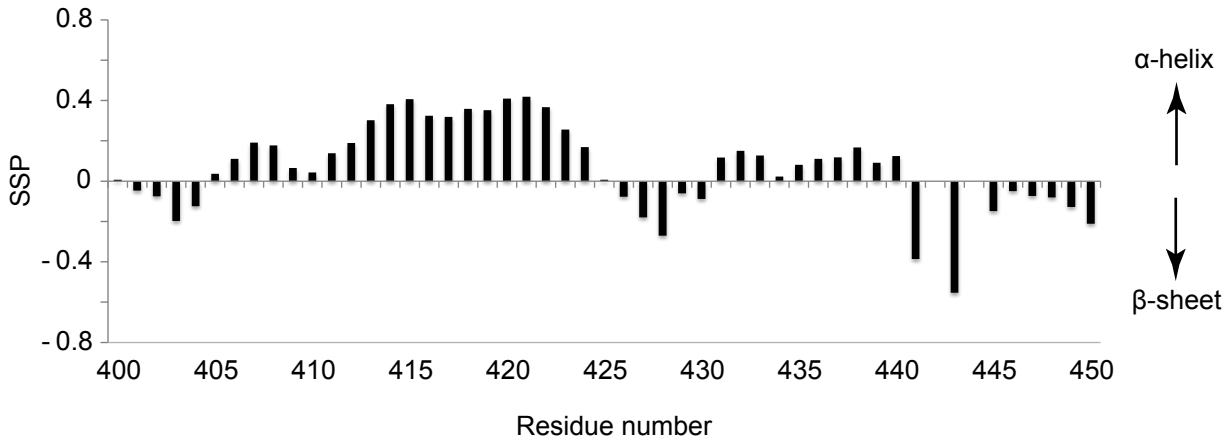

Figure 2.3.8. Secondary structure propensity (SSP) of sPBD

SSP scores for sPBD were calculated using $^{13}C_{\alpha}$ and $^{13}C_{\beta}$ chemical shifts, plotted against residue number. Positive values specify α-helix propensity and negative values specify β-structure propensity.

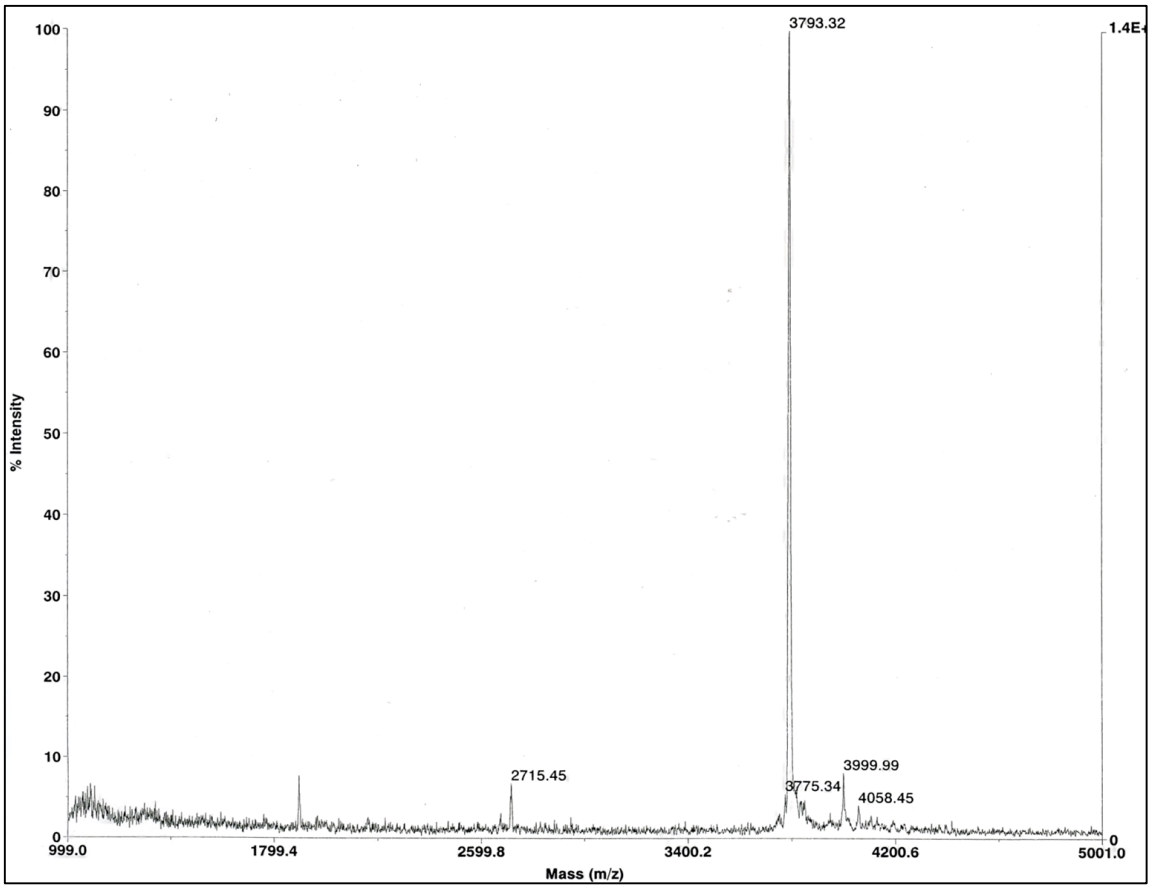

Figure 2.3.9. Mass spectrum of the presequence peptide pSu9N

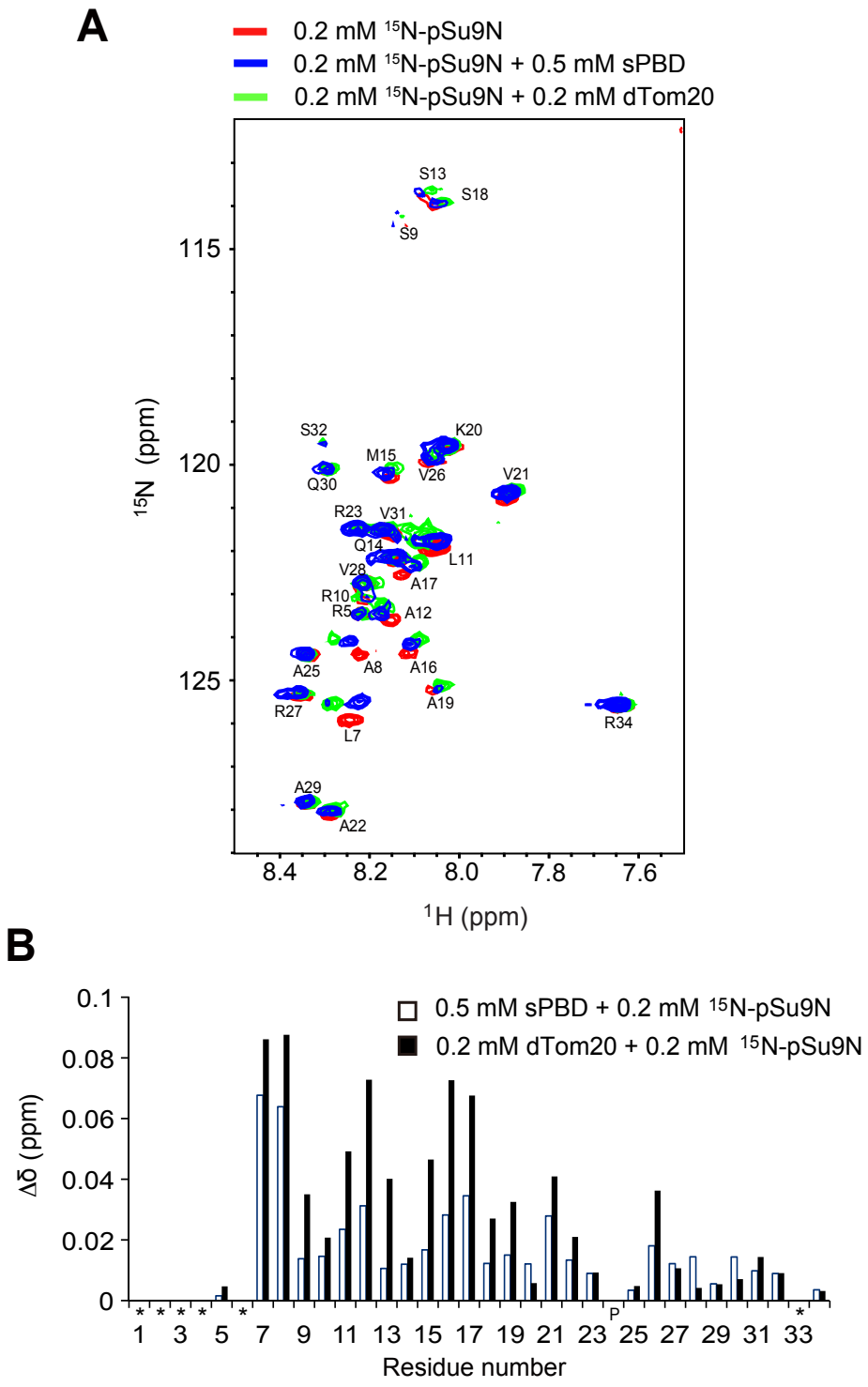

Figure 2.3.10. Binding elements of pSu9N are similar for sPBD and dTom20

(A) [^{1}H, ^{15}N]-HSQC spectra of ^{15}N-labeled pSu9N (0.2 mM) were recorded before (red) or after addition of 0.5 mM sPBD (blue) or 0.2 mM dTom20 (green) in 20 mM KPi, pH 6.7, 50 mM KCl, D_2O/H_2O (7/93) at 26 °C.

(B) The chemical-shift perturbations of backbone amides in [^{1}H, ^{15}N]-HSQC spectra of 0.2 mM ^{15}N-labeled pSu9N in the presence or absence of 2.5-fold excess of sPBD (blank bar) or the same concentration of dTom20 (filled bar).

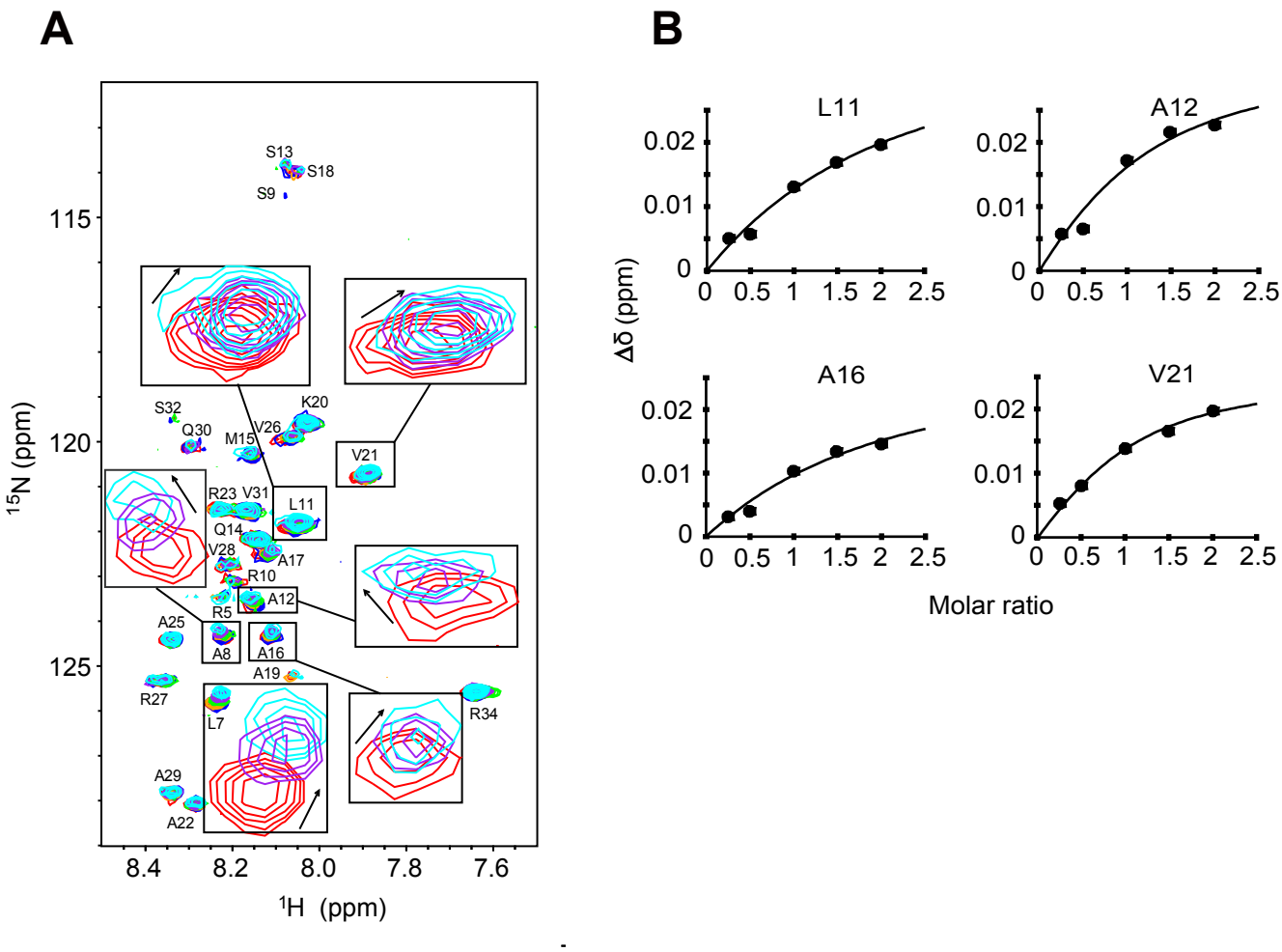

Figure 2.3.11. Binding affinity of the pSu9N to sPBD

(A) Superposition of two dimensional [^{1}H, ^{15}N]-HSQC spectra of pSu9N without sPBD (red) and upon addition of sPBD at molar ratios (pSu9N : sPBD) of 1 : 0.25 (Blue), 1 : 0.5 (orange), 1 : 1 (green), 1 : 1.5 (purple), 1 : 2 (cyan). Shift directions for each signal are indicated by arrows in the magnifications (showing peaks for pSu9N : sPBD = 1:0, 1:1.5, and 1:2).

(B) Chemical shift perturbations as a function of sPBD concentration for residues L11, A12, A16, and V21 of pSu9N in [^{1}H, ^{15}N]-HSQC spectra were analysed and fitted well to binding curves obtained by an nonlinear iterative fitting procedure. The dissociation constant, K_d were obtained for pSu9N binding to sPBD as shown in Table 2.3.4.

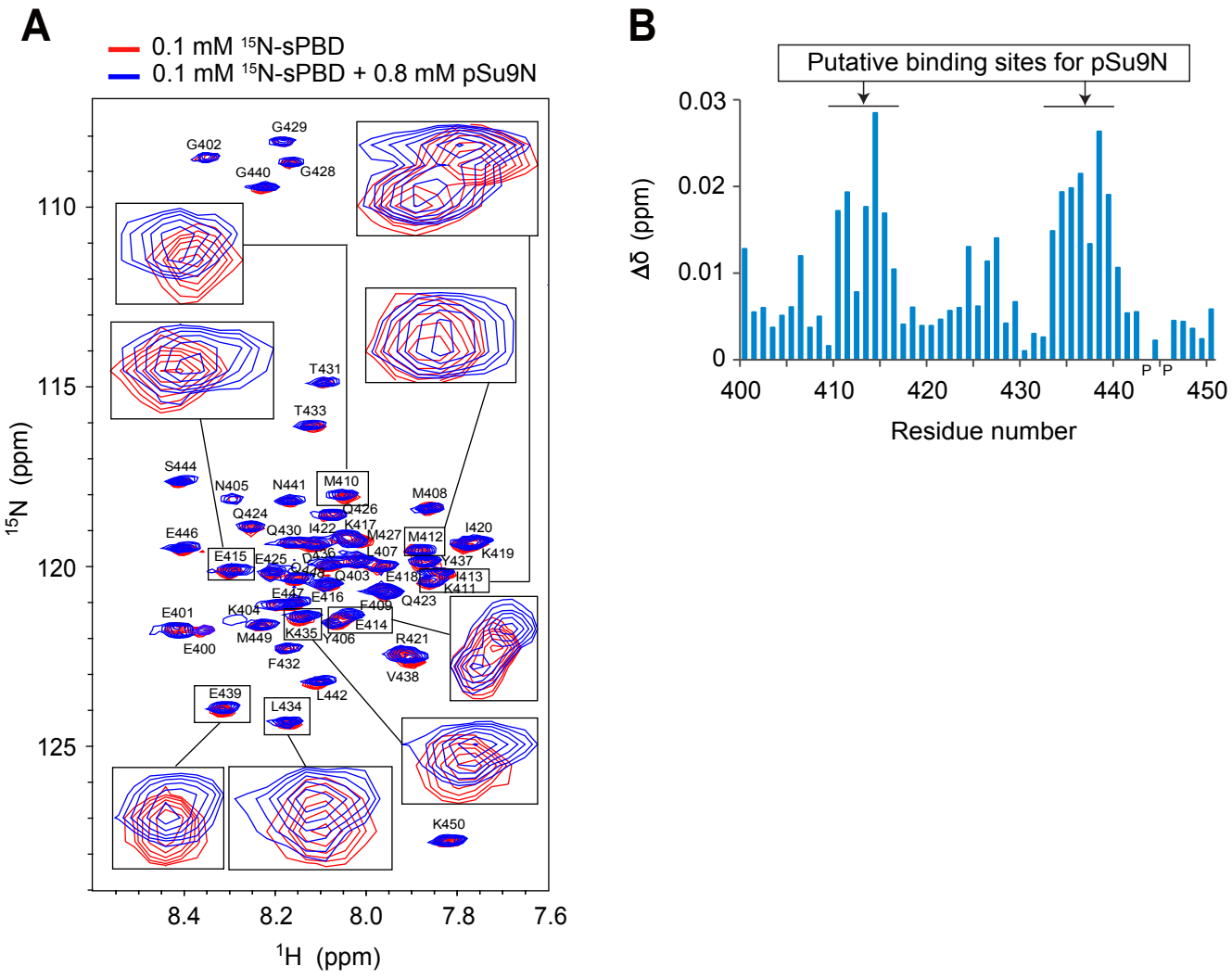

Figure 2.3.12. Two distinct binding sites of sPBD map out for pSu9N

(A) [^{1}H, ^{15}N]-HSQC spectra of ^{15}N-labeled sPBD (0.1 mM) were recorded before (red) or after (blue) addition of 0.8 mM pSu9N in 20 mM KPi, pH 6.7, 50 mM KCl, D_2O/H_2O (7/93) at 26°C.

(B) pSu9N (0.8 mM) induced chemical shift changes of backbone amides in [^{1}H, ^{15}N]-HSQC spectra of ^{15}N-labeled sPBD (0.1 mM) was calculated according to the equation of $[(\Delta\delta\ (^{1}H))^2 + (\Delta\delta\ (^{15}N)/15)^2]^{1/2}$; P, Pro.

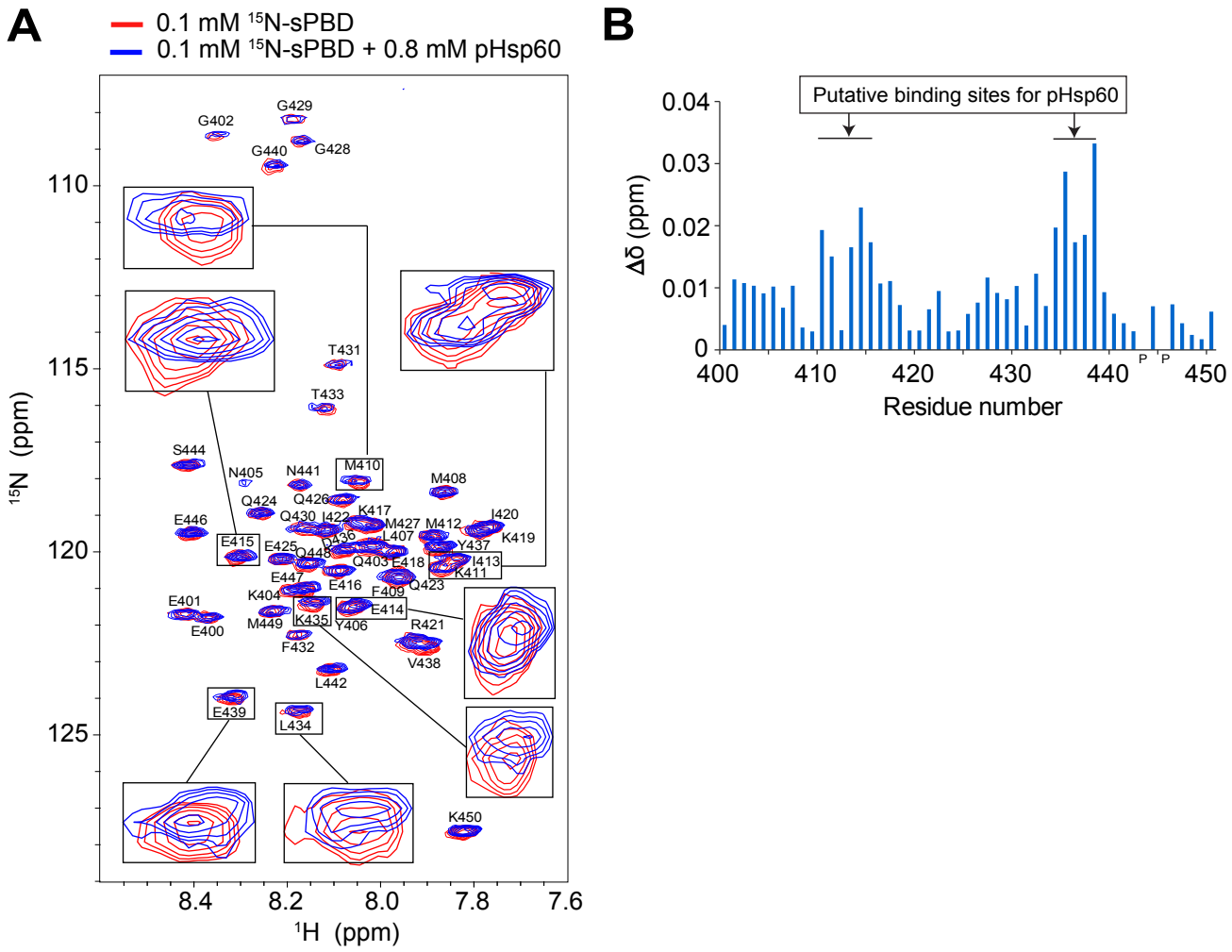

Figure 2.3.13. Binding segment of sPBD for the mitochondrial Hsp60 presequence (pHsp60)

(A) [^{1}H, ^{15}N]-HSQC spectra of 0.1 mM ^{15}N-labeled sPBD with (blue) and without (red) 0.8 mM pHsp60. (B) Chemical shift changes of backbone amides in [^{1}H, ^{15}N]-HSQC spectra spectra of 0.1 mM ^{15}N-labeled sPBD with or without 0.8 mM pHsp60. P, Pro.

.

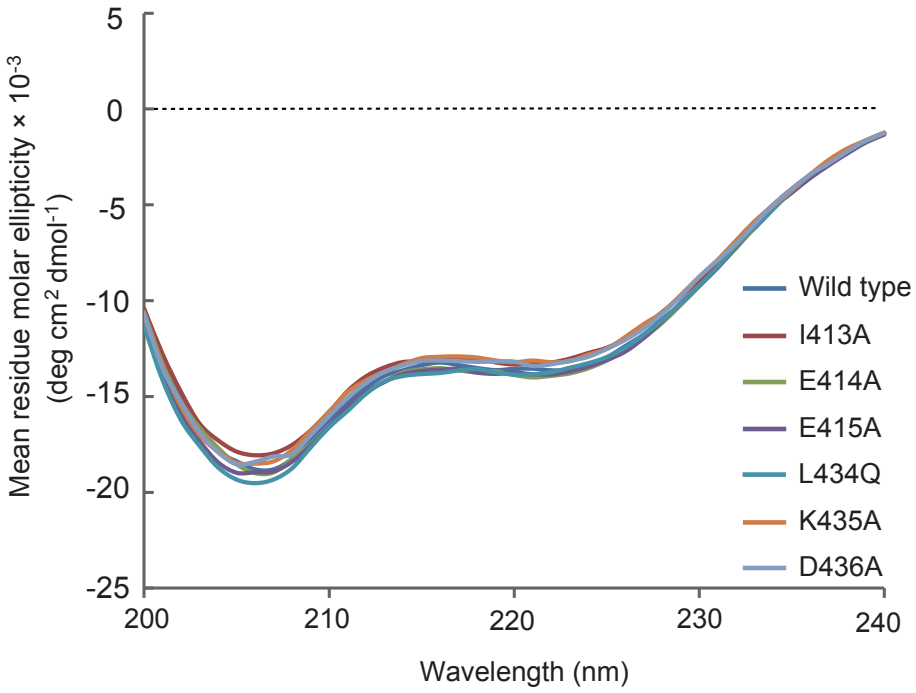

Figure 2.3.14. Mutants sPBD have nearly the same secondary structure as wild type

Superposition of circular dichroism (CD) spectra of wild type sPBD (WT) and six sPBD mutants (I413A, E414A, E415A, L434Q, K435A and D436A), were recorded at 10 μM protein concentration in 20 mM KPi, pH 6.7, containing 50 mM KCl at 25°C

.

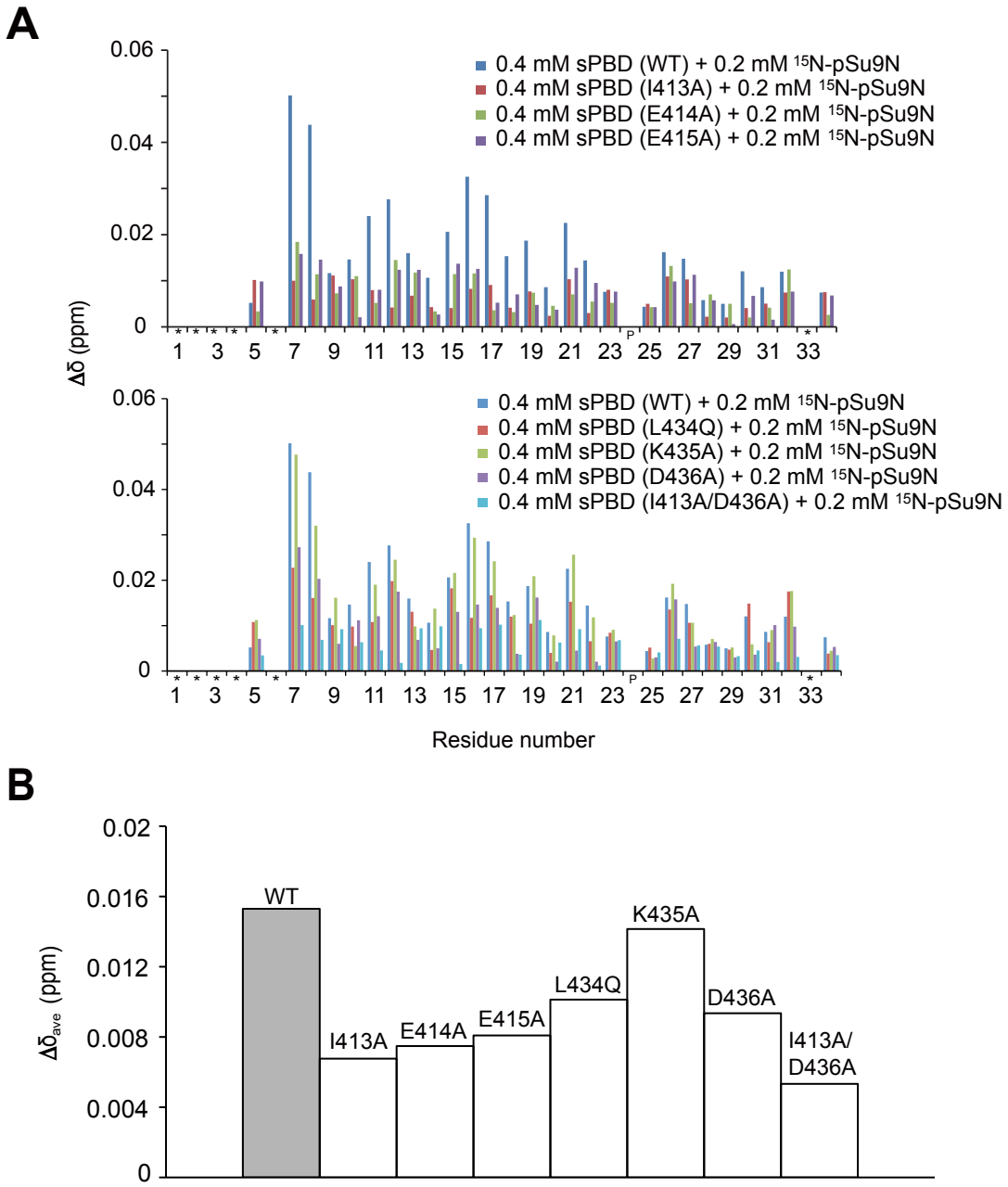

Figure 2.3.15. Effects of mutations on binding of sPBD to pSu9N

(A) Chemical shift changes of backbone amides in [^{1}H, ^{15}N]-HSQC spectra of 0.2 mM ^{15}N-labeled pSu9N with or without 0.4 mM wild-type (WT) and indicated mutant of sPBD. P, Pro; asterisk, signals from these residues were not detected.

(B) Average chemical shift changes for each backbone amide in [^{1}H, ^{15}N]-HSQC spectra of 0.2 mM ^{15}N-labeled pSu9N with or without 0.4 mM wild-type (WT) and indicated mutant of sPBD.

.

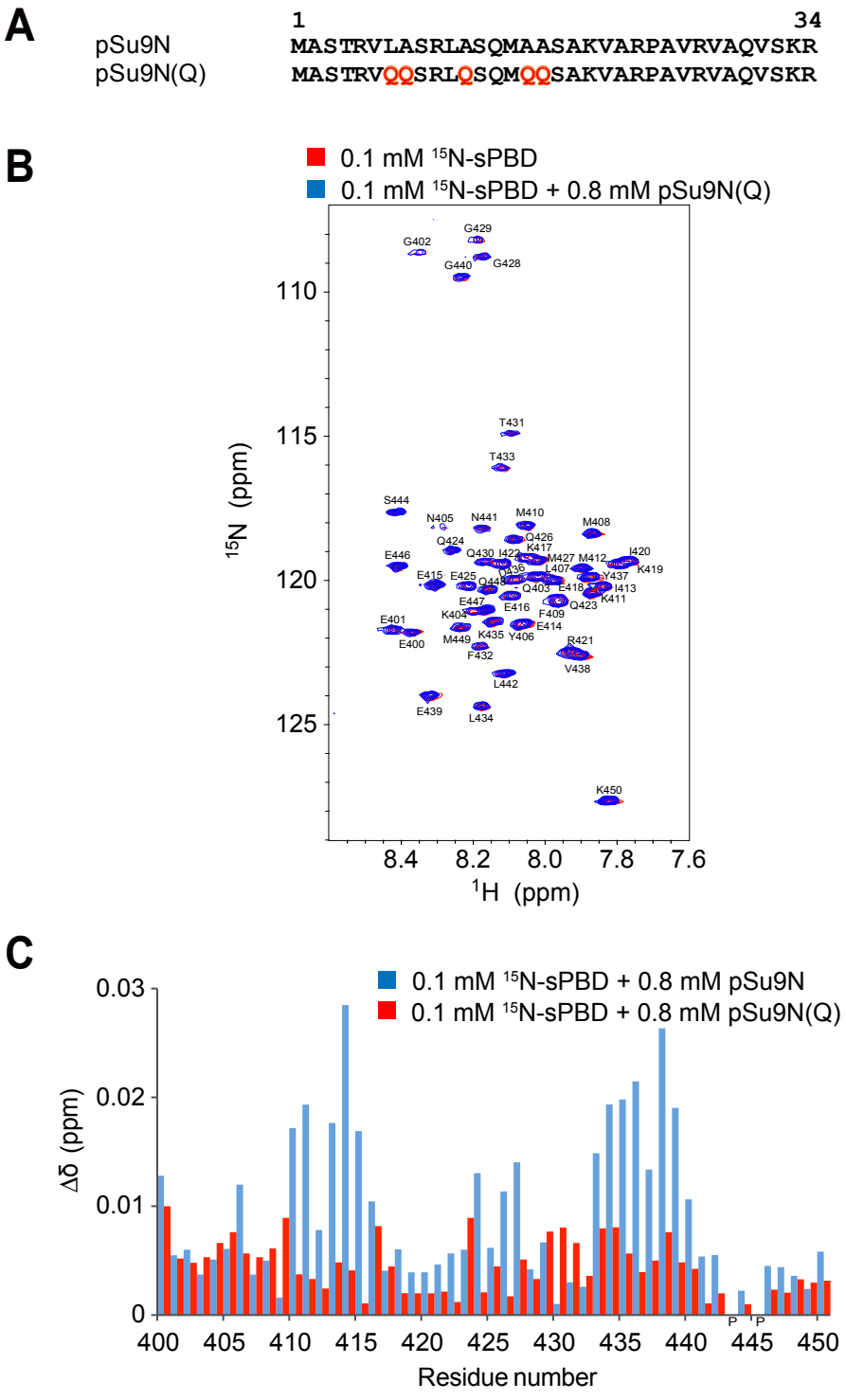

Figure 2.3.16. Hydrophobic residues in pSu9N are important for its binding to sPBD

(A) Amino acid sequences of wild type pSu9N and its mutant pSu9N(Q) with 5 Gln replacement.

(B) [^{1}H, ^{15}N]-HSQC spectra of ^{15}N-labeled sPBD (0.1 mM) were recorded before (red) or after (blue) addition of 0.8 mM presequence pSu9N(Q) in 20 mM KPi, pH 6.7, 50 mM KCl, D_2O/H_2O (7/93) at 26°C.

(C) Chemical shift changes of backbone amides in [^{1}H, ^{15}N]-HSQC spectra of 0.1 mM ^{15}N-labeled sPBD before or after addition of 0.8 mM pSu9N (blue bar) or 0.8 mM pSu9N(Q) (red bar).

.

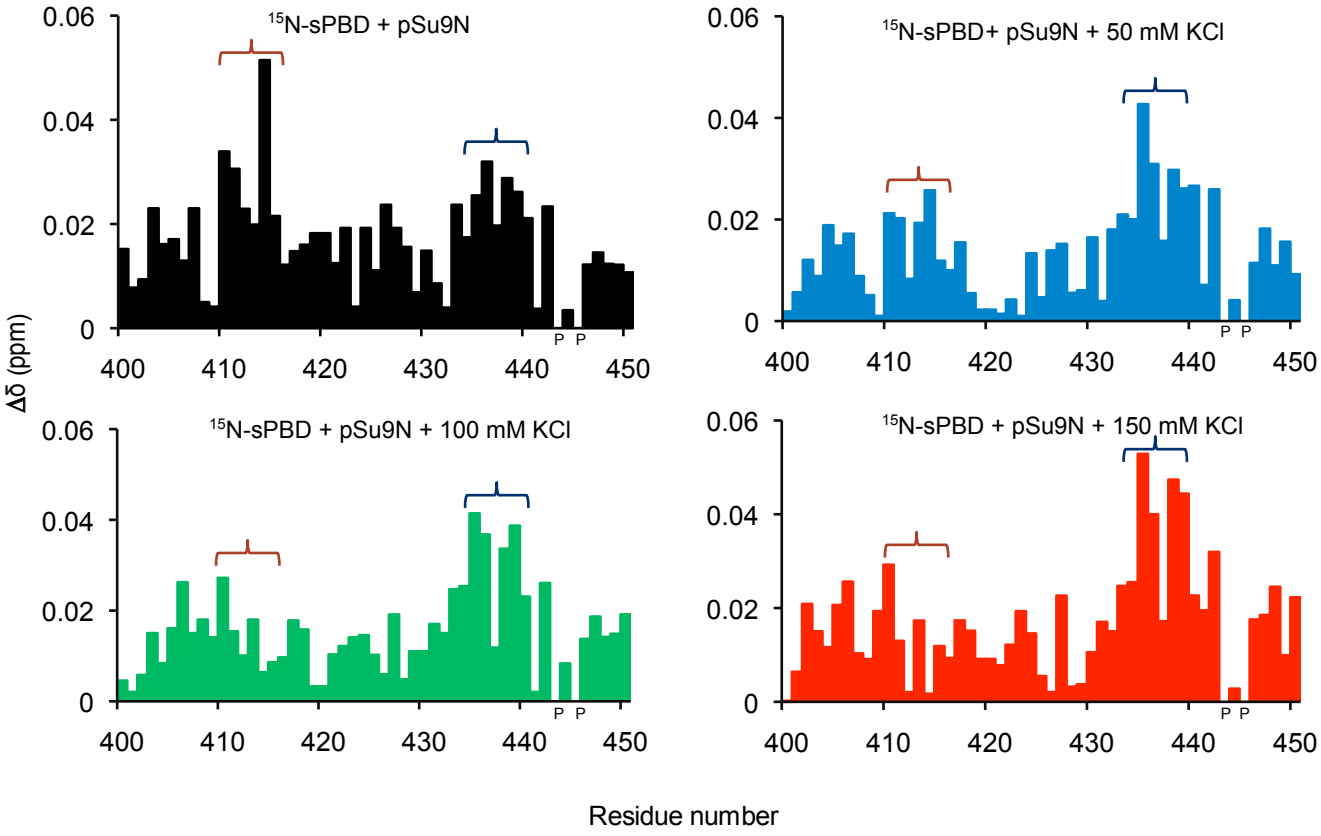

Figure 2.3.17. Effects of salt concentration on sPBD-presequence interactions

Chemical shift changes of the backbone amides in [^{1}H, ^{15}N]-HSQC spectra of 0.1 mM ^{15}N-labeled sPBD with or without 0.8 mM pSu9N in 20 mM KPi, pH 6.7, with KCl at 0 mM (black), 50 mM (blue), 100 mM (green), or 150 mM (red).

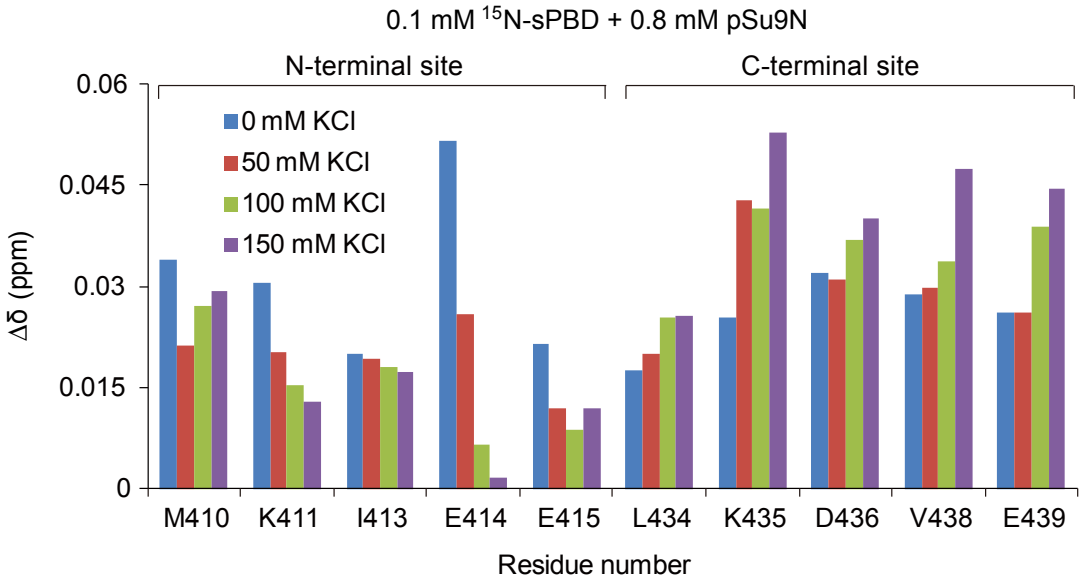

Figure 2.3.18. sPBD-presequence interaction is responsive to high-salt concentrations

Chemical shift changes of the indicated backbone amides in [^{1}H, ^{15}N]-HSQC spectra of 0.1 mM ^{15}N-labeled sPBD with or without 0.8 mM pSu9N in 20 mM KPi, pH 6.7, with KCl at 0 mM (blue), 50 mM (red), 100 mM (green), or 150 mM (purple).

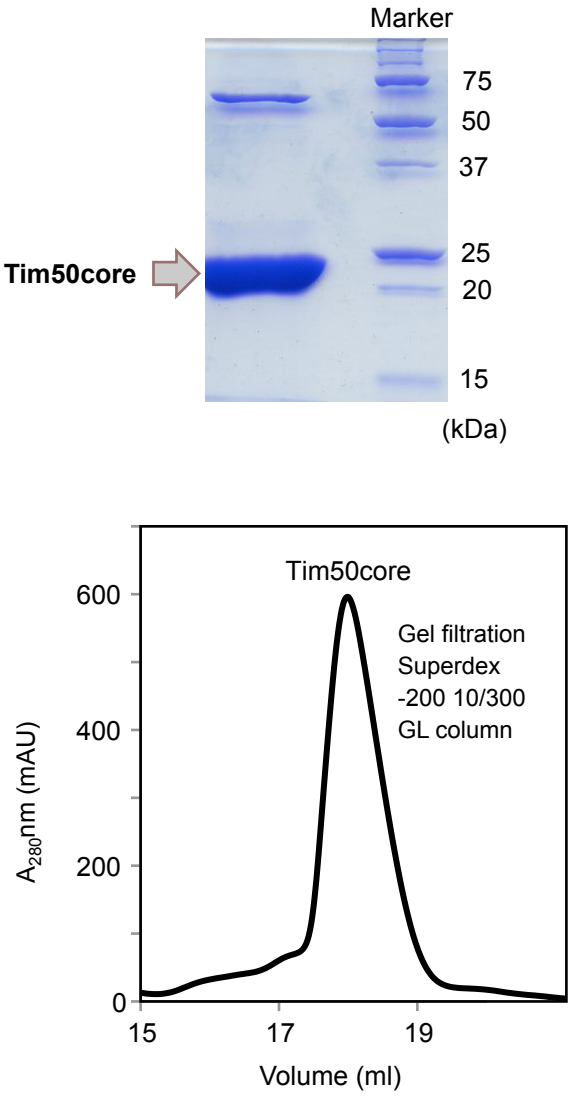

Figure 2.3.19. Purification of Tim50core

(A) Purified Tim50core protein was analysed by SDS-PAGE and CBB staining

(B) Elution pattern of Tim50core was captured by gel-filtraion chromatography

.

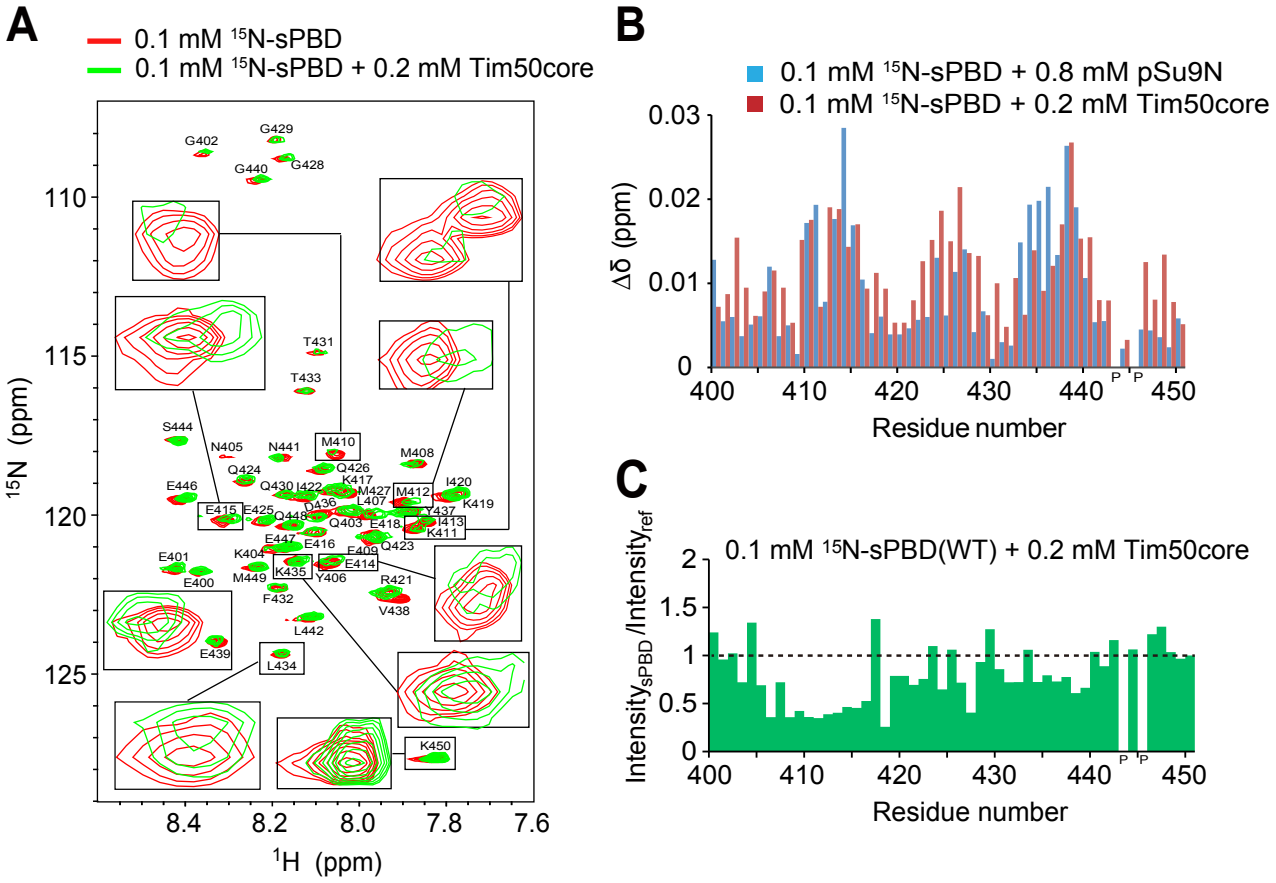

Figure 2.3.20. sPBD binds to Tim50core and pSu9N in a similar manner

(A) [^{1}H, ^{15}N]-HSQC spectra of 0.1 mM ^{15}N-labeled sPBD with (green) and without (red) 0.2 mM Tim50core.

(B) Chemical shift changes of backbone amides in [^{1}H, ^{15}N]-HSQC spectra of 0.1 mM ^{15}N-labeled sPBD with or without 0.8 mM pSu9N (blue bar) or 0.2 mM Tim50core (red bar). P, Pro.

(C) Signal intensity changes of backbone amides in [^{1}H, ^{15}N]-HSQC spectra of 0.1 mM ^{15}N-labeled sPBD with or without 0.2 mM Tim50core as in (A). The signal intensity of K450 is used as an internal reference. P, Pro.

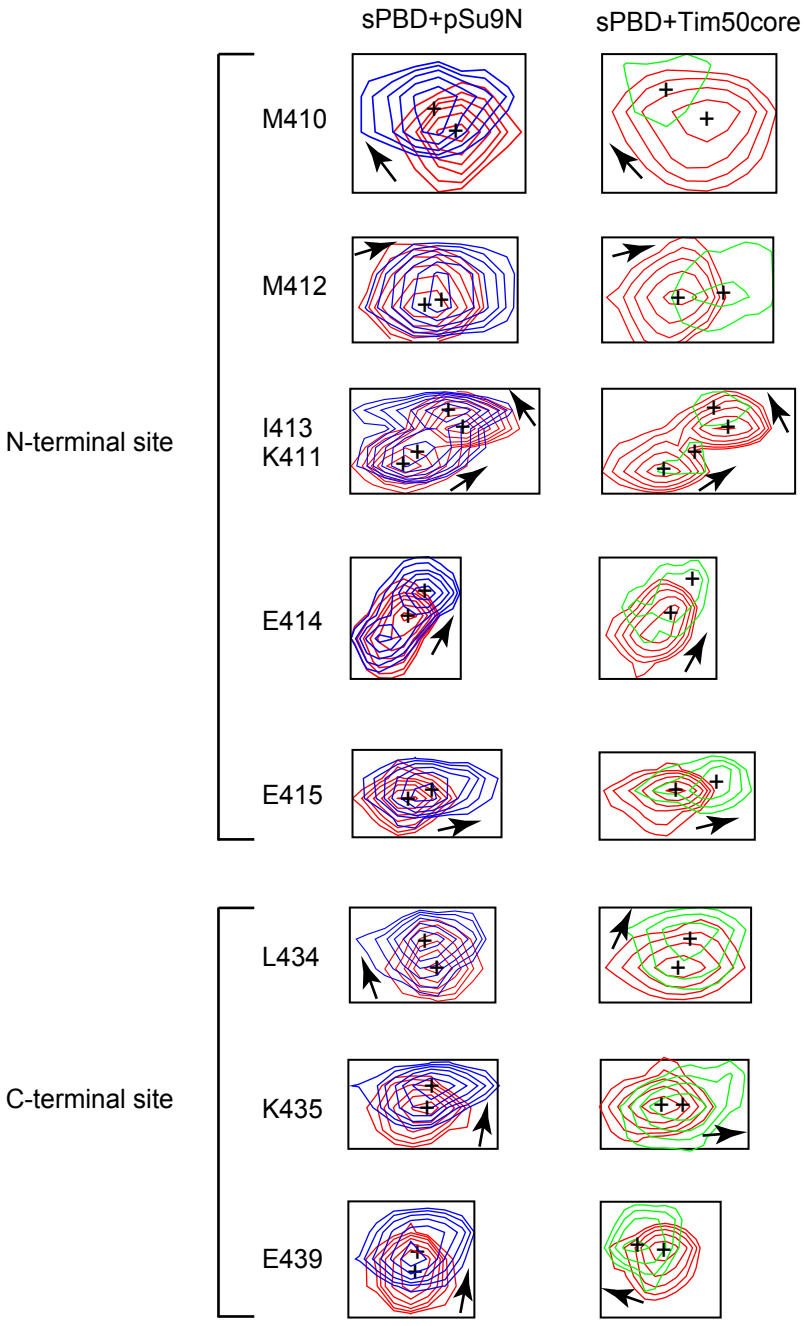

Figure 2.3.21. Direction of the sPBD signals upon addition of pSu9N and Tim50core

Comparison of chemical shift changes for the indicated signals between Fig. 2.3.12A and Fig. 2.3.20A. Peak top positions and shift directions for each signal are indicated by "+" and arrows, respectively, in the magnifications.

.

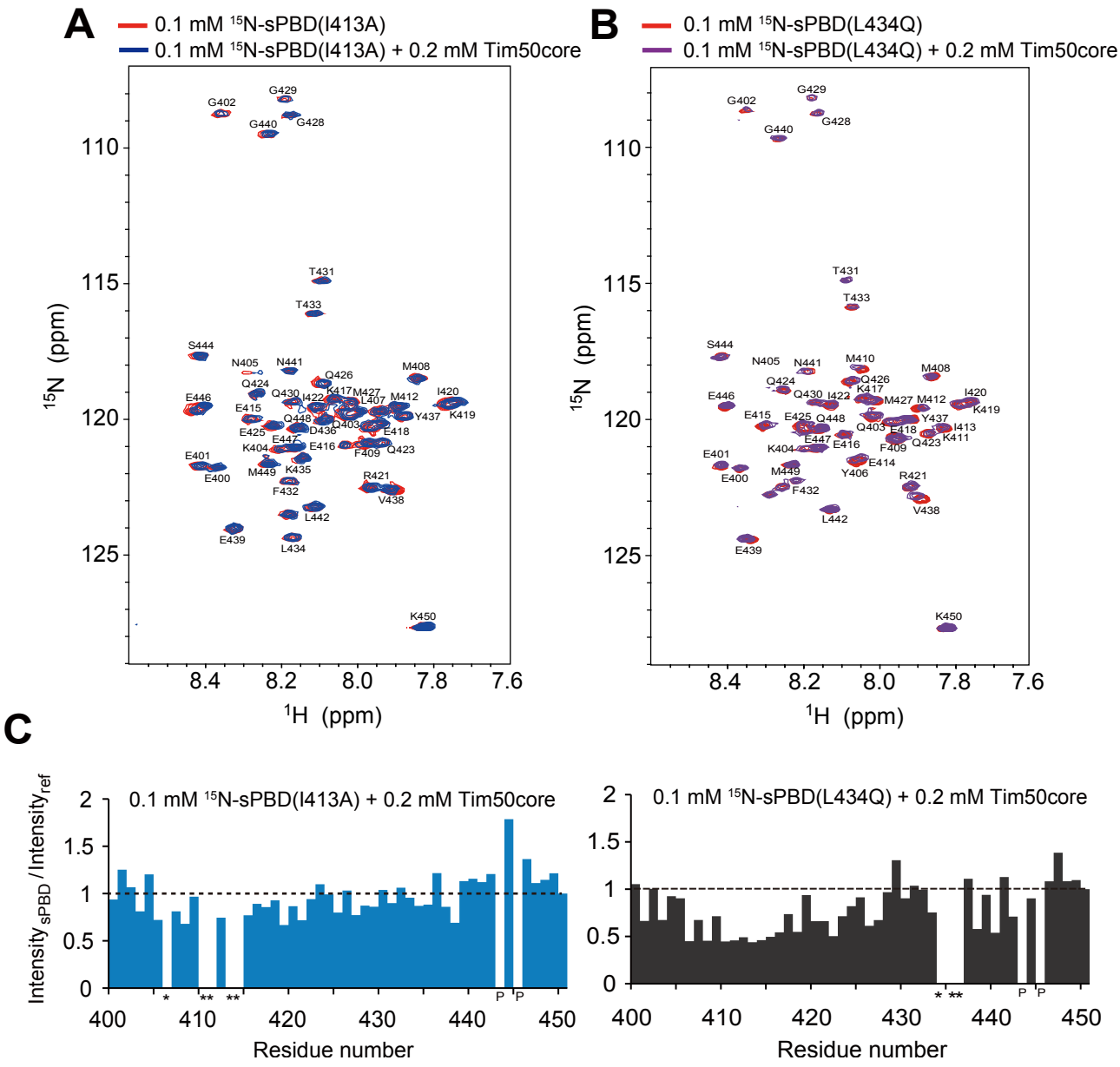

Figure 2.3.22. Effects of mutations on binding of sPBD to Tim50core

(A) [^{1}H, ^{15}N]-HSQC spectra of 0.1 mM ^{15}N-labeled sPBD (I413A) with (blue) and without (red) 0.2 mM Tim50core in 20 mM KPi, pH 6.7, 50 mM KCl, D_2O/H_2O (7/93) at 26°C.

(B) [^{1}H, ^{15}N]-HSQC spectra of 0.1 mM ^{15}N-labeled sPBD (L434Q) with (purple) and without (red) 0.2 mM Tim50core in 20 mM KPi, pH 6.7, 50 mM KCl, D_2O/H_2O (7/93) at 26°C.

(C) Signal intensity changes of backbone amides in [^{1}H, ^{15}N]-HSQC spectra of 0.1 mM ^{15}N-labeled sPBD(I413A) (left panel) or sPBD(L434Q) (right panel) with or without 0.2 mM Tim50core. The signal intensity of K450 is used as an internal reference. P, Pro; asterisk, signals from these residues were not detected.

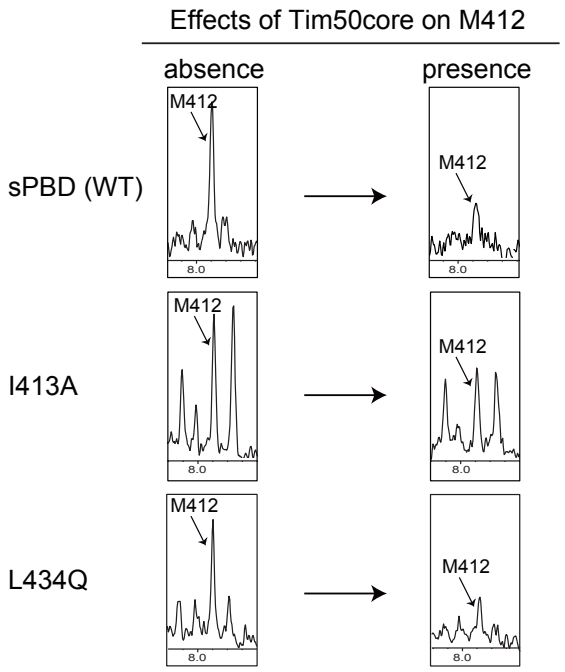

Figure 2.3.23. Effects of mutations on binding of sPBD to Tim50core

Cross sections for the signals of M412 in [^{1}H, ^{15}N]-HSQC spectra of 0.1 mM ^{15}N-labeled sPBD or its mutants (I413A and L434Q) with or without 0.2 mM Tim50core.

.

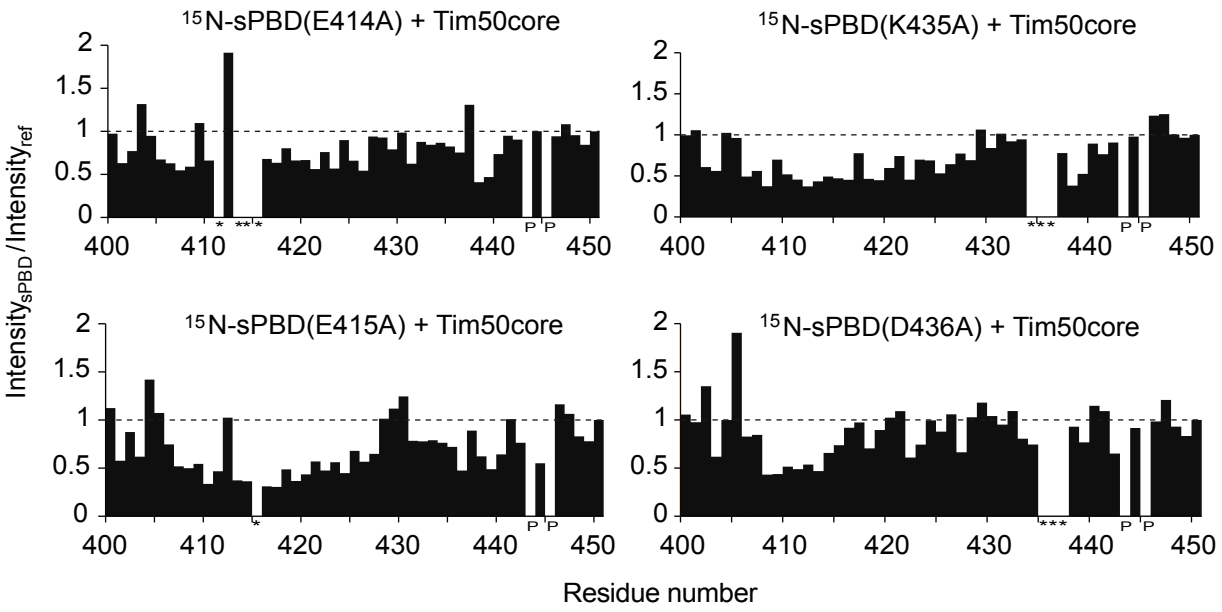

Figure 2.3.24. Effects of mutations on binding of sPBD to Tim50core

Signal intensity changes of backbone amides in [^{1}H, ^{15}N]-HSQC spectra of 0.1 mM ^{15}N-labeled sPBD(E414A) (left upper panel) or or sPBD(E415A) (left lower panel) or sPBD(K435A) (right upper panel) or sPBD(D436A) (right lower panel) with or without 0.2 mM Tim50core. The signal intensity of K450 is used as an internal reference. P, Pro; asterisk, signals from these residues were not detected.

.

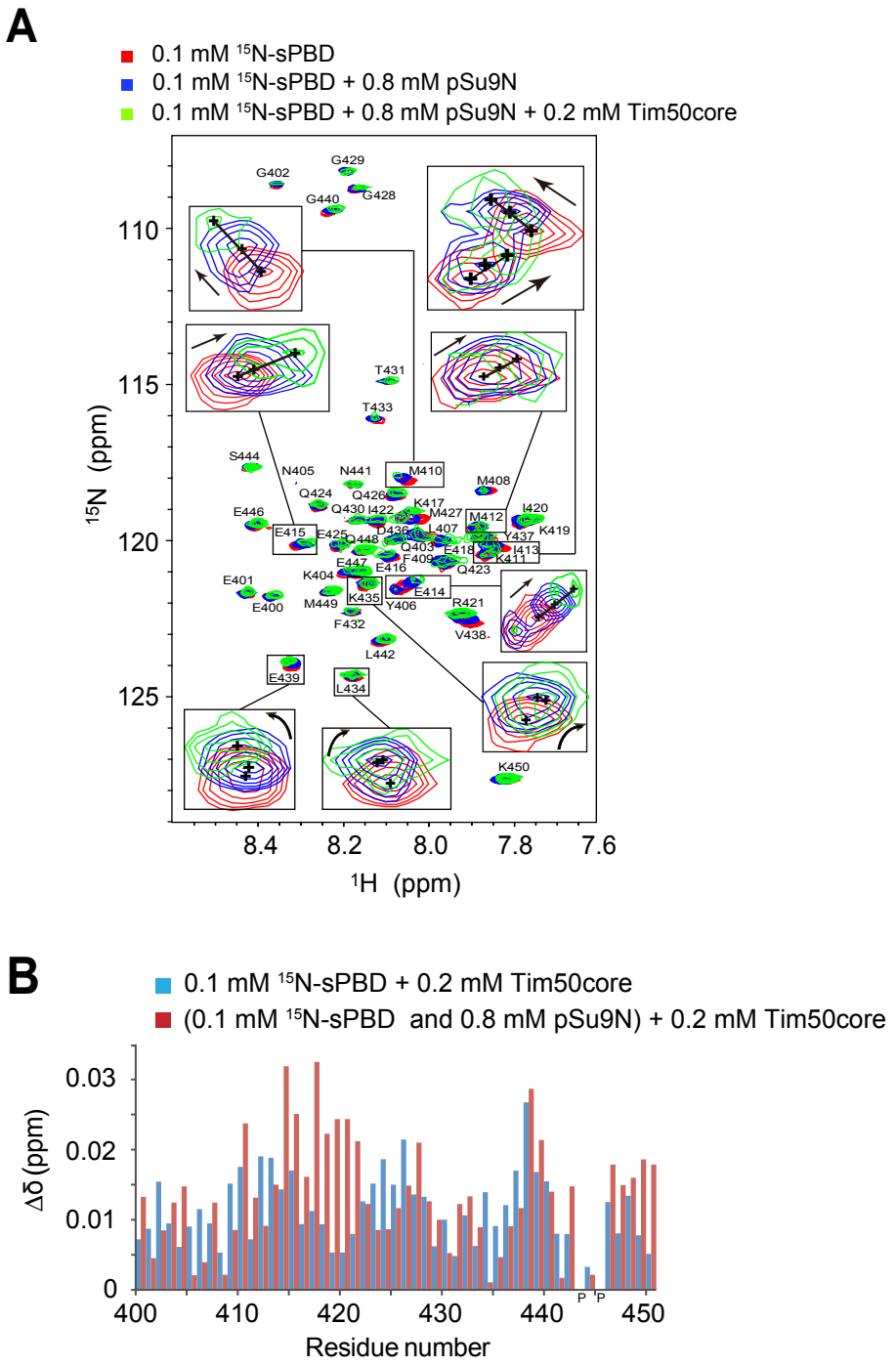

Figure 2.3.25. sPBD likely forms a partial ternary complex

(A) Superposition of [^{1}H, ^{15}N]-HSQC spectra of 0.1 mM ^{15}N-labeled sPBD (red), upon addition of 0.8 mM pSu9N (blue), and upon further addition of 0.2 mM Tim50core (green). Peak top positions and shift directions for each signal are indicated by "+" and arrows, respectively, in the magnifications. (B) Chemical shift changes of backbone amides in [^{1}H, ^{15}N]-HSQC spectra of 0.1 mM ^{15}N-labeled sPBD with or without 0.2 mM Tim50core (blue bar) or those of 0.1 mM ^{15}N-labeled sPBD with or without 0.2 mM Tim50core in the presence of 0.8 mM pSu9N (red bar). P, Pro

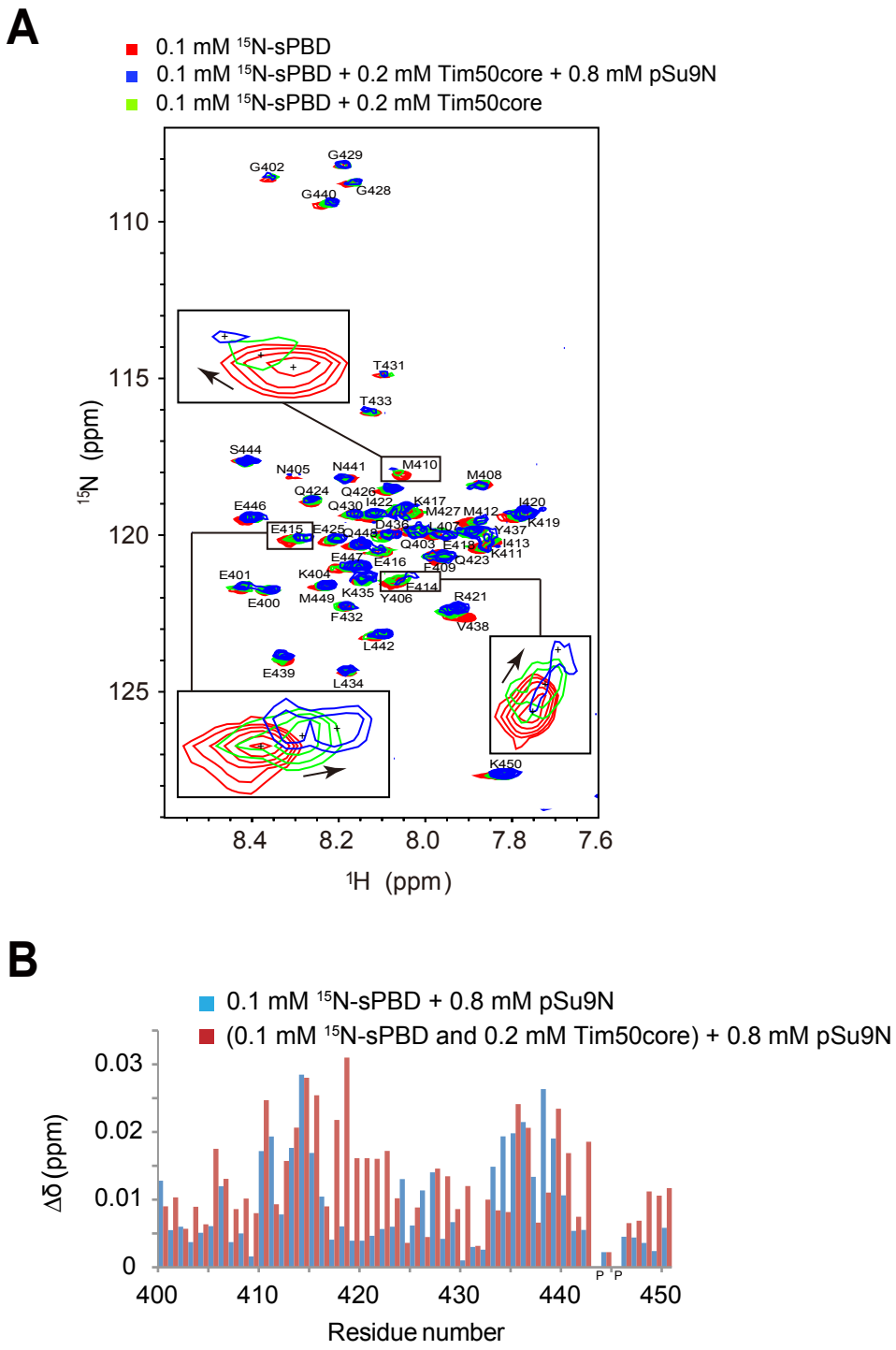

Figure 2.3.26. sPBD partially form a ternary complex

(A) Superposition of [^{1}H, ^{15}N]-HSQC spectra of 0.1 mM ^{15}N-labeled sPBD (red), upon addition of 0.2 mM Tim50core (green), and upon further addition of 0.8 mM pSu9N (blue). Peak top positions and shift directions for each signal are indicated by "+" and arrows, respectively, in the magnifications. (B) Chemical shift changes of backbone amides in [^{1}H, ^{15}N]-HSQC spectra of 0.1 mM ^{15}N-labeled sPBD with or without 0.8 mM pSu9N (blue bar) or those of 0.1 mM ^{15}N-labeled sPBD with or without 0.8 mM Tim50core in the presence of 0.2 mM Tim50core (red bar). P, Pro

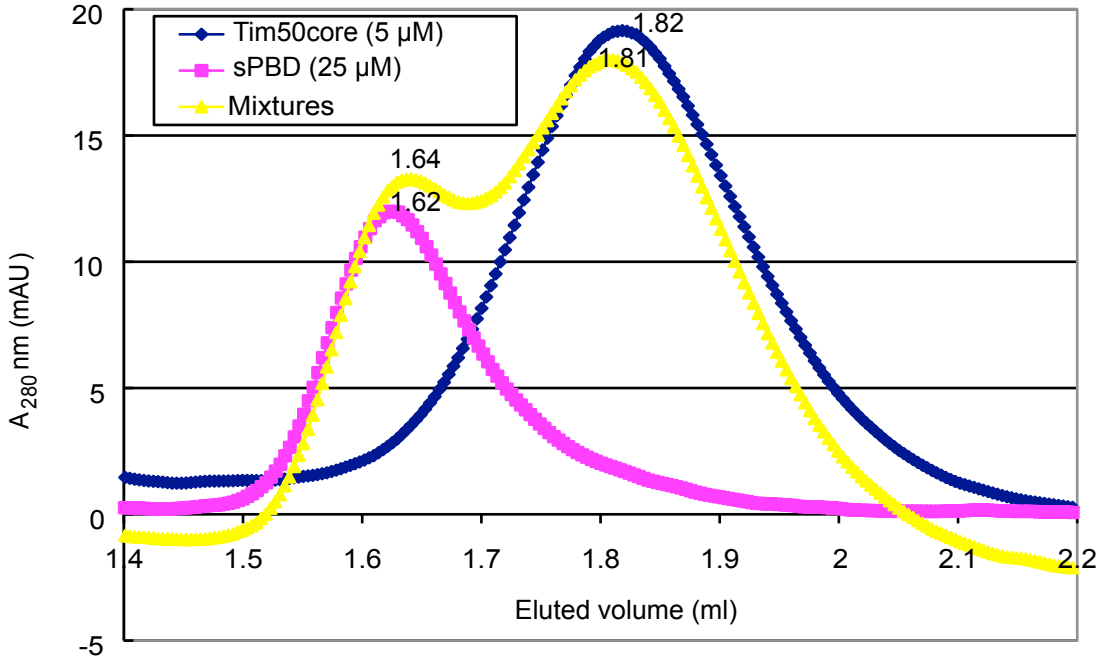

Figure 2.3.27. Analytical gel-filtration analysis of complex formation between sPBD and Tim50core

sPBD, Tim50core and mixtures of them were run on Superdex-75 5/150 GL in a buffer of 20 mM Tris/HCl, pH 7.4, 50 mM NaCl at a flow rate of 0.3 ml/min.

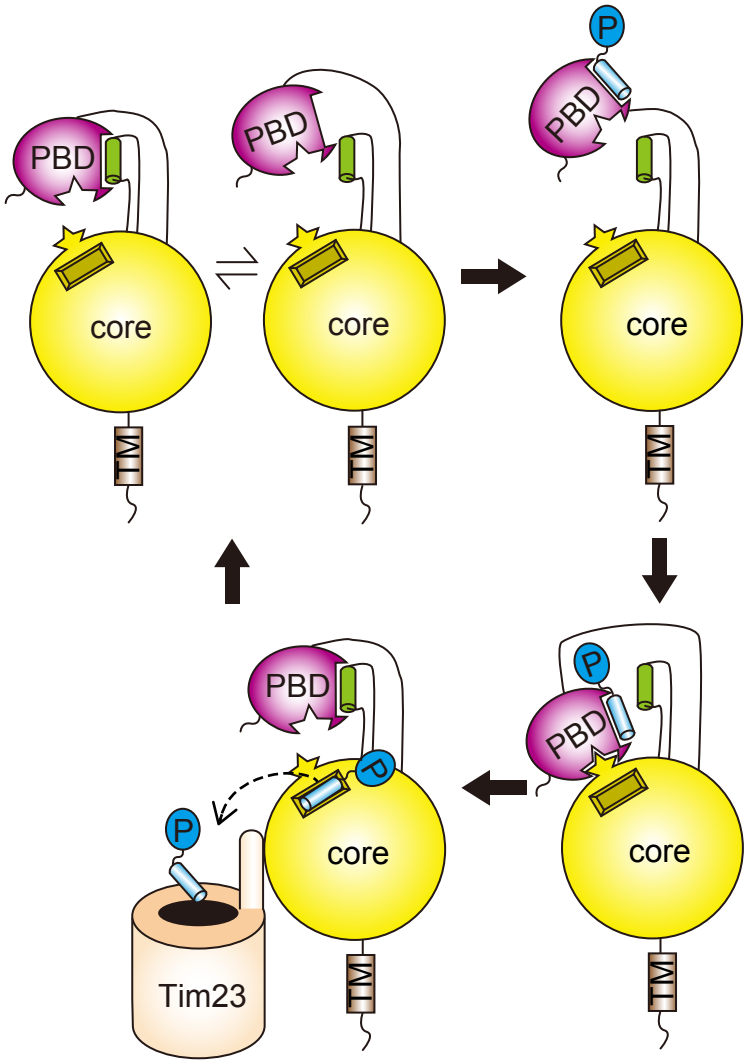

Figure 2.3.28. Proposed model for presequence recognition by PBD and the core domain of Tim50

2.5. References

1. Neupert, W. and Herrmann, J. M. (2007) Translocation of proteins into mitochondria. Annu. Rev. Biochem. 76, 723–749.
2. Chacinska, A., Koehler, C. M., Milenkovic, D., Lithgow, T. and Pfanner, N. (2009) Importing mitochondrial proteins: machineries and mechanisms. Cell 138, 628–644.
3. Endo, T. and Yamano, K. (2010) Transport of proteins across or into the mitochondrial outer membrane. Biochim. Biophys. Acta. 1803, 706–714.
4. Mick, D. U., Fox, T. D. and Rehling, P. (2011) Inventory control: cytochrome c oxidase assembly regulates mitochondrial translation. Nat. Rev. Mol. Cell Biol. 12, 14–20.
5. Dudek, J., Rehling, P. and van der Laan, M. (2013) Mitochondrial protein import: Common principles and physiological networks. Biochim. Biophys. Acta. 1833, 274–285.
6. Vögtle, F. -N. et al. (2009) Global analysis of the mitochondrial N-proteome identifies a processing peptidase critical for protein stability. Cell 139, 428–439.
7. Taylor, A. et al. (2001) Crystal structures of mitochondrial processing peptidase reveal the mode for specific cleavage of import signal sequences. Structure 9, 615–625.
8. Mossmann, D., Meisinger, C. and Vögtle, F.-N. (2012) Processing of mitochondrial presequences. Biochim. Biophys. Acta. 1819, 1098-1106.
9. Endo, T. and Kohda, D. (2002) Functions of outer membrane receptors in mitochondrial protein import. Biochim. Biophys. Acta. 1592, 3–14.
10. Koehler, C. M. (2004) New developments in mitochondrial assembly. Annu. Rev. Cell Dev. Biol. 20, 309–335.
11. Endo, T. and Yamano, K. (2009) Multiple pathways for mitochondrial protein traffic. Biol. Chem. 390, 723–730.
12. Abe, Y., Shodai, T, Muto, T., Mihara, K., Torii, H., Nishikawa, S., Endo, T. and Kohda, D. (2000) Structural basis of presequence recognition by the mitochondrial protein import receptor Tom20. Cell 100, 551–560.
13. Saitoh, T., Igura, M., Obita, T., Ose, T., Kojima, R., Maenaka, K., Endo, T. and Kohda, D. (2007) Tom20 recognizes mitochondrial presequences through dynamic equilibrium among multiple bound states. EMBO J. 26, 4777–4787.

14. Geissler, A., Chacinska, A., Truscott, K.N., Wiedemann, N., Brandner, K., Sickmann, A., Meyer, H.E., Meisinger, C., Pfanner, N. and Rehling, P. (2002) The mitochondrial presequence translocase: an essential role of Tim50 in directing preproteins to the import channel. Cell 111, 507–518.
15. Yamamoto, H., Esaki, M., Kanamori, T., Tamura, Y., Nishikawa, S. and Endo, T. (2002) Tim50 is a subunit of the TIM23 complex that links protein translocation across the outer and inner mitochondrial membranes. Cell 111, 519–528.
16. Mokranjac, D., Paschen, S.A., Kozany, C., Prokisch, H., Hoppins, S.C., Nargang, F.E., Neupert, W. and Hell, K. (2003) Tim50, a novel component of the TIM23 preprotein translocase of mitochondria. EMBO J. 22, 816-825.
17. Shiota, T., Mabuchi, H., Tanaka-Yamano, S., Yamano, K. and Endo, T. (2011) In vivo protein-interaction mapping of a mitochondrial translocator protein Tom22 at work. Proc. Natl. Acad. Sci. USA. 108, 15179–15183.
18. Qian, X., Gebert, M., Höpker, J., Yan, M., Li, J., Wiedemann, N., van der Laan, M., Pfanner, N. and Sha, B. (2011) Structural basis for the function of Tim50 in the mitochondrial presequence translocase. J. Mol. Biol. 411, 513–519.
19. Schulz, C., Lytovchenko, O., Melin, J., Chacinska, A., Guiard, B., Neumann, P., Ficner, R., Jahn, O., Schmidt, B. and Rehling, P. (2011) Tim50's presequence receptor domain is essential for signal driven transport across the TIM23 complex. J. Cell Biol. 195, 643–656.
20. Lytovchenko, O., Melin, J., Schulz, C., Kilisch, M., P Hutu, D. and Rehling, P. (2013) Signal recognition initiates reorganization of the presequence translocase during protein import. EMBO J. 32, 886–898.
21. Yamamoto, H., Itoh, N., Kawano, S., Yatsukawa, Y., Momose, T., Makio, T., Matsunaga, M., Yokota, M., Esaki, M. Shodai, T., Kohda, D., Hobbs, A.E.A., Jensen, R.E. and Endo, T. (2011) Dual role of the receptor Tom20 in specificity and efficiency of protein import into mitochondria. Proc. Natl. Acad. Sci. U.S.A. 108, 91−96.
22. Sikorski, R. S. and Hieter, P. (1989) A system of shuttle vectors and yeast host strains designed for efficient manipulation of DNA in Saccharomyces cerevisiae. Genetics 122, 19–27.
23. Tamura, Y., Harada, Y., Shiota, T., Yamano, K., Watanabe, K., Yokota, M., Yamamoto, H., Sesaki, H., and Endo, T. (2009) Tim23-Tim50 pair coordinates functions of

translocators and motor proteins in mitochondrial protein import. J. cell. Biol. 184 (1), 129-41.

24. Marom, M., Dayan, D., Demishtein-Zohary, K., Mokranjac, D., Neupert, W. and Azem A. (2011) Direct interaction of mitochondrial targeting presequences with purified components of the TIM23 complex. J. Biol. Chem. 286, 43809–43815.
25. Louis-Jeune , C., Andrade-Navarro, MA., and Perez-Iratxeta, C. (2011) Prediction of protein secondary structure from circular dichroism using theoretically derived spectra. Proteins: Structure, Function, and Bioinformatics, 80 (2), 374-381.
26. Marsh, J.A., Singh, V.K., Jia, Z. and Forman-Kay, J.D. (2006) Sensitivity of secondary structure propensities to sequence differences between α- and γ-synuclein: implications for fibrillation. Protein Sci. 15, 2795–2804.
27. Yamano, K., Yatsukawa, Y., Esaki, M., Hobbs, A.E.A, Jensen, R.E. and Endo, T. (2008) Tom20 and Tom22 share the common signal recognition pathway in mitochondrial protein import. J. Biol. Chem. 283, 3799-3807.
28. Dolezal, P., Likic, V., Tachezy, J., and Lithgow, T. (2006) Evolution of the molecular machines for protein import into mitochondria. Science 313, 314–318.
29. de la Cruz, L., Bajaj, R., Becker, S. and Zweckstetter, M. (2010) The intermembrane space domain of Tim23 is intrinsically disordered with a distinct binding region for presequences. Protein Sci. 19, 2045–2054.
30. Zhang, Y., Deng, H., Zhao, Q. and Jie Li, S. (2012) Interaction of Presequence with Human Translocase of the Inner Membrane of Mitochondria Tim50. J. Phys. Chem. B. 116, 2990−2998.